Diploma thesis

Bose-Einstein condensation of photons

Tobias Rexin

July 24, 2012

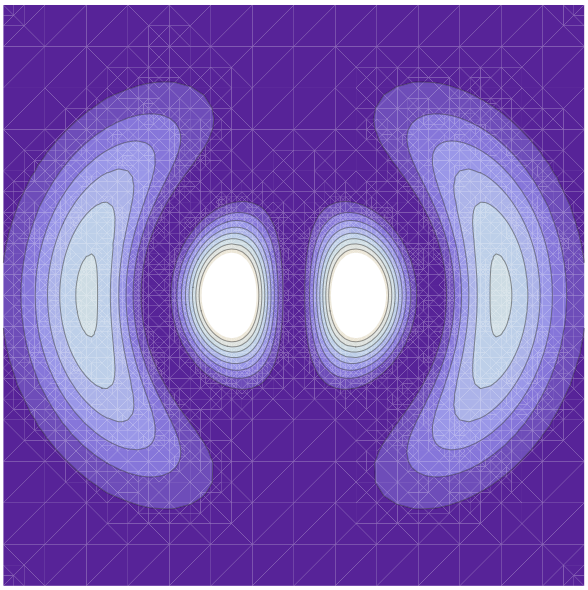

first supervisor: Prof. Martin Wilkens
second supervisor: PD Dr. Axel Pelster

Institut für Physik und Astronomie, Universität Potsdam

The title shows the transverse electromagnetic mode (TEM_{11}) with radial quantum number $l = 1$ and angular momentum quantum number $m = 1$ in a cylinder-symmetrical optical micro cavity.

Selbstständigkeitserklärung

Hiermit versichere ich, die vorliegende Arbeit ohne unzulässige Hilfe Dritter und ohne Benutzung anderer als der angegebenen Hilfsmittel angefertigt zu haben. Die aus fremden Quellen direkt oder indirekt übernommenen Gedanken sind als solche kenntlich gemacht. Die Arbeit wurde bisher weder im In- noch im Ausland in gleicher oder ähnlicher Form einer anderen Prüfungsbehörde vorgelegt.

Potsdam, den 24.Juli 2012

_____

(Tobias Rexin)

Kurzzusammenfassung

1995 wurden die ersten Bose-Einstein-Kondensate (BEC) mit ultrakalten Atomen experimentell beobachtet [1, 2]. Seither konnte dieses makroskopische Quantenphänomen in einer Vielzahl von physikalischen Systemen realisiert werden, angefangen bei ultrakalten Atomen bis hin zu Quasiteilchen in Halbleiterstrukturen bei Zimmertemperatur [3, 4, 5, 6, 7]. Aktuelle Experimente in der Arbeitsgruppe von Martin Weitz an der Universität Bonn [8, 9] machten es sogar experimentell möglich, Photonen in ein Bose-Einstein Kondensat zu überführen. Obwohl sie weder eine Ruhemasse noch ein chemisches Potential aufweisen, konnte durch geschicktes Modifizieren des thermischen Gleichgewichts in einem Resonator dieser Phasenübergang bei einem Photonengas beobachtet werden. Die vorliegende Diplomarbeit verbindet nun die Elektrodynamik mit der Bose-Einstein-Kondensation und unterstützt somit theoretisch die bereits durchgeführten Experimente. Ausgehend von den Maxwell-Gleichungen in einer Kavität leiten wir die zugrundeliegende Modenstruktur der dreidimensionalen Resonatorphotonen her, welche effektiv einem zweidimensionalen massiven Bose-Gas entspricht. Das resultierende Randwertproblem in einem gekrümmten Resonator beinhaltet bereits die relevanten Informationen, die für ein in einer harmonischen Falle gefangenes massives Bose-Gas erforderlich sind. Die berechneten Moden bieten Zugang zu thermodynamischen und statistischen Größen wie der kritischen Photonenzahl, Intensitäten und Korrelationsfunktionen. In diesem Sinne bietet die explizite Kenntnis des elektromagnetischen Feldes ein perfektes Werkzeug für weitergehende Untersuchungen.

Abstract

The first Bose-Einstein condensate (BEC) was experimentally observed with ultra cold atoms in 1995 [1, 2]. Since then, this macroscopic quantum phenomenon has been realized in various physical systems from ultra cold atoms to quasi-particles in semi-conductors at room-temperature [3, 4, 5, 6, 7]. Recent experiments [8, 9] made it experimentally feasible to Bose-Einstein condensate even photons. Possessing neither a rest mass nor a chemical potential, an adept modification of the thermal equilibrium in a micro cavity permits the observation of the phase transition for a photon gas. This diploma thesis links electrodynamics with the Bose-Einstein condensation of photons and therefore theoretically supports the performed experiments on a photonic BEC. Starting from the three-dimensional Maxwell equations in a cavity, we derive the underlying mode structure of the cavity photons which then corresponds to an effective two-dimensional massive Bose gas. The resulting boundary value problem in a curved resonator already contains all relevant information which is required for a massive harmonically trapped Bose gas. The calculated modes grant access to thermodynamical and statistical quantities such as the critical photon number, intensity and correlation functions. In this sense the knowledge of the explicit electromagnetic field provides a perfect tool for further investigations.

Contents

1 Introduction **3**
- 1.1 Experimental setup . . . 5
- 1.2 Experimental results . . . 6

2 Photon field in a micro resonator **9**
- 2.1 Maxwell equations in matter . . . 9
- 2.2 Boundary value problem . . . 11
- 2.3 Oblate spheroidal coordinates . . . 14
- 2.4 Scalar Helmholtz equation in oblate spheroidal coordinates . . . 15
  - 2.4.1 Transverse modes . . . 17
  - 2.4.2 Axial modes . . . 20
  - 2.4.3 Higher order correction to axial modes . . . 21
  - 2.4.4 Scalar solution . . . 22
- 2.5 Vector solution . . . 23
- 2.6 Boundary values and eigenvalues . . . 25
- 2.7 Polarization vectors and ground-state energy . . . 28
- 2.8 Field quantization . . . 31

3 Calculating the BEC **35**
- 3.1 Ultra cold versus room temperature Bose gas . . . 35
- 3.2 Density matrix . . . 36
- 3.3 Effective action . . . 37
  - 3.3.1 Condensate and fluctuations . . . 40
  - 3.3.2 Two-dimensional phase transitions . . . 41
  - 3.3.3 Perturbation theory in the interacting Hamiltonian . . . 42
- 3.4 Effective action for ideal cavity photon gas . . . 43
- 3.5 Critical number for non-interacting cavity photon gas . . . 45
- 3.6 Effective action for interacting cavity photon gas . . . 47
- 3.7 Shift of chemical potential due to interaction . . . 49
- 3.8 Critical number for the interacting cavity photon gas . . . 50
- 3.9 Density and correlation . . . 52

4 Conclusion and outlook **57**

A Normalizing the vector modes **59**

B Transverse delta function **63**

C Correlation function **67**

Bibliography **71**

Outline of this thesis

This thesis represents a link between electrodynamics and the BEC theory which obviously both apply to a BEC of photons. In particular, we transfer the results for electromagnetic fields in the cavity obtained from classical electrodynamics to the bosonic field theory for weakly interacting Bose gases.
After the brief presentation of the performed experiment in the **introduction**, the **second chapter** starts with the Maxwell equations and develops the boundary value problem for the cavity photons. To this end, the vectorial Maxwell equations are decomposed into a vector constraint and a scalar differential equation. In paraxial approximation and with suitable coordinates, the boundary value problem for the curved resonator system can be explicitly solved. The obtained mode structure is then used to quantize the electromagnetic field. The **third chapter** takes advantage of the field quantization and establishes an effective two-dimensional description for the Bose gas. The main part of this chapter is dedicated to the calculation of the BEC phase transition for the cavity photons, which is performed quantum mechanically exact. With the full mode structure at hand, the spatial correlation of the photon gas can be studied. Finally, the thesis is concluded in the **fourth chapter**. The methods and experimental proposals for further investigation of a photonic BEC are discussed. Worth mentioning are the occurring different polarizations in the BEC and the possible creation of a left- and right-handed BEC or doughnut-shaped ground state mode. In particular, the theoretical description of the two-dimensional phase transition and the calculation of the corresponding time-dependent correlations are fundamental ongoing questions for the photonic BEC.

Chapter 1

Introduction

This diploma thesis links the experiments on a Bose-Einstein condensate (BEC) of photons [8, 9, 10, 11, 12] performed by the Bonn group of Martin Weitz with electrodynamics.
What is special about Bose-Einstein condensation of photons in an optical micro cavity? One of the most omnipresent Bose gases is the black-body radiation. It is not feasible to cool down a black body-radiator in order to achieve a phase transition towards a BEC of photons with thermal distribution. The Stefan-Boltzmann law tells us already that the radiated energy, and therefore the number of emitted photons, is proportional to T^4 with T being the temperature. This just states that cooling provides an effective loss of photons but it does not end up in a macroscopic occupation of the lowest possible energy level. In case of massive particles, as for a rubidium gas, it is clear that you just have to reduce the average kinetic energy of the particles to reach the ground state with the whole ensemble. However, with a rest mass of zero and a vanishing chemical potential we cannot cool down photons in number conserving way. How can we experimentally circumvent this problem? A promising ansatz is to put the photons into a micro cavity. The setting of a resonator discretizes the spectrum of possible modes inside the cavity. The resonance condition $L = 0.5\ n\lambda$ naturally selects the allowed cavity modes, here L denotes the spatial extension of the cavity, λ is a possible wavelength and n is the integer number of nodes in the resonator. Obviously a wavelength with

$$\lambda > 2L \tag{1.1}$$

is not resonant, because $n = 1$ is the lowest available node number. Thus, we conclude that every finite system has a certain cut-off wavelength. Via the linear dispersion relation for light in a homogeneous medium

$$E = \hbar\omega = \hbar c\frac{2\pi}{\lambda} \tag{1.2}$$

the resonator defines the lowest available energy level. By setting a high energy cut-off, it is no longer required to cool down to the absolute zero point to reach the corresponding ground state. Thus, especially micro cavities with ultra small mirror distances L implement enhanced cut-offs. The thermalization of photons in a cavity is still problematic, how can one populate the ground state macroscopically

without loosing the photons. The answer is a dye solution between the cavity mirrors. Every electromagnetic wave can be described by a certain wave vector $\mathbf{k}$. In three dimensions, this vector has three distinct vector components. Imagine a resonator in z-direction and an open rim in the other two transverse directions. The transverse direction has a continuous spectrum, while the z-direction possesses an energy cut-off. Translated into the proportions of the wave vector $\mathbf{k}$, this means that the two transverse components can become arbitrarily small, whereas the k_z-component cannot. The spectral properties of the dye-solution thermalize the light inside the cavity. Due to the large overlap between its absorption and its emission coefficient, the dye depopulates states with great transversal components and emits exactly electromagnetic waves with the appropriate k_z-component. Thus, this is not cooling down photons, but the modified thermal equilibrium with the high energy cut-off effectively leads to a significant population of the photons with wave vector k_z and small transverse components. This is essentially distinct from lasing, where the gain medium and the light field are far removed from thermal equilibrium to produce coherent light. In the case of the photon BEC the macroscopic population of one photon mode is achieved by an equilibrium phase transition. Strongly coupled mixed states of photons and polaritons can also thermalize due to interparticle interaction. However the difference between these exciton polaritons and the photon BEC is the coupling mechanism. While polaritons require coherent back scattering to reach a quasi-equilibrium, the frequent collisions of the dye with the solvent hinder coherent energy exchange between the photons and the dye molecules. Thus, the coupling process for the thermalization is incoherent which contravenes the condition for strong matter-field coupling.
Of course, electromagnetic waves in a curved resonator obey the Maxwell equations. In appropriate gauge, the Maxwell equations encode the Fourier transformed three-dimensional wave equation or so called Helmholtz equation

$$-\Delta\Psi(\mathbf{x}) = k^2\Psi(\mathbf{x}), \tag{1.3}$$

with some additional boundary conditions arising from the curved mirrors. An explicit analysis of the underlying mode structure should reveal similarities to a massive trapped bosonic gas whose corresponding partial differential equation (PDE) for the mode function is reminiscent of the two-dimensional stationary Schrödinger equation

$$\left\{-\frac{\hbar^2}{2m_{\mathrm{ph}}}\Delta + V(\mathbf{x})\right\}\Psi(\mathbf{x}) = k^2\Psi(\mathbf{x}). \tag{1.4}$$

This diploma thesis is guided by the idea of taking the normal mode expansion for cavity photons as an ansatz for equivalently massive trapped bosons. The intention is to derive the occurrence of BEC from the Helmholtz equation (1.3), which is classical electrodynamics. Inspired by the analogy to the massive trapped boson Hamiltonian (1.4), we set up a boundary value problem for the electromagnetic field and develop the underlying normal modes. The explicit mode structure gives full access to various important quantities as for instance intensities, correlation functions and the critical photon number. Therefore this diploma thesis provides also theoretical support for the photonic BEC experiment in Bonn. Before we analyze the problem in detail, it is useful to have in mind a precise scheme of the performed experiment.

1.1 Experimental setup

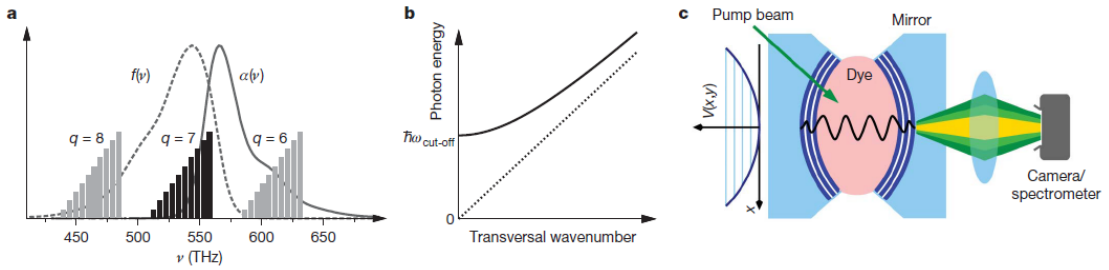

Figure 1.1: a) Schematic spectrum of cavity modes with absorption coefficient $\alpha(\nu)$ and fluorescence strength $f(\nu)$ b) Dispersion relation of photons in the cavity (solid line) with fixed longitudinal mode ($q = 7$) and the free photon dispersion (dashed line) c) Schematic experimental setup with trapping potential imposed by the curved mirrors [9].

The experiment described here is the basic setting for our further theoretical investigation. It was performed by Martin Weitz and his group at the University of Bonn. Photons are trapped in a curved optical micro resonator, where the curvature of the mirrors induces an effective harmonic trapping potential, see Figure 1.1. Outside the center of the mirrors, the distance d becomes shorter and the absolute value of allowed wave vectors

$$|\mathbf{k}| = \frac{2\pi}{d} \tag{1.5}$$

grows. Thus, we conclude that the energy $E = \hbar c|\mathbf{k}|$ of the photons to remain in this region of the cavity is higher than in the center. Here, c denotes the speed of light in the dye medium defined as $c = c_0/n$ with the refraction index of the dye solution $n = 1.4$ and the vacuum speed of light c_0. Thus, we have to distinguish the cavity wavelength and the outside wavelength according to

$$\nu = \frac{c_0}{\lambda_0} = \frac{c}{\lambda}, \tag{1.6}$$

which results in a shorter cavity wavelength

$$\lambda = \frac{\lambda_0}{n}. \tag{1.7}$$

The two mirrors are spaced $L = 1.46$ μm away from each other, which amounts to 3.5 times the optical wavelength. Corresponding to a vacuum wavelength of $\lambda_0 = 585$ nm or a cavity wavelength $\lambda = 412$ nm, Figure 1.1 shows a great overlap between the absorption coefficient $\alpha(\nu)$ and the fluorescence strength $f(\nu)$ of the dye at the quantum number $q = 7$. This modifies the spontaneous emissions such that the emission of the longitudinal mode with quantum number $q = 7$ dominates

over all other emission processes.
Due to the extremely short mirror distance and the spectral properties of the dye solution, there is an effective longitudinal low frequency cut-off $\omega_{\mathrm{cut}} = ck_z = 2\pi \cdot 5.1 \cdot 10^{14}$ Hz with the longitudinal cut-off wave vector

$$k_z = \frac{q\pi}{L} = \frac{2\pi}{\lambda}. \tag{1.8}$$

The energy $E = \hbar\omega_{\mathrm{cut}}$ of the longitudinal mode k_z is far above thermal energy at room-temperature $\beta\hbar\omega_{\mathrm{cut}} = 80$ with the inverse temperature $\beta = 1/(k_{\mathrm{B}}T)$. The photon statistics yields

$$n_{\mathrm{ph}} = \frac{1}{\mathrm{e}^{\beta\hbar\omega_{\mathrm{cut}}} - 1} \approx \mathrm{e}^{-80} \tag{1.9}$$

i.e. the cavity photon number n_{ph} is almost not altered by the temperature T of the surrounding dye solution. The thermalization process conserves the average photon number. Thermal equilibrium can be achieved by absorption and reemission processes in the dye solution, which is acting as a heat bath for the photons. In Figure 1.1, the reemission and absorption in the longitudinal mode k_z dominates all other modes. There the largest overlap between the emission coefficient $\alpha(\nu)$ and the fluorescence strength $f(\nu)$ occurs. Most of the $(q = 7)$-photons absorbed by the dye will be reemitted inside the cavity, whereas there is an imbalance between absorption and emission for all other longitudinal modes. The k_z-mode is frozen out and the transversal modes $k_\perp$ can thermalize due to the rovibrational energy levels of the dye solution.

1.2 Experimental results

The BEC of the photons inside the dye-filled cavity has been proven experimentally by investigating both the spatial and the temporal coherence. Figure 1.2 shows the measured spectral distribution which is a classical thermal distribution at room temperature plus an increased intensity for the wavelength $\lambda = 585$ nm. The latter corresponds to the frozen longitudinal wave vector k_z, which yields $\lambda = n_0 2\pi/k_z$. This proves the BEC of photons in the frequency domain. The experimental setup also allows to check the spatial domain. Hence, another evidence for the achieved BEC is the in-situ spot captured by the camera in Figure 1.2. Below criticality, there is only a thermal cloud of the cavity photons, but above criticality, one finds a rather sharp yellow spot sitting in the center of the cavity in the minimum of the harmonic potential, which is induced by the curvature of the cavity mirrors.

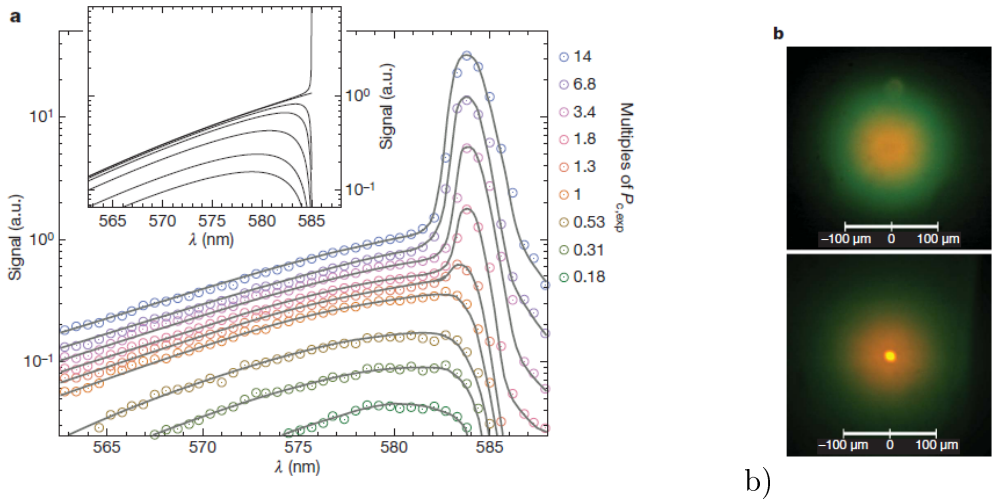

a) b)

Figure 1.2: a) Spectral intensity distributions (connected circles) transmitted through one cavity mirror, as measured with a spectrometer for different pump powers. b) Images of the spatial radiation distribution below criticality (upper panel) and above criticality (lower panel) [9].

Chapter 2

Photon field in a micro resonator

Starting from the three-dimensional Maxwell equations, we derive a theoretical description of the electromagnetic field that can be used to mimic the Hamiltonian of two-dimensional massive trapped bosons. To this end, we formulate a boundary value problem for the Maxwell equations in the curved resonator environment. This classical description yields the eigenmodes which are necessary for the quantization of the cavity field. Within the **paraxial approximation**, it can be shown that solving the Maxwell equations for the photon modes in three dimensions is formally equivalent to looking for eigenfunctions of the stationary Schrödinger equation for matter-like bosons in two dimensions. Thus, we can identify the Fock space of the cavity photons with the Fock space of trapped massive bosons.

2.1 Maxwell equations in matter

The electromagnetic field in the resonator, which we investigate, is modified by the presence of the dye solution. Thus we have to consider the macroscopic Maxwell equations which read in the units of the *système international* (SI)

$$\begin{aligned} \nabla \cdot \mathbf{D} &= \rho & \nabla \cdot \mathbf{B} &= 0 \\ \nabla \times \mathbf{E} &= -\dot{\mathbf{B}} & \nabla \times \mathbf{H} &= \mathbf{j} + \dot{\mathbf{E}}. \end{aligned} \tag{2.1}$$

The following material equations for media featuring electric or magnetic polarization $\mathbf{P}$ or $\mathbf{M}$, respectively, connect the dielectric displacement $\mathbf{D}$ and the magnetic induction $\mathbf{B}$ with the electric and the magnetic field $\mathbf{E}$ and $\mathbf{H}$ respectively,

$$\mathbf{D} = \epsilon_0 \mathbf{E} + \mathbf{P} \tag{2.2}$$

$$\mathbf{B} = \mu_0 (\mathbf{H} + \mathbf{M}), \tag{2.3}$$

where ϵ_0 is the vacuum permittivity and μ_0 the vacuum permeability. For the moment, we assume that the dye is an isotropic linear material which leads to

$$\mathbf{D} = \epsilon_0 \mathbf{E} + \mathbf{P} = \epsilon_0 (\mathbf{E} + \chi_{\mathrm{el}} \mathbf{E}) = \epsilon \mathbf{E} \tag{2.4}$$

$$\mathbf{B} = \mu_0 (\mathbf{H} + \mathbf{M}) = \mu_0 (\mathbf{H} + \chi_{\mathrm{m}} \mathbf{H}) = \mu \mathbf{H}, \tag{2.5}$$

where χ_{el} and χ_{m} are the scalar susceptibilities. Thus, here the permeability μ and the permittivity ϵ are scalar quantities, too. More generally, the susceptibilities are

tensor-valued and depend on the orientation of the medium which then also covers non-linear optical effects like the parametric down conversion or the Kerr effect [13]. The present system does not involve any free charges or free currents, thus we set the charge density $\rho = 0$ and the current $\mathbf{j} = \mathbf{0}$. Combining these assertions with the material equations (2.4) and (2.5), the Maxwell equations read now

$$\begin{aligned} \nabla \cdot \epsilon\mathbf{E} &= 0 & \nabla \cdot \mu\mathbf{H} &= 0 \\ \nabla \times \mathbf{E} &= -\mu\dot{\mathbf{H}} & \nabla \times \mathbf{H} &= \dot{\mathbf{E}}. \end{aligned} \tag{2.6}$$

Within the potential formalism, we reexpress the electric and the magnetic field in terms of a scalar potential ϕ and a vector potential $\mathbf{A}$,

$$\mathbf{E} = -\nabla\varphi - \dot{\mathbf{A}} \tag{2.7}$$

$$\mathbf{H} = \nabla \times \mathbf{A}. \tag{2.8}$$

Note here, that two of the four equations (2.6) are always satisfied by the vector identities

$$\nabla \times \nabla\varphi = \mathbf{0} \tag{2.9}$$

$$\nabla \cdot \nabla \times \mathbf{A} = 0. \tag{2.10}$$

From a mathematical point of view, we can add the gradient of an arbitrary function to $\mathbf{A}$ and still get the same physical field $\mathbf{H}$,

$$\tilde{\mathbf{H}} = \nabla \times \tilde{\mathbf{A}} = \nabla \times (\mathbf{A} + \nabla\Xi) = \mathbf{H}. \tag{2.11}$$

Correspondingly, also the electric field is left unchanged

$$\tilde{\mathbf{E}} = -\nabla\tilde{\varphi} - \frac{\partial}{\partial t}\tilde{\mathbf{A}} = -\nabla\tilde{\varphi} - \frac{\partial}{\partial t}(\mathbf{A} + \nabla\Xi) \stackrel{!}{=} \mathbf{E}, \tag{2.12}$$

provided the scalar function is given by

$$\tilde{\varphi} = \varphi - \frac{\partial}{\partial t}\Xi. \tag{2.13}$$

Clearly, the Maxwell equations are invariant under such gauge transformations. From Emmy Noether's theorem we know that symmetries underlie conserved quantities, in the present case it is simply charge conservation. However, the information we obtain from (2.11) is that the vector potential $\mathbf{A}$ is not exactly determined. There are many ways for a gauge fixation, i.e ways to fix the arbitrary function Ξ as for example

$$\sin(\mathbf{A} \cdot \mathbf{x}) = \frac{\pi}{7|\mathbf{x}|} \tag{2.14}$$

$$\nabla \cdot \mathbf{A} = 0. \tag{2.15}$$

Equation (2.14) is probably not a good choice for a gauge fixation, but (2.15) represents the Coulomb gauge or the so-called transversal gauge, which is of tremendous

physical relevance. Plugging Equation (2.7) into Equation (2.6) and applying (2.26), one immediately finds that φ is an harmonic function

$$\Delta\varphi = 0. \tag{2.16}$$

Setting the Dirichlet boundary condition $\varphi = 0$ on the boundary $\partial\Omega$ and applying the minimum and maximum principle for harmonic functions, φ must be 0. The Coulomb gauge together with $\varphi = 0$ represents the radiation gauge.
Using the vector identity

$$\nabla \times \nabla \times \mathbf{A} = \nabla\nabla \cdot \mathbf{A} - \Delta\mathbf{A} \tag{2.17}$$

and the Coulomb gauge (2.15), the Maxwell equations (2.6) reduce to the vectorial wave equation

$$\left[\Delta - \frac{1}{c^2}\frac{\partial^2}{\partial t^2}\right]\mathbf{A} = \mathbf{0}, \tag{2.18}$$

where $c = (\mu\epsilon)^{-1/2}$ denotes the speed of light in the dye solution given by $c = c_0/n$. The linear refraction index n of the dye solution is 1.33. Performing the Fourier transformation from the time domain to the frequency domain by taking into account the linear dispersion relation $\omega = c|\mathbf{k}|$ in homogeneous media, we end up with the homogeneous vectorial Helmholtz equation

$$\left[\Delta + |\mathbf{k}|^2\right]\mathbf{A} = \mathbf{0}, \tag{2.19}$$

with the length of a yet arbitrary wave vector $|\mathbf{k}| = \sqrt{k_z^2 + k_y^2 + k_x^2}$. This equation is the starting point for further investigations.

2.2 Boundary value problem

In order to establish proper boundary conditions, we must take a closer look at the experimental setup. The whole system exhibits cylindrical symmetry, since it is invariant under rotations of the azimuthal angle. These are rotations around the z-axis, see Figure 2.1. Additionally we have to parametrize the curved caps of the cylinder as the boundary for the curved resonator.
A few geometrical considerations for this bi-convex cavity lead to a parametrization of the mirrors, here denoted by $\partial\Omega_\pm$. Hence the coordinate z is parametrized as a function of the distance ρ perpendicular to the optical axis

$$z|_{\partial\Omega_\pm}(\rho) = \pm\left(\frac{L}{2} - R + \sqrt{R^2 - \rho^2}\right), \tag{2.20}$$

where R is the curvature radius of the mirrors and L the mirror distance. In paraxial approximation, where $\rho \ll R$ is assumed, these boundary conditions reduce to

$$z|_{\partial\Omega_\pm}(\rho) \approx \pm\left(\frac{L}{2} - \frac{\rho^2}{2R}\right). \tag{2.21}$$

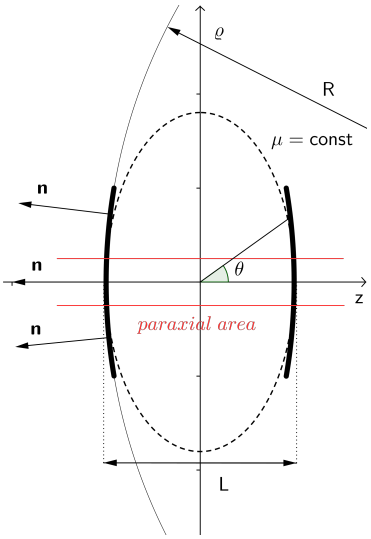

Figure 2.1: Schematic of the geometrical setup within the bi-convex micro resonator. The system is invariant under rotations around the z-axis. The indicated polar angle θ does not play a role in cylindrical coordinates, but it is relevant in curvilinear coordinates to describe the mirror surfaces (bold black). The large radius vector R indicates the curvature of the mirrors. L is the mirror distance on the optical axis, which decreases in radial direction ρ.

To justify that $\rho \ll R$, we evaluate ρ at $z = 0$ in (2.21), where theoretically the two mirror surfaces get together,

$$z = \pm \left(\frac{L}{2} - \frac{\rho^2}{2R} \right) \stackrel{!}{=} 0. \tag{2.22}$$

A first estimation leads to

$$\rho_{\max} \approx \sqrt{LR}. \tag{2.23}$$

Just for comparison, the mirror distance L is about 1.46 μm in contrast to a huge curvature radius R of about 1 m. Thus $\rho_{\max}$ is at least a thousand times smaller than R.
Furthermore, we assume perfectly conducting cavity walls which yields the boundary conditions [14]

$$\mathbf{n} \times \mathbf{E}|_{\partial\Omega_\pm} = \quad -\mathbf{n} \times \dot{\mathbf{A}}|_{\partial\Omega_\pm} \quad = \mathbf{0} \tag{2.24}$$

$$\mathbf{n} \cdot \mathbf{H}|_{\partial\Omega_\pm} = \quad \mathbf{n} \cdot \nabla \times \mathbf{A}|_{\partial\Omega_\pm} \quad = 0, \tag{2.25}$$

where $\mathbf{n}$ is the normal vector to the curved mirror surface in Figure 2.1. Due to continuity, the tangential component of the electric field and the normal component of the magnetic field have to vanish on the cavity boundary. However, a normal component of electric field on the cavity surface is allowed. The same applies for the tangential magnetic field. There is a non-zero field inside the cavity, but outside

the cavity the field should vanish. This is modeled by the ideal cavity walls which guarantee a field-free environment. Figure 2.1 clearly shows that the tangential and normal vectors are not constant vectors, but depend on the base point.
In the previous section, we have cast the Maxwell equations into the form of the vectorial Helmholtz equation (2.19) with a vector constraint arising from Coulomb gauge (2.15)

$$\nabla \cdot \mathbf{A} = 0 \tag{2.26}$$

$$\left[\Delta + |\mathbf{k}|^2\right] \mathbf{A} = \mathbf{0}. \tag{2.27}$$

The actual advantage of the Coulomb gauge is that the Helmholtz differential operator is scalar and acts separately on each of the three field components of $\mathbf{A}$. The coupling of the various vector components is still present in the divergence constraint.
Solving the Maxwell equations for the cavity modes amounts to solving Equations (2.26), (2.27) with the boundary conditions given by Equations (2.24), (2.25) and a specific boundary parametrization (2.21) making the variable z dependent on ρ.
In three dimensions, one has three independent variables for the Helmholtz equation. It would be tempting to separate these three variables in order to solve the ordinary differential equations (ODEs), however the boundary condition induces a dependence which destroys this scheme afterwards. One can simplify the problem by using coordinates (ξ_1, ξ_2, ξ_3) adapted to the boundary condition, such that no dependencies among the variables are induced on the boundary, for example

$$\mathbf{A}(\mathbf{x})|_{\partial\Omega} = \mathbf{A}(\xi_1 = \text{const}, \xi_2, \xi_3). \tag{2.28}$$

The curved mirrors are then just isolines in the chosen curvilinear coordinate system. In this representation the boundary value problem can be handled more readily.
In a next step, I subdivide the system of two partial differential equations into the vector constraint and the scalar Helmholtz equation for each vector component. The separability of partial differential equations (PDEs) is the criterion whether or not it is possible to cast a PDE of certain variables into separated ordinary differential equations (ODEs) for the respective single variables. This is advantageous as ODEs are generally easier to solve than PDEs. Morse and Feshbach have already shown that the homogeneous scalar Helmholtz equation in three dimensions [15], i.e.

$$\left[\Delta + |\mathbf{k}|^2\right] A_i(\xi_1, \xi_2, \xi_3, \omega) = 0 \tag{2.29}$$

is separable in eleven different coordinate systems [15, 16]. Of course the scalar Helmholtz equation can also be solved in non-separable coordinates, but this is rather hard to achieve. In general it is convenient to choose one of these eleven coordinate systems such that the boundary is parametrized in a simple form, while the scalar Helmholtz equation still remains separable, although the Laplace operator can get more complicated.
In this section we deduced that it is sufficient to solve the scalar Helmholtz equations in separable coordinates. The following section provides a possible coordinate system matching the boundary condition. Once we have a scalar solution A_i [17] at hand, we have to construct a vector field which fulfills the additional constraint $\nabla \cdot \mathbf{A}(\mathbf{x}) = 0$.

2.3 Oblate spheroidal coordinates

With the previous considerations in mind, we choose the oblate spheroidal coordinates

$$x = a\cosh(\mu)\sin(\theta)\cos(\phi), \tag{2.30}$$
$$y = a\cosh(\mu)\sin(\theta)\sin(\phi), \tag{2.31}$$
$$z = a\sinh(\mu)\cos(\theta), \tag{2.32}$$

where a is scale factor, one has to determine from the geometry of the cavity. The coordinate μ runs mainly along the z-axis, while $\theta > 0$ is off-axis. For a fixed μ one gets an ellipsoid in the xz-plane which is rotated around the z-axis by the angle ϕ. Restricting the polar angle θ to $0 < \theta < \pi/2$, the sign of z is carried by μ. Then the sign of x and y is defined by ϕ, for further illustration see Figure 2.2. The limitation of the polar angle θ enables us to distinguish between the left $(-)$ and right $(+)$ mirror side.

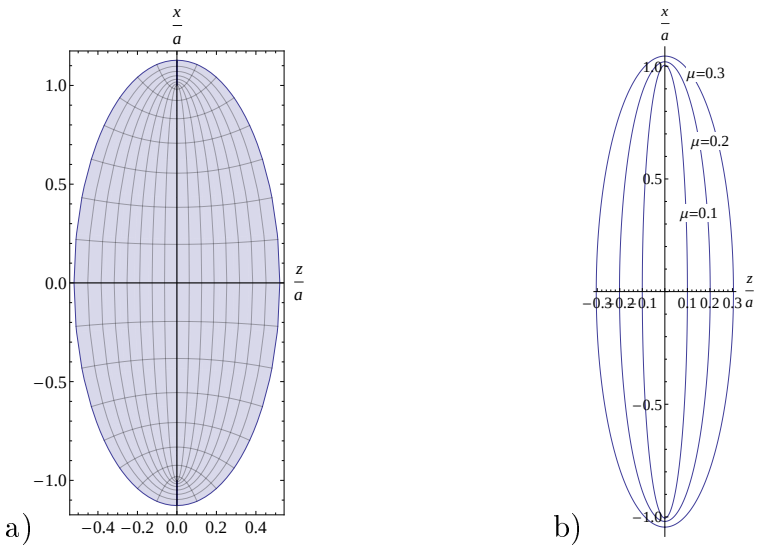

Figure 2.2: Oblate spheroidal coordinates. a) Equations (2.30)–(2.32) as a cut in the xz-plane for ϕ=0. b) Coordinate surfaces at constant μ are ellipses. The short half axis is defined by μ and the two focal points are defined by the parameter a.

Now we link this coordinate system to the oblate cavity. First of all, the mirror distance L is small in comparison to all other involved spatial dimensions, $L \ll \rho \ll R$. This already implies that the coordinate μ, which determines the mirror distance on the z axis, is much smaller than 1. The isolines for $\mu = \text{const}$ in Figure 2.2 highlight this fact. Thus, an expansion for small μ corresponds to a micro cavity and a plain mirror expansion. Additionally, expanding for small θ, which is actually the paraxial expansion, yields an approximate form of the oblate spheroidal coordinates

$$x \approx a\theta \cos\phi \tag{2.33}$$
$$y \approx a\theta \sin\phi \tag{2.34}$$
$$z \approx a\mu - \frac{a\mu\theta^2}{2}. \tag{2.35}$$

Inserting now (2.33) and (2.34) into (2.35) yields

$$z = a\mu - \frac{\mu(x^2+y^2)}{2a}. \tag{2.36}$$

Starting with the coordinate surface for $\mu_0 = \text{const}$, we impose the boundary conditions from Equation (2.21)

$$z|_{\partial\Omega_-} = \frac{x^2+y^2}{2R} - \frac{L}{2} \stackrel{!}{=} \frac{\mu_0(x^2+y^2)}{2a} - a\mu_0, \tag{2.37}$$
$$z|_{\partial\Omega_+} = \frac{L}{2} - \frac{x^2+y^2}{2R} \stackrel{!}{=} a\mu_0 - \frac{\mu_0(x^2+y^2)}{2a}. \tag{2.38}$$

This determines the scaling factor a and the oblate coordinate $\pm\mu_0$ for the mirror surfaces

$$a = \sqrt{\frac{LR}{2}}, \tag{2.39}$$
$$\mu_0 = \sqrt{\frac{L}{2R}} \ll 1. \tag{2.40}$$

Note here again that the expansion above is valid for an oblate cavity where the mirror distance L is much smaller than the curvature radius R. We have assured that the coordinates match the boundary condition in a way that we can simply parametrize it by $\mu = \text{const}$.

2.4 Scalar Helmholtz equation in oblate spheroidal coordinates

The oblate spheroidal coordinates are one of the eleven orthogonal coordinate systems in which the scalar Helmholtz equation is separable [16]. Now we are going to solve

$$\left[\Delta + |\mathbf{k}|^2\right] u(x,y,z,\omega) = 0 \tag{2.41}$$

with $|\mathbf{k}| = \omega/c$. Here the scalar function u is a Fourier transformed solution to the scalar wave equation in Cartesian coordinates. It turns out to be convenient to transform the variables according to [18]

$$\xi = \cos\theta \qquad 0 \le \xi < 1 \tag{2.42}$$
$$\zeta = \sinh\mu \qquad -\infty \le \zeta < \infty. \tag{2.43}$$

Then the Cartesian coordinates in (2.30)–(2.32) read as follows

$$x = a\sqrt{(1+\zeta^2)(1-\xi^2)}\cos\phi, \tag{2.44}$$

$$y = a\sqrt{(1+\zeta^2)(1-\xi^2)}\sin\phi, \tag{2.45}$$

$$z = a\zeta\xi. \tag{2.46}$$

Since we treat the micro cavity in a set of orthogonal coordinates, the metric involving the Jacobian is diagonal, so in three dimensions there are only three non-zero metric components. In general orthogonal coordinates the Laplace operator can be written as [19]

$$\Delta u = \frac{1}{h_1 h_2 h_3}\left[\partial_1\left(\frac{h_2 h_3}{h_1}\partial_1 u\right) + \partial_2\left(\frac{h_1 h_3}{h_2}\partial_2 u\right) + \partial_3\left(\frac{h_1 h_2}{h_3}\partial_3 u\right)\right], \tag{2.47}$$

where h_1, h_2, h_3 are the diagonal entries of the metric. In our case we get

$$h_\xi = \left\|\frac{\partial \mathbf{x}}{\partial \xi}\right\| = a\sqrt{\frac{\zeta^2+\xi^2}{1-\xi^2}}, \tag{2.48}$$

$$h_\zeta = \left\|\frac{\partial \mathbf{x}}{\partial \zeta}\right\| = a\sqrt{\frac{\zeta^2+\xi^2}{1+\zeta^2}}, \tag{2.49}$$

$$h_\phi = \left\|\frac{\partial \mathbf{x}}{\partial \phi}\right\| = a\sqrt{(1+\zeta^2)(1-\xi^2)}. \tag{2.50}$$

The Laplacian then takes the form

$$\begin{aligned}\Delta =& \frac{1}{a^2\left(\zeta^2+\xi^2\right)}\left\{\frac{\partial}{\partial\zeta}\left[\left(1+\zeta^2\right)\frac{\partial}{\partial\zeta}\right] + \frac{\partial}{\partial\xi}\left[\left(1-\xi^2\right)\frac{\partial}{\partial\xi}\right]\right\} \\ &+ \frac{1}{a^2\left(1+\zeta^2\right)\left(1-\xi^2\right)}\frac{\partial^2}{\partial\phi^2}.\end{aligned} \tag{2.51}$$

The azimuthal term can be split into a difference

$$\frac{1}{\left(1+\zeta^2\right)\left(1-\xi^2\right)} = \frac{1}{\left(\zeta^2+\xi^2\right)}\left[\frac{1}{1-\xi^2} - \frac{1}{1+\zeta^2}\right], \tag{2.52}$$

so we are able to separate the Helmholtz equation as

$$\left(\zeta^2+\xi^2\right)a^2\left(\Delta + |\mathbf{k}|^2\right)u(\xi,\zeta,\phi) = 0. \tag{2.53}$$

The multiplication with $(\zeta^2+\xi^2)$ cancels the prefactor in the Laplacian (2.51), such that separation with a constant is possible.
Plugging the separation ansatz $u(\xi,\zeta,\phi) = Q(\zeta)R(\xi)e^{im\phi}$ with an integer angular momentum quantum number m into Equation (2.53), the separated Helmholtz equation is

$$\left[\frac{\mathrm{d}}{\mathrm{d}\zeta}(1+\zeta^2)\frac{\mathrm{d}}{\mathrm{d}\zeta} + \frac{m^2}{(1+\zeta^2)} + (|\mathbf{k}|a)^2\zeta^2\right]Q(\zeta) = -\gamma^2 Q(\zeta), \tag{2.54}$$

$$\left[\frac{\mathrm{d}}{\mathrm{d}\xi}(1-\xi^2)\frac{\mathrm{d}}{\mathrm{d}\xi} - \frac{m^2}{(1-\xi^2)} + (|\mathbf{k}|a)^2\xi^2\right]R(\xi) = +\gamma^2 R(\xi), \tag{2.55}$$

with γ as a separation constant. The separation scheme endows the two brackets with eigenvalues of opposite sign e.g $\pm\gamma^2$. Furthermore, a kind of harmonic potential emerges in the form of two quadratic terms. The task is now to simultaneously solve both eigenvalue problems. Thus, it remains to determine the connection between γ and $|\mathbf{k}|$. The azimuthal angular momentum eigenvalue m was already identified by separating the variables. For simplification we set from now on $|\mathbf{k}| = k$.

2.4.1 Transverse modes

Rewriting the eigenvalue problem (2.55) from $\xi = \cos(\theta)$ into the θ coordinate, we find

$$-\frac{1}{\sin\theta}\frac{\mathrm{d}}{\mathrm{d}\theta}\sin\theta\frac{\mathrm{d}R}{\mathrm{d}\theta} + \frac{m^2}{\sin^2\theta}R + (ak)^2\sin^2\theta R = (qa)^2 R \tag{2.56}$$

with the following decomposition of the absolute value of wave vector $\mathbf{k}$

$$(qa)^2 = (ak)^2 - \gamma^2. \tag{2.57}$$

The allover sign in Equation (2.56) is chosen in analogy to the kinetic energy from quantum mechanics, which is $-\Delta$. Within the paraxial approximation we gain access to analytic solutions, namely to modes which are strongly confined close to the cavity axis, i.e. to the z-axis. Anticipating a typical axial wavelength of the order L, we expect the dimensionless parameter

$$ka \sim \frac{1}{L}\sqrt{\frac{RL}{2}} = \sqrt{\frac{R}{2L}} \tag{2.58}$$

to be large. Hence, we have a large potential $ka\sin^2\theta$ confining the transverse modes near the cavity axis.
The previous observation motivates the paraxial expansion $\sin\theta \approx \theta = \rho/a$, so that we find the following approximated equation

$$-\frac{1}{\rho}\frac{\mathrm{d}}{\mathrm{d}\rho}\rho\frac{\mathrm{d}R}{\mathrm{d}\rho} + \left(\frac{m^2}{\rho^2} + \frac{k^2}{a^2}\rho^2\right)R = q^2 R, \tag{2.59}$$

where $(k/a)^2\rho^2$ is the leading order potential term. Note here, that we have omitted higher order potential terms.
Equation (2.59) is formally equivalent to the radial differential equation for a quantum mechanical **two-dimensional harmonic oscillator** with the transversal eigenvalue q^2. Thus finding eigenmodes in a curved resonator and, therefore, solving the scalar Helmholtz equation in paraxial approximation is formally equivalent to the quantum mechanical two-dimensional harmonic oscillator.
Since the total wave vector is given by $k^2 = q^2 + \gamma^2/a^2$, we already conclude that $k_\parallel = \gamma/a$ must be the absolute value of the axial wave vector. Equation (2.59) is well studied, so we restrain ourselves in specifying its solution.
Second order differential equations generally have two linearly independent solutions, but here, only one of them is of physical relevance, the one which is not singular at $\rho = 0$, i.e.

$$R(q,k,m;\rho) = \mathrm{e}^{-\rho^2 k/2a}\rho^{|m|}{}_1F_1\left(\frac{|m|+1}{2} - \frac{aq^2}{4k}; |m|+1; \frac{k}{a}\rho^2\right), \tag{2.60}$$

where ${}_1F_1(d;b;z)$ is the confluent hypergeometric function

$$ {}_1F_1(d;b;z) = \sum_{n=0}^{\infty} \frac{d^{(n)} z^n}{b^{(n)} n!} \tag{2.61} $$

with the raising factorial $d^{(n)} = d(d+1)\cdots(d+n-1)$. The solution R is regular except for poles at negative integer b and can be normalized if d is zero or a negative integer, so that the infinite series terminates and the leading exponential function guarantees that $R \in L^2$ is a square integrable function. Checking these conditions, we find

$$ b = |m| + 1 \geq 0 \tag{2.62} $$

$$ d = \frac{|m|+1}{2} - \frac{aq^2}{4k} \stackrel{!}{=} -l \qquad l = 0, 1, ... \tag{2.63} $$

which leads to a relation between q, k and m. Recalling that $k = \sqrt{q^2 + \gamma^2/a^2}$ we determine $q(\gamma, |m|)$ from

$$ q^2 = 2\frac{2k}{a}(2l + |m| + 1). \tag{2.64} $$

For negative integers d, the confluent hypergeometric function ${}_1F_1(d;b;z)$ can be rewritten in terms of generalized Laguerre polynomials L_l^m in the form

$$ R(q,k,m,\rho) = \mathrm{e}^{-\rho^2 k/2a} \rho^m L_l^m \left(\frac{k}{a}\rho^2 \right). \tag{2.65} $$

Remarks on the transverse solution

Before we can analyze the eigenvalues depending on γ, m, q in more detail, we have to investigate the longitudinal differential equation (2.54) and the boundary conditions. This will give further constraints and requirements to the separation constant γ. We can already estimate the order of the radial eigenvalue q from Equation (2.63). In leading order k will be proportional to $1/L$. Solving Equation (2.63) for q leads to

$$ q \sim \sqrt{\frac{k}{a}} \sim \frac{1}{L^{3/4}} \tag{2.66} $$

with $a = \sqrt{RL/2}$. For L in the μm regime, we anticipate that the transversal eigenvalues are around 10-100 times smaller than the axial ones which means their contribution to $|\mathbf{k}| = \sqrt{(\gamma/a)^2 + q^2}$ compared with the axial ones are about 100-10000 times smaller because they appear squared in the absolute value of the total wave vector. Due to the fact that the energy of an harmonic oscillator is equi-partite between kinetic and potential energy, there is a way to estimate the order of the transverse spatial extension of the eigenmodes. Omitting the kinetic energy term and taking half of the energy eigenvalue yields

$$ \frac{k^2}{a^2}\rho^2 = \frac{q^2}{2} \quad \Longrightarrow \quad \Delta\rho \approx \sqrt{\frac{(l+1)a}{2k}} \approx \sqrt{(l+1)} 10\ \mu\mathrm{m} \tag{2.67} $$

which is typically much larger than the wavelength. This is well known for the waist of a beam that is not deeply focused, so that its wave fronts have a small curvature. If l is not particularly large, the transverse modes are much narrower than the cavity width, which is of the order a. This is good since conceptual, the cavity is actually open in radial direction. Thus the edge effects should be only a small perturbation, if the modes are localized close to the optical axis. Note also that the quantization of q arises naturally from the fact that the Laguerre functions can be normalized and not from any boundary condition. By approximating the Helmholtz equation we acquired a curvature-induced harmonic confinement which makes the solution to the radial equation automatically normalizable, even in an open cavity. In contrast, a simple plane wave is only normalizable in a finite volume. Figure 2.3 shows the open and closed cavity definition. We can choose the open one, because we do not expect large contributions from afar. On the one hand this micro cavity setup involves large longitudinal wave numbers $1/L$ which implicate huge trapping potentials (2.59). On the other hand, the large radius of curvature does not significantly deform the wave fronts.

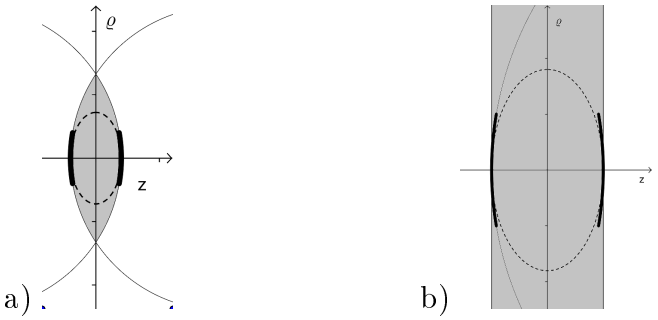

Figure 2.3: Schematic of a) closed and b) open cavity. The gray shaded area indicates the effective cavity volume and the fat black lines represent the mirrors. Due to the curvature of the two mirrors, they would enclose a finite volume. However strong confinement to the optical axis, normalizable mode functions and a large curvature radius permit an open cavity model b).

Higher order corrections to the axial modes

Rewritten in the θ-variable and expanded to the next order, the transverse eigenvalue equation (2.56) yields the following terms in units of the dimensionless variable $x = \theta/\sqrt{ak}$, which is adapted to the harmonic oscillator limit

$$\begin{aligned} &-\frac{1}{x}\frac{\mathrm{d}}{\mathrm{d}x}x\frac{\mathrm{d}R}{\mathrm{d}x}+\frac{m^2}{x}R+x^2R \\ &+\frac{x}{3ka}\frac{\mathrm{d}R}{\mathrm{d}x}+\frac{m^2}{3ka}R-\frac{x^4}{3ka}R=\frac{(qa)^2}{ka}R. \end{aligned} \tag{2.68}$$

The second line can only be treated with perturbation theory, otherwise the negative x^4 potential would make the system unstable. Since the harmonic oscillator in the first line is dimensionless, all quantities related to x are of the order of the dimensionless transverse extent, say $\sqrt{l}$ according to (2.67), we anticipate a correction

of the order $l^2/ka \sim \sqrt{L}$ from the quartic potential. Compared to the eigenvalue $2l = (qa)^2/ka$, this correction is small.

2.4.2 Axial modes

The axial part of the Helmholtz equation (2.54) can be cast into a Schrödinger-like form if we rescale the function $Q(\zeta) = (1+\zeta^2)^{-1/2}P(\zeta)$, which leads to

$$-\frac{\mathrm{d}^2 P}{\mathrm{d}\zeta^2} + V(\zeta)P = (ka)^2 P. \tag{2.69}$$

Here, the potential is

$$V(\zeta) = -\frac{m^2-1}{(1+\zeta^2)^2} + \frac{(qa)^2}{1+\zeta^2}, \tag{2.70}$$

where $\zeta = \sinh\mu$.
Since the coordinate μ is small for our micro resonator system, as it lies between $\pm\mu_0 = \sqrt{L/2R}$, we can treat the potential term as being essentially constant with a maximum value at $\zeta = 0$ of $V_0 = (qa)^2 + 1 - m^2$. The higher order non-constant contributions in ζ may be treated as small perturbations within the semiclassical WKB-theory. First of all we are only interested in propagating solutions, which means that the energy $(ka)^2 - V(\zeta)$ should always be positive. In zeroth order approximation with the notation $(ka)^2 - V_0 = \gamma^2 + m^2 - 1 > 0$, Equation (2.69) is

$$-\frac{\mathrm{d}^2 P(\mu)}{\mathrm{d}\mu^2} = (\gamma^2 + m^2 - 1)P(\mu). \tag{2.71}$$

This is equation is solved by

$$P(\mu) = Ae^{i\sqrt{(\gamma^2+m^2-1)}\,\mu} + Be^{-i\sqrt{(\gamma^2+m^2-1)}\,\mu}. \tag{2.72}$$

The longitudinal eigenvalue problem (2.71) involves also the angular momentum quantum number m, which mixes here with the axial eigenvalue due to the curvature. Solving the Cartesian z coordinate (2.32) for μ, we get the approximate form

$$\mu(\rho, z) \approx \frac{z}{a}\left(1 + \frac{\rho^2}{2a^2} + \frac{z^3}{6a^2}\right), \tag{2.73}$$

where the leading order term z/a is proportional to $\sqrt{L}$ and the next-to-leading order term $z\rho^2/2a^3$ already goes with L. This means once again that the off-axis correction is about three magnitudes smaller than the leading order. So at first sight the function P is a plane wave in z-direction with small corrections. We cannot yet specify another equation for γ, until we construct the full vector solution and finally implement the boundary conditions for the perfect conducting cavity walls (2.24) and (2.25). The general solution P in (2.72) still contains some arbitrary constants A and B which will also be fixed later.

2.4.3 Higher order correction to axial modes

In this section we use the WKB technique to calculate the next order correction term of the axial modes. This semiclassical approach is useful since, we treat the regime where the energy eigenvalue is larger than the given potential $(ka)^2 \gg V_0$. This is the region where the classical motion is possible. If the transverse quantum numbers are sufficiently small, we already know that $(ka)^2 \gg V_0 = (qa)^2 - m^2 + 1$. To apply the WKB method we rewrite Equation (2.69) in the form

$$\epsilon^2 \frac{\mathrm{d}^2 P}{\mathrm{d}\upsilon^2} = \left\{ V(\upsilon) - (ka)^2 \right\} P(\upsilon), \tag{2.74}$$

where we have introduced the rescaled variable $\upsilon = \epsilon\zeta$ with a small dimensionless scaling parameter ϵ. The parameter provides a separation of scales between the kinetic energy term and the potential term. If one thinks in terms of the Schrödinger equation, one finds $\epsilon \sim \hbar$ with appropriate dimensions.
With the ansatz for P

$$P = \exp\left(\Phi(\upsilon)\right), \tag{2.75}$$

Equation (2.74) turns into a differential equation for Φ

$$\frac{\mathrm{d}^2\Phi}{\mathrm{d}\upsilon^2} + \left(\frac{\mathrm{d}\Phi}{\mathrm{d}\upsilon}\right)^2 = \frac{1}{\epsilon^2}\left\{ V(\upsilon) - (ka)^2 \right\}. \tag{2.76}$$

The first derivative of Φ can be split into its real and imaginary part

$$\frac{\mathrm{d}\Phi(\upsilon)}{\mathrm{d}\upsilon} = A(\upsilon) + iB(\upsilon). \tag{2.77}$$

Integrating this equation we obtain immediately the amplitude and the phase of the function P. Applying the ansatz (2.77) to Equation (2.76), we find an equation for the imaginary and one for the real part of P

$$\frac{\mathrm{d}A(\upsilon)}{\mathrm{d}\upsilon} + A(\upsilon)^2 - B(\upsilon)^2 = \frac{1}{\epsilon^2}\left\{ V(\upsilon) - (ka)^2 \right\}, \tag{2.78}$$

$$\frac{\mathrm{d}B(\upsilon)}{\mathrm{d}\upsilon} + 2A(\upsilon)B(\upsilon) = 0. \tag{2.79}$$

Performing an expansion in the small parameter ϵ for A and B

$$A = \frac{1}{\epsilon}\sum_{n=0}^{\infty} \epsilon^n A_n \tag{2.80}$$

$$B = \frac{1}{\epsilon}\sum_{n=0}^{\infty} \epsilon^n B_n, \tag{2.81}$$

and taking the limit $\epsilon \to 0$ the zeroth order of (2.78) and (2.79), yields

$$A_0^2 - B_0^2 = \left\{ V(\upsilon) - (ka)^2 \right\}, \tag{2.82}$$

$$2A_0 B_0 = 0. \tag{2.83}$$

If the amplitude A varies sufficiently slowly as compared to the phase B, we can set $A_0 = 0$ and find an equation for the determination of the WKB phase

$$B_0 = \pm\sqrt{(ka)^2 - V(\upsilon)}. \tag{2.84}$$

This is of course only valid if $(ka)^2 > V$, otherwise we will not find any classical oscillating motion, since the square root becomes imaginary and the total wave function is then exponentially damped, which corresponds to quantum mechanical tunneling.
Now we are able to calculate the WKB phase between the points $\pm\upsilon_0 = \pm\epsilon\zeta_0 = \pm\epsilon\sinh\mu_0$, where the axial mode function vanishes, thus the phase must be a multiple of π. Expanding the potential $V(\zeta)$ from (2.70) in the old variable ζ under the square root (2.84) and then integrating it, yields the phase

$$\int_{-\zeta_0}^{\zeta_0} B(\zeta')d\zeta' \approx 2k_\parallel a\zeta_0 - \frac{((qa)^2 - (2m^2-2))\zeta_0^3}{3k_\parallel a} \stackrel{!}{=} n\pi \tag{2.85}$$

with the definition of the longitudinal wave vector $(ka)_\parallel^2 = (ka)^2 - (qa)^2 + (m^2-1)$ and the axial quantum number n. The first term is the zeroth order potential term we have already found in the previous section. The next curvature correction is then

$$\frac{(qa)^2}{ka}\mu_0^3 \approx 2l\mu_0^3 \approx 2l\frac{1}{(ka)^3}, \tag{2.86}$$

where we used the estimated result for q^2 from (2.66) and the fact that the parameter μ is $\mu_0 = L/2a \sim 1/ka$. In terms of these dimensionless units, the axial next order correction is about a factor $1/(ka)^2$ smaller than the transverse one. Thus the transverse anharmonicity is more relevant, although is scales with $1/ka$.

2.4.4 Scalar solution

The separation scheme of the scalar Helmholtz equation in oblate spheroidal coordinates provided two differential equations. One of them is connected to the transversal modes and the quantum mechanical two-dimensional harmonic oscillator. The other one involved the μ coordinate whose isolines represent the curved mirrors. In summary we obtain a total scalar wave function that solves the Helmholtz equation in the paraxial approximation. It contains an effective two-dimensional oscillator for the radial part and a plane wave for the μ coordinate,

$$u_{\gamma qm}\left(\rho,\phi,\mu(\rho,z),k=\sqrt{\gamma^2/a^2+q^2}\right) = \mathrm{e}^{-\rho^2 k/2a}\rho^m L_l^m\left(\frac{k}{a}\rho^2\right) P\left(\mu(\rho,z)\right)\mathrm{e}^{im\phi}, \tag{2.87}$$

where $k = \sqrt{\gamma^2/a^2+q^2}$. Here, the expression $\gamma/a = k_\parallel$ represents the absolute value of the axial wave vector.
The boundary condition cannot be implied properly, before we have a vector solution at hand. Thus, at present we are not able to give exact eigenvalues for the wave function P. The WKB-phase method in (2.85) for the scalar function P yields the provisional result $k_\parallel = n\pi/L$. The wave vector $k_\parallel$ is the result of the axial modes and it resembles k_z, but they are not necessarily exactly the same.

2.5 Vector solution

The precedent steps, which led to the scalar Helmholtz equation, are only valid under the constraint $\nabla \cdot \mathbf{A} = 0$. Starting with the scalar solution (2.87), we have to construct an adequate vector solution. Fortunately, there exists a representation theorem for the vector Helmholtz equation [20, 10.41] which states:
If u is a solution to the scalar Helmholtz equation

$$\Delta u + |\mathbf{k}|^2 u = 0, \tag{2.88}$$

and $\mathbf{e}$ is a constant vector, then the vectors

$$\mathbf{f} = \nabla \times (\mathbf{e}u) \tag{2.89}$$

$$\mathbf{g} = \frac{1}{|\mathbf{k}|} \nabla \times \mathbf{f} \tag{2.90}$$

are independent solutions of the vector Helmholtz equation

$$\Delta \mathbf{A} + |\mathbf{k}|^2 \mathbf{A} = \mathbf{0} \tag{2.91}$$

involving a solenoidal vector $\mathbf{A}$, i.e. the Coulomb gauge $\nabla \cdot \mathbf{A} = 0$ is fulfilled. The general transverse solution of this equation is a linear combination of both

$$\mathbf{A} = C_1 \nabla \times (\mathbf{e}u) + \frac{C_2}{|\mathbf{k}|} \nabla \times \nabla \times (\mathbf{e}u). \tag{2.92}$$

The general vector solution for the potential $\mathbf{A}$ in (2.92) is a superposition of two orthogonal vector fields corresponding to the different polarizations ϵ_1 and ϵ_1 of the electromagnetic field. Together with the wave vector $\mathbf{k}$, they form an orthogonal basis of the cavity system. In order to distinguish between the two orthogonal vector modes, we introduce

$$\mathbf{A}_{\gamma q m \epsilon_1}(\mathbf{x}) = \nabla \times (\mathbf{e}u_{\gamma q m}) \tag{2.93}$$

$$\mathbf{A}_{\gamma q m \epsilon_2}(\mathbf{x}) = \frac{1}{|\mathbf{k}|} \nabla \times \nabla \times (\mathbf{e}u_{\gamma q m}). \tag{2.94}$$

The indices on the scalar solution $u_{\gamma q m}$ from (2.87) remind us of the yet undetermined wave vectors and quantum numbers. The divergence condition is satisfied trivially due to the identity $\nabla \cdot \nabla \times = 0$. One only has to make a good choice for the constant unit vector $\mathbf{e}$. The theorem holds for constant vectors, because the operation $\nabla \times$ acts only on the scalar solution and not on the unit vector.
In the non-constant vector case the product rule for scalar function times vector results in additional terms to the vector Helmholtz equation. As the normal vector $\mathbf{n}$ is non-constant, we also want to admit non-constant vectors and therefore allow some kind of corrections.
Due to the curl construction it also possible to choose unit vectors of a gradient form without loosing transversality, i.e.

$$\nabla \times [(\nabla f)u] = u \underbrace{\nabla \times \nabla f}_{=0} + \nabla u \times \nabla f = -\nabla f \times \nabla u. \tag{2.95}$$

In the oblate spheroidal coordinates the corresponding unit vectors are not constant as they still depend on the local coordinates. However a good starting point is the μ-surface from (2.73) and its gradient which, by definition, is the normal vector to the $\mu = \text{const}$-surface spanned by the θ and ϕ unit vectors, see Figure 2.4,

$$\mathbf{n} = a\nabla\mu = a\nabla\frac{z}{a}\left(1 + \frac{\rho^2}{2a^2} + \frac{z^3}{6a^2}\right) = \begin{pmatrix} xz/a^2 \\ yz/a^2 \\ 1 + x^2/2a^2 + y^2/2a^2 - z^2/2a^2 \end{pmatrix}. \quad (2.96)$$

Hence, the leading order of normal vector $\mathbf{n}$ points into the Cartesian z-direction. This is illustrated in Figure 2.4.

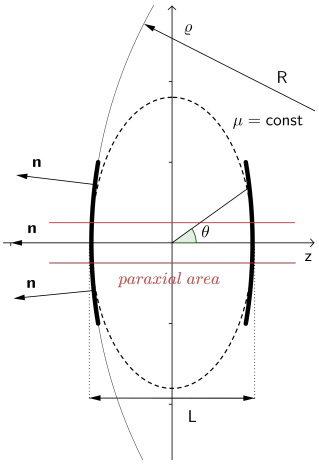

Figure 2.4: Illustration of paraxial area and the non-constant normal vectors $\mathbf{n}(\rho)$. Ellipses of small $\mu = 10^{-3}$ are almost plane. For small polar angle θ the paraxial approximated oblate spheroidal coordinates are close to cylindrical coordinates.

The electric (2.7) and magnetic field (2.8) is

$$\mathbf{E} = i\omega\mathbf{A}_{\gamma qm\epsilon_1}(\mathbf{x}) + i\omega\mathbf{A}_{\gamma qm\epsilon_2}(\mathbf{x}), \quad (2.97)$$

$$\mathbf{H} = \nabla \times \mathbf{A}_{\gamma qm\epsilon_1}(\mathbf{x}) + \nabla \times \mathbf{A}_{\gamma qm\epsilon_2}(\mathbf{x}) \quad (2.98)$$

Imposing the perfect conductor boundary conditions (2.24) and (2.25), the fields have satisfy

$$\mathbf{n} \times \mathbf{E}|_{\partial\Omega_\pm} = i\omega\mathbf{n} \times \nabla \times (\mathbf{n}u_{\gamma qm})|_{\partial\Omega_\pm} + i\frac{\omega}{k}\mathbf{n} \times \nabla \times \nabla \times (\mathbf{n}u_{\gamma qm})|_{\partial\Omega_\pm} \stackrel{!}{=} \mathbf{0}, \quad (2.99)$$

$$\mathbf{n} \cdot \mathbf{H}|_{\partial\Omega_\pm} = \mathbf{n} \cdot \nabla \times \nabla \times (\mathbf{n}u_{\gamma qm})|_{\partial\Omega_\pm} + \frac{1}{k}\mathbf{n} \cdot \nabla \times \nabla \times \nabla \times (\mathbf{n}u_{\gamma qm})|_{\partial\Omega_\pm} \stackrel{!}{=} 0. \quad (2.100)$$

An explicit analysis of these terms yields in leading order the Dirichlet boundary condition for the scalar function $P(\mu)$ of the polarization ϵ_1 and the von Neumann condition for the other vector mode with its respective electric and magnetic field. The performed expansion is the micro cavity expansion for $k_\parallel \gg 1$, $z \ll 1$ and the

plain cavity expansion, which allows to expand in the geometric variable $a \gg 1$. The leading order of these expansions is

$$\mathbf{n} \times \mathbf{E}_{\epsilon_1}|_{\partial\Omega_\pm} \approx (\Psi_3 \mathbf{e}_{\perp \mathbf{3}} + \Psi_4 \mathbf{e}_{\perp \mathbf{4}}) P(\mu)|_{\partial\Omega_\pm} + \mathcal{O}\left(k_\perp^2 \rho^2 \frac{\rho z}{a^2}\right) \stackrel{!}{=} \mathbf{0}, \tag{2.101}$$

$$\mathbf{n} \times \mathbf{E}_{\epsilon_2}|_{\partial\Omega_\pm} \approx (\Psi_1 \mathbf{e}_{\perp \mathbf{1}} + \Psi_2 \mathbf{e}_{\perp \mathbf{2}}) \frac{\partial P}{\partial \mu}|_{\partial\Omega_\pm} + \mathcal{O}\left(k_\perp^2 \rho^2 \frac{\rho z}{a^2}\right) \stackrel{!}{=} \mathbf{0}, \tag{2.102}$$

$$\mathbf{n} \cdot \mathbf{H}_{\epsilon_1}|_{\partial\Omega_\pm} \approx \Psi_5 P(\mu)|_{\partial\Omega_\pm} + \mathcal{O}\left(\frac{k_\perp^2}{k_\parallel^2} \frac{\rho^2}{a^2}\right) \stackrel{!}{=} 0. \tag{2.103}$$

$$\mathbf{n} \cdot \mathbf{H}_{\epsilon_2}|_{\partial\Omega_\pm} = 0. \tag{2.104}$$

Here Ψ_i is an arbitrary scalar function containing the two-dimensional harmonic oscillator and its derivatives. Note that the only boundary dependent variable is the μ coordinate. Therefore the only function we can adjust to the boundary conditions is the function P. It is evident that we can not satisfy both conditions at once. However this is no problem, since we started with a superposition of two distinct linearly independent vector modes. The constructed electromagnetic field is purely transverse, whereas the boundary condition holds only up to a certain order of perturbation theory which is also listed in the equations above. The obtained information is

$$\mathbf{A}_{\gamma q m \epsilon_1}(\mathbf{x}) = \nabla \times (\mathbf{e} u_{\mathrm{D}\gamma q m}), \tag{2.105}$$

$$\mathbf{A}_{\gamma q m \epsilon_2}(\mathbf{x}) = \frac{1}{|\mathbf{k}|} \nabla \times \nabla \times (\mathbf{e} u_{\mathrm{vN}\gamma q m}), \tag{2.106}$$

$$\mathbf{A}_{\gamma q m}(\mathbf{x}) = \mathbf{A}_{\gamma q m \epsilon_1}(\mathbf{x}) + \mathbf{A}_{\gamma q m \epsilon_2}(\mathbf{x}), \tag{2.107}$$

$$\mathbf{A}(\mathbf{x}) = \sum_{\gamma q m} \mathbf{A}_{\gamma q m \epsilon_1}(\mathbf{x}) + \mathbf{A}_{\gamma q m \epsilon_2}(\mathbf{x}). \tag{2.108}$$

The general vector solution is a superposition of Dirichlet and von Neumann modes, where the subscript D or vN indicates the boundary condition for the scalar function P. Thus the vector field to ϵ_1 has a scalar Dirichlet seed function u, whereas the other polarization ϵ_2 requires a von Neumann seed function.

2.6 Boundary values and eigenvalues

The scalar function P from (2.72) contains two undetermined constants A and B. Imposing the Dirichlet boundary condition for mode function we get

$$P(\mu) = A e^{i\sqrt{(\gamma^2+m^2-1)}\,\mu} + B e^{-i\sqrt{(\gamma^2+m^2-1)}\,\mu} \stackrel{!}{=} 0. \tag{2.109}$$

Since P has to be real, this can be either sin or cos. Let us define the Dirichlet seed function with $P = \sin$. By choosing the von Neumann seed function with $P = \cos$, we can consider the two vector modes to the same value of γ, because the von Neumann seed function requires the derivative of P to be zero. By demanding

$$P(\mu_0) = \sin\left(\sqrt{(\gamma^2 + m^2 - 1)}\,\mu_0\right) \stackrel{!}{=} 0 \tag{2.110}$$

we determine the unknown separation constant γ. This yields

$$\sqrt{(\gamma^2 + m^2 - 1)}\sqrt{\frac{L}{2R}} \stackrel{!}{=} n\pi, \tag{2.111}$$

which is solved by

$$\gamma_{nm} = \pm\sqrt{\frac{2(n\pi)^2 R}{L} + 1 - m^2}. \tag{2.112}$$

The newly introduced quantum number n labels the axial modes. This quantum number is a pure result of the chosen boundary conditions. Usually plane waves in an infinite volume have a continuous spectrum. The corresponding eigenvalue of the longitudinal Schrödinger-like Equation (2.71) is then

$$k_{\parallel nm} = \frac{\gamma_{nm}}{a} = \sqrt{\frac{2}{RL}\frac{2(n\pi)^2 R}{L} + \frac{2(1-m^2)}{RL}} \approx \frac{2n\pi}{L}, \tag{2.113}$$

where in the last step we omitted the mixture of the angular momentum quantum number with the axial one, because its contribution only behaves as $1/L$, whereas the first term is proportional to $1/L^2$. Of course, this is only valid, as long as the angular momentum quantum number m is sufficiently small. A careful look on the argument μ and its paraxial expansion (2.73) grants deeper insight in the obtained result

$$\gamma_{nm}\mu = k_\parallel z\left(1 + \frac{\rho^2}{2a^2}\right). \tag{2.114}$$

The leading order term represents the plane wave in a box and the additional contribution arises from the curved mirrors. With the help of the Helmholtz equation in oblate spheroidal coordinates we were able to construct the absolute value of the total wave vector $|\mathbf{k}|$. The final result after evaluating the differential equations and boundary conditions is

$$|\mathbf{k}| = \sqrt{k_\parallel^2 + q^2}, \tag{2.115}$$

$$q^2 = \frac{2k(2l + |m| + 1)}{a}, \tag{2.116}$$

$$k_\parallel^2 = \frac{(2\pi n)^2}{L^2}. \tag{2.117}$$

Unless the radial quantum number l and the angular quantum number m are sufficiently small, we have already shown that $k_\parallel^2 \gg q^2$. Thus we can expand the square root for small transversal eigenvalues and obtain in leading order

$$|\mathbf{k}| \approx k_\parallel + \frac{q^2}{2k_\parallel} = k_\parallel + \frac{(2l + |m| + 1)}{a}. \tag{2.118}$$

Our investigation started with the electromagnetic field in the micro cavity. In free space and homogeneous media, electromagnetic waves or light have a linear dispersion relation in $|\mathbf{k}|$

$$E_{nlm} = \hbar c|\mathbf{k}| \approx \hbar c\left(\frac{2\pi n}{L} + \frac{(2l + |m| + 1)}{a}\right). \tag{2.119}$$

Clearly, ω splits into $\omega_\perp = c/a$ and $\omega_\parallel = 2\pi nc/L$ with a cut-off frequency of $\omega_\parallel = 7\pi c/L = 2\pi 5.1 \cdot 10^{14}$ Hz, where the resonator length L is exactly 3.5 λ. From the experimental side we already know that it is possible to effectively fix the longitudinal quantum number n with an appropriate choice of the dye in the resonator. Therefore considering $k_\parallel$ as frozen out yields the energy

$$E = E_{\text{cut}} + E_{lm}, \tag{2.120}$$

where $E_{\text{cut}} = \hbar c k_{\text{cut}}$ is an energy offset from the fixed longitudinal mode and $E_{lm} = \hbar\omega_\perp(2l + |m| + 1)$ is the energy eigenvalue of the two-dimensional harmonic oscillator with radial quantum number l, azimuthal quantum number m and the typical vacuum fluctuations in D dimensions of $D\hbar\omega_\perp/2 = \hbar\omega$. The steps performed so far were just a reinterpretation of the Helmholtz equation for the electromagnetic field as an eigenvalue equation for massive bosonic particles. Due to the experimental setting, which means $k_\parallel \gg k_\perp$ and the fixed $k_\parallel = k_{\text{cut}}$, we were able to deduce an effective two-dimensional oscillator from the linear dispersion relation of light. In analogy, we will have a look at the dispersion relation of relativistic massive particles

$$E = \sqrt{m^2c^4 + c^2\mathbf{p}^2}, \tag{2.121}$$

which we expand for small velocities $\mathbf{p}^2 \ll c^2$. Rewriting the momentum $\mathbf{p}$ in terms of the wave vector $\mathbf{k}$, we get

$$E = mc^2 + \frac{\hbar^2\mathbf{k}^2}{2m}. \tag{2.122}$$

Comparing Equations (2.118) and (2.119), we interpret

$$mc^2 = \hbar c k_\parallel \tag{2.123}$$

$$\frac{\hbar^2\mathbf{k}^2}{2m} = \frac{\hbar c q^2}{2k_\parallel}. \tag{2.124}$$

Here the effective mass term is identified with the fixed longitudinal wave number $k_\parallel$, then the remaining part of $\mathbf{k}^2$ is the absolute value of an effective two-dimensional transverse wave vector $\mathbf{q}$. Hence, the effective photon mass m_{ph} is

$$m_{\text{ph}} = \frac{\hbar 7\pi}{cL} = 7 \cdot 10^{-36} \text{ kg}. \tag{2.125}$$

Furthermore, the trap frequency of the two-dimensional harmonic oscillator can be specified to

$$\omega = \frac{c}{a} = 2\pi \cdot 4.1 \cdot 10^{10} \text{ Hz}. \tag{2.126}$$

The trap frequency from the boundary value problem is the same as in Ref. [9]. The wave vector $\mathbf{k}$ of the cavity photons possesses a large constant $k_\parallel$-component and the transverse components can be counted in the energy level spacing of the harmonic oscillator $\hbar\omega$. Spectrally resolved, there is a huge gap between two longitudinal modes $\Delta\omega = \omega_{n+1} - \omega_n = 2\pi \cdot 1.5 \cdot 10^{14}$ Hz in comparison to the transverse trap frequency of $\omega = 2\pi \cdot 4.1 \cdot 10^{10}$ Hz, which is about three magnitudes smaller.

2.7 Polarization vectors and ground-state energy

This section is devoted to the vector solution and its properties. The transversality of vector modes is guaranteed by construction. So we have to check how the eigenvalues $|\mathbf{k}|^2$ of the scalar function u_{lm} correspond to the vectorial Helmholtz equation. It is sufficient to investigate the vector potential $\mathbf{A}$ from which the electric and magnetic fields can be obtained. The non-constant unit vector $\mathbf{n}$ will give further contributions to the Helmholtz equation. In order to evaluate the additional expressions, we compare them with $k\mathbf{A}/a$ which represents the order of the transverse modes. There are three important scales in the system $k_\parallel \gg 1$, $a \gg z$ and $z \ll 1$ which determine whether a term is large or negligible. By taking the micro cavity limes $k_\parallel z = \text{const}$ while $z \to 0$ and the plain cavity limes $k/a = \text{const}$ while $a = \sqrt{LR/2} \to \infty$, we can analyze the leading order of the eigenvalue problem

$$-\Delta\mathbf{A} = |\mathbf{k}|^2\mathbf{A}. \tag{2.127}$$

For the ground state $l = m = 0$ the eigenvalue is

$$-\Delta\mathbf{A} = (k_\parallel^2 + 2k_\perp^2)\mathbf{A}. \tag{2.128}$$

The factor two in front of $k_\perp^2$ is due to the non-constant unit vector. Indeed if we only take into account the leading order of the normal vector $\mathbf{n} = \mathbf{e}_z$, we get

$$-\Delta\mathbf{A}^{(\mathbf{0})} = (k_\parallel^2 + k_\perp^2)\mathbf{A}^{(\mathbf{0})}. \tag{2.129}$$

This can be explained by a rotation around the z-axis, where now higher order terms arising from $\mathbf{n}$ lead to an effective tilt off-axis. This shift from the energetically favored $\mathbf{e}_z$ costs a small amount of energy. This effect may be related to the geomtric spin hall effect of light [21].

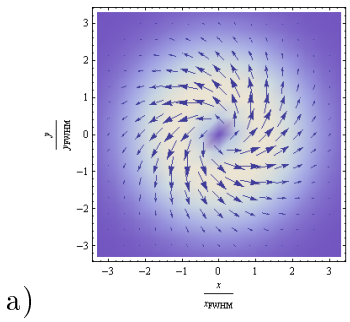

a)

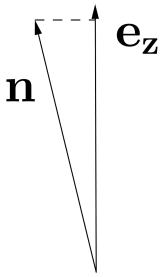

b)

Figure 2.5: a) Vector field $\mathbf{A}_{00}^n$ for $z = 0.25\ L$. b) Schematic of the vectorial tilt induced by the non-constant unit vector $\mathbf{n}$.

Furthermore, we should have a look at the intensity profile $|\mathbf{A}_{00}|^2$. The scalar function u_{00} is proportional to a Gaussian. However, the vectorial ground state is not of a Gaussian form due to its curl

$$\mathbf{A}_{00} = \nabla \times (\mathbf{n}u_{\mathrm{D}00}) + \frac{1}{k_\parallel}\nabla \times \nabla \times (\mathbf{n}u_{\mathrm{vN}00}) \tag{2.130}$$

with the scalar functions

$$u_{\mathrm{D}00} = \mathrm{e}^{-\rho^2 k/2a} \sin\left[k_\parallel z(1+\rho^2/2a^2)\right], \tag{2.131}$$

$$u_{\mathrm{vN}00} = \mathrm{e}^{-\rho^2 k/2a} \cos\left[k_\parallel z(1+\rho^2/2a^2)\right], \tag{2.132}$$

where the derivatives of the Gaussian part lead to expressions $\sim \rho\exp(\rho^2)$ which do not have any contribution to the center intensity. Only the next-to-leading order term arising from the operator $\nabla\times\nabla\times$ gives a negligible contribution $\sim 1/(k_\parallel a)$. This is the case even for a constant unit vector $\mathbf{e}_z$. For further illustration, see Figure 2.6. Thus constructing the vectorial ground state with $\mathbf{n}$ and u_{00} does not produce a proper Gaussian profile. Intuitively expected, it is interesting to ask what is the condition for a purely transverse clean Gauss mode.

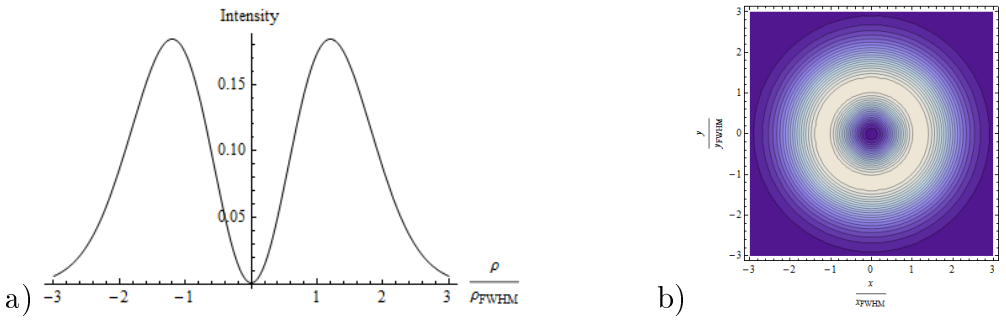

Figure 2.6: a) Ground-state intensity profile in radial direction for $z = 0.25\ L$. b) Contour plot of the intensity profile in xy-plane for $z = 0.25\ L$.

For spherical symmetry, there exists a method from Berestetski, Lifshitz and Pitaevskii, where one directly constructs the longitudinal mode and the transversal modes [22]. The length of the $\mathbf{k}$-vector is fixed and the transversal field is then the tangent space to the radial pointing $\mathbf{k}$-vector. In this case it is impossible to obtain a purely transversal field with total angular momentum $|\mathbf{J}| = 0$. The lowest spherical harmonic Y_{00} is a constant, but within this frame work, it always appears with a derivative. In the textbook of Messiah [23] the multipole expansion chapter provides a general argument, why it is impossible to have a transverse field with $|\mathbf{J}| = 0$: The state $|\mathbf{J}| = 0$ always corresponds to a longitudinal state. We will sketch the proof, because it helps to understand and construct alternative solutions. The total angular momentum is

$$\mathbf{J} = \mathbf{L} + \mathbf{S} \tag{2.133}$$

with $\mathbf{L} = \mathbf{r} \times \mathbf{p}$ as the orbital angular momentum and $\mathbf{S}$ as the spin angular momentum. The action of $\mathbf{L}$ is to rotate the coordinates, while $\mathbf{S}$ rotates the vector components itself. The spin angular momentum in three dimension consists of the three spin matrices S_1, S_2, S_3 defined in (2.136)

$$\mathbf{S} := \begin{pmatrix} S_1 \\ S_2 \\ S_3 \end{pmatrix}. \tag{2.134}$$

The helicity is the projection of the spin onto the momentum $\mathbf{p} = \hbar\mathbf{k}$

$$h = \frac{\mathbf{k}}{k} \cdot \mathbf{S}, \tag{2.135}$$

where we can represent the spin $\mathbf{S}$ as the infinitesimal generator of rotations in three dimensions

$$S_1 = -i \begin{pmatrix} 0 & 0 & 0 \\ 0 & 0 & 1 \\ 0 & -1 & 0 \end{pmatrix}, \qquad S_2 = -i \begin{pmatrix} 0 & 0 & -1 \\ 0 & 0 & 0 \\ 1 & 0 & 0 \end{pmatrix}, \qquad S_3 = -i \begin{pmatrix} 0 & 1 & 0 \\ -1 & 0 & 0 \\ 0 & 0 & 0 \end{pmatrix}. \tag{2.136}$$

Note here that the components S_i satisfy the commutation relation

$$[S_i, S_j] = i\epsilon_{ijk} S_k. \tag{2.137}$$

This is natural, since $\mathbf{J}$ follows the same commutation relations. The definition of the helicity can be identified with the vector operation

$$\mathbf{S} \cdot \mathbf{p} = \nabla \times \tag{2.138}$$

$$(\mathbf{S} \cdot \mathbf{p})^2 - \mathbf{p}^2 = \nabla \nabla \cdot \qquad . \tag{2.139}$$

The transverse fields fulfill $(\mathbf{S} \cdot \mathbf{p})^2 - \mathbf{p}^2 = \mathbf{0}$, while the longitudinal fields satisfy $(\mathbf{S} \cdot \mathbf{p})^2 = \mathbf{0}$. The longitudinal modes can have the helicity $h = 0$ corresponding to $|\mathbf{S}| = 0$. Thus lowest possible total angular momentum for longitudinal modes is $|\mathbf{J}| = 0$ while transverse modes start at least with $|\mathbf{J}| = 1$. The key idea is now to hide the $|\mathbf{J}| = 1$ in the spin component. Therefore it useful to introduce eigenvectors to the helicity operator which are chosen as circularly polarized unit vectors with eigenvalues $+1$ and -1

$$\mathbf{e}_+ = \mathbf{e}_x + i\mathbf{e}_y, \tag{2.140}$$

$$\mathbf{e}_- = \mathbf{e}_x - i\mathbf{e}_y. \tag{2.141}$$

So instead of $\mathbf{n}$, we use $\mathbf{e}_+$ as a unit vector for the construction of the vector modes. The advantage is that the theorem for the vector solution to Helmholtz equation holds now exactly. Considering again the boundary conditions (2.24) and (2.25), we get the following result for the vector mode

$$\mathbf{A}_{00} = \nabla \times (\mathbf{e}_+ u_{\mathrm{vN}00}) + \frac{1}{k_\parallel} \nabla \times \nabla \times (\mathbf{e}_+ u_{\mathrm{D}00}), \tag{2.142}$$

where as usual the subscript D or vN indicates the boundary condition for the scalar function $P(\mu)$. Due to the new unit vector the boundary condition for the scalar solution swapped. This state has of course the lowest energy eigenvalue

$$-\Delta \mathbf{A}_{00} = (k_\parallel^2 + k_\perp^2)\mathbf{A}_{00}. \tag{2.143}$$

Its intensity profile is shown in Figure 2.7.
In principle, the vector solution $\mathbf{A}_{00}^{e_z}$ with $\mathbf{e}_z$, u_{00} and $|\mathbf{J}| = 0$ but also $\mathbf{A}_{00}^{e_+}$ with $\mathbf{e}_+$, u_{00} and $|\mathbf{J}| = 1$ meet all requirements for the solution of the vectorial Helmholtz equation and its boundary conditions in leading order. Since $\mathbf{A}_{00}^{e_z}$ possesses zero angular momentum, the next order expansion of the oblate spheroidal coordinate $\mu(z, \rho)$ reveals a bigger transversal component than the state with $|\mathbf{J}| = 1$. That is why we will prefer the Gaussian ground state for later considerations.

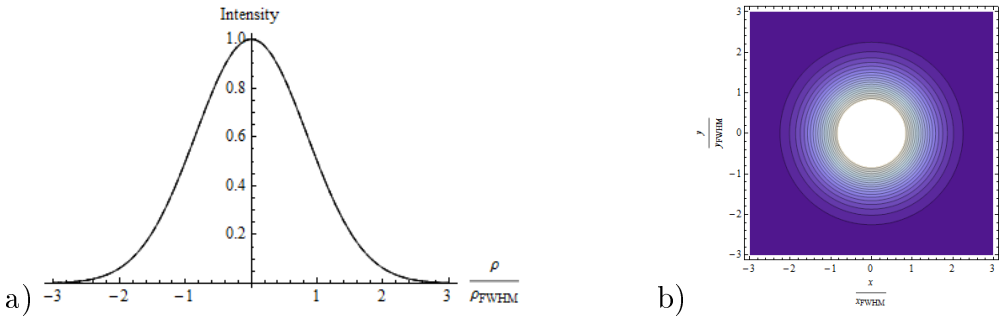

Figure 2.7: a) Ground state intensity profile in radial direction for $z = 0.25\ L$. b) Contour plot of the intensity profile in xy plane for $z = 0.25\ L$.

2.8 Field quantization

We now have constructed suitable vector eigenmodes for the Maxwell equations. In this section, we will take advantage of the eigenmodes and its eigenvalues in order to quantize the electromagnetic field inside the resonator. It is helpful to start with normalized mode functions. Therefore we demand

$$\int_{\mathrm{vol_c}} dA\, \mathbf{A}^*_{lm} \cdot \mathbf{A}_{lm} \stackrel{!}{=} 1, \tag{2.144}$$

where $\mathbf{A}_{lm}$ is the total vector field containing both polarizations (2.107) labeled with the radial quantum number l and the angular momentum quantum number m. The quantization volume is two-dimensional. The integral yields a normalization constant for the mode $\mathbf{A}_{lm}$. The explicit calculation of the normalization can be found in Appendix A. In this section, we just provide the normalized mode function

$$\mathbf{A}_{lm} = \Gamma_{lm}(\nabla \times \mathbf{e}_+ u_{\mathrm{vN}lm}) + \frac{\Gamma_{lm}}{k_{lm}}(\nabla \times \nabla \times \mathbf{e}_+ u_{\mathrm{D}lm}) \tag{2.145}$$

with the normalization constant for each of the vector mode (A.23)

$$\Gamma_{lm} = \sqrt{\left(\frac{k_{lm}}{a}\right)^{m-1} \frac{1}{\pi a^2} \frac{l!}{(l+m)!}}. \tag{2.146}$$

Here k_{lm} is the absolute value of wave vector $\mathbf{k}$ with a fixed longitudinal quantum number n and two parameter-like transverse quantum numbers l, m.
In terms of the vector field $\mathbf{A}$ and its spectral decomposition (2.108), the energy of the electromagnetic field in homogeneous polarized medium is

$$H = \frac{\epsilon_0}{2} N^2 \int_{\mathrm{vol_c}} dA\ \left\{\mathbf{E}^* \cdot \mathbf{E} + c^2 \mathbf{B}^* \cdot \mathbf{B}\right\} \tag{2.147}$$

$$= \frac{\epsilon_0}{2} \int_{\mathrm{vol_c}} dA \sum_{lm} \left\{N_{lm}^2 \omega_{lm}^2 \mathbf{A}^*_{lm} \cdot \mathbf{A}_{lm} + c^2 N_{lm}^2 \nabla \times \mathbf{A}^*_{lm} \cdot \nabla \times \mathbf{A}_{lm}\right\} \tag{2.148}$$

$$= \frac{\epsilon_0}{2} \int_{\mathrm{vol_c}} dA \sum_{lm} \left\{N_{lm}^2 \omega_{lm}^2 \mathbf{A}^*_{lm} \cdot \mathbf{A}_{lm} - c^2 N_{lm}^2 \Delta \mathbf{A}^*_{lm} \cdot \mathbf{A}_{lm}\right\}. \tag{2.149}$$

The occurring factor c is the speed of light in the medium and N normalizes the electromagnetic field to correct dimension. In the last step partial integration, zero divergence and the vanishing fields on boundary were used. This is similar to the calculation of the mode function, where one also has to shift the operator $\nabla\times$, see Appendix (A.3). We replace $-c^2\Delta$ by $c^2|\mathbf{k}_{lm}|^2 = \omega_{lm}^2$ to find

$$H = \epsilon_0 \sum_{lm} N_{lm}^2 \omega_{lm}^2 \left\{ \int_{\mathrm{vol_c}} dA\, \mathbf{A}_{lm}^* \cdot \mathbf{A}_{lm} \right\}. \tag{2.150}$$

The integral over the mode functions is normalized to 1 and can be found in Appendix A. Note here that the two-dimensional volume integral is performed in polar coordinates. The actual advantage of the eigenmodes is that the Hamiltonian becomes simply a sum over eigenvalues

$$H = \epsilon_0 \sum_{lm} N_{lm}^2 \omega_{lm}^2 \stackrel{!}{=} \hbar \sum_{lm} \omega_{lm}. \tag{2.151}$$

This finally fixes the normalization constant to

$$N_{lm} = \sqrt{\frac{\hbar}{c k_{lm} \epsilon_0}}. \tag{2.152}$$

Knowing the mode function, we perform the canonical field quantization. Therefore, we introduce the creation and annihilation operators, which obey the canonical commutation relation

$$[\widehat{a}_{lm\epsilon}, \widehat{a}_{jk\epsilon'}] = \left[\widehat{a}_{lm\epsilon}^\dagger, \widehat{a}_{jk\epsilon'}^\dagger\right] = 0 \qquad \left[\widehat{a}_{lm\epsilon}, \widehat{a}_{jk\epsilon'}^\dagger\right] = \delta_{lj}\delta_{mk}\delta_{\epsilon\epsilon'}, \tag{2.153}$$

where the commutator is $[\widehat{A}, \widehat{B}] = \widehat{A}\widehat{B} - \widehat{B}\widehat{A}$ and the subscript ϵ denotes the respective polarization. Applying the corresponding operators on the Fock space yields

$$\widehat{a}_{lm\epsilon} |\mathbf{n}_\epsilon\rangle = \sqrt{n_{lm}}\, |n_{00}, \ldots, n_{lm} - 1, \ldots\rangle_\epsilon \tag{2.154}$$

$$\widehat{a}_{lm\epsilon}^\dagger |\mathbf{n}_\epsilon\rangle = \sqrt{n_{lm} + 1}\, |n_{00}, \ldots, n_{lm} + 1, \ldots\rangle_\epsilon . \tag{2.155}$$

Note here that the distinct polarizations have distinct operators. The ket vector $|\mathbf{n}_\epsilon\rangle$ is the number base counting cavity photons with the quantum numbers l, m and polarization ϵ. With the help of these operators acting on the Fock space, we define the operator-valued vector potential $\widehat{\mathbf{A}}$

$$\begin{aligned} \widehat{\mathbf{A}}(\mathbf{x}) &= \sum_{lm} \mathbf{A}_{lm\epsilon_1}(\mathbf{x}) \widehat{a}_{lm\epsilon_1} + \mathbf{A}_{lm\epsilon_2}(\mathbf{x}) \widehat{a}_{lm\epsilon_2}, \\ \widehat{\mathbf{A}}^\dagger(\mathbf{x}) &= \sum_{lm} \mathbf{A}_{lm\epsilon_1}^*(\mathbf{x}) \widehat{a}_{lm\epsilon_1}^\dagger + \mathbf{A}_{lm\epsilon_2}^*(\mathbf{x}) \widehat{a}_{lm\epsilon_2}^\dagger. \end{aligned} \tag{2.156}$$

Since the double sum over the quantum numbers l and m appears frequently, we define the short hand notation

$$\sum_{lm} = \sum_{l=0}^{\infty} \sum_{m=-\infty}^{\infty}. \tag{2.157}$$

These field operators have to obey the canonical commutation relation

$$\left[\widehat{A}_i^\dagger(\mathbf{x}), \widehat{A}_j(\mathbf{x}')\right] = \delta_\perp^{(2)}(\mathbf{x}-\mathbf{x}')\delta_{ij} \tag{2.158}$$

$$\left[\widehat{A}_i(\mathbf{x}), \widehat{A}_j(\mathbf{x}')\right] = \left[\widehat{A}_i^\dagger(\mathbf{x}), \widehat{A}_j^\dagger(\mathbf{x}')\right] = 0 \tag{2.159}$$

where $\delta_\perp^{(2)}(\mathbf{x}-\mathbf{x}')\delta_{ij}$ is the transverse delta function in two dimensions with modulation in z-direction. The calculation of the transverse delta function is presented in Appendix B. We are automatically in the transverse subspace due to the Coulomb gauge (2.15). In fact one should evalutate commutator of the canonical conjugate fields $\mathbf{A}$ and $\mathbf{\Pi} = \dot{\mathbf{A}}$ arising from the Lagrangian of the elecromagnetic field $\left[\widehat{A}_i^\dagger, \widehat{\Pi}_j\right] = i\hbar\delta_\perp(\mathbf{x}-\mathbf{x}')\delta_{ij}$, but this exactly corresponds to (2.158) and (2.159).
The vector character of these operators is carried by the orthonormalized mode functions $\mathbf{A}_{lm\epsilon_i}$. The subscript ϵ_i indicates the two different polarizations arising from the two different vector modes proportional to $\nabla\times$ and $\nabla\times\nabla\times$. Replacing the vector modes by the operators (2.156), the electromagnetic field Hamiltonian in Equation (2.150) is equivalent to

$$\begin{aligned}\widehat{H} &= \hbar\sum_{lm}\omega_{lm}\left\{\int_{\mathrm{vol_c}} dA\left(\mathbf{A}^*_{lm\epsilon_1}\cdot\mathbf{A}_{lm\epsilon_1}\widehat{a}^\dagger_{lm\epsilon_1}\widehat{a}_{lm\epsilon_1} + \mathbf{A}^*_{lm\epsilon_2}\cdot\mathbf{A}_{lm\epsilon_2}\widehat{a}^\dagger_{lm\epsilon_2}\widehat{a}_{lm\epsilon_2}\right)\right\} \\ &= \hbar\sum_{lm}\omega_{lm}\left\{\widehat{a}^\dagger_{lm\epsilon_1}\widehat{a}_{lm\epsilon_1} + \widehat{a}^\dagger_{lm\epsilon_2}\widehat{a}_{lm\epsilon_2}\right\},\end{aligned} \tag{2.160}$$

where we have explicitly used the orthonormality of the mode function $\mathbf{A}_{lm\epsilon_1}$ and $\mathbf{A}_{lm\epsilon_2}$. The quantized cavity photon field can be described by a set of harmonic oscillators. Equivalently, massive bosons in a harmonic trap can be described with Equation (2.160). This will be shown in the next section.

Chapter 3

Calculating the BEC

The normal mode expansion (2.156) of the cavity photon field is an ideal starting point for investigating the possible occurrence of Bose-Einstein condensation. In order to determine the critical particle number of the two-dimensional phase transition, we need to introduce some methods of thermodynamics and quantum many-body theory.
From classical electrodynamics, we could already obtain the effective photon mass and the effective two-dimensional trap frequency. The quantization of the electromagnetic field with normal modes always yields continuous distributed harmonic oscillators in space. In this sense, it is natural to reinterpret this field as a many-body ensemble of trapped bosons. The most important thing is, that this point of view holds in the special case of the cavity photon field. Here, the various photons with their distinct wave vectors $\mathbf{k}$ were given a huge non-vanishing $k_{\parallel}$-component. Even the reinterpretation of the three-dimensional Helmholtz equation as a two-dimensional Schrödinger equation would fail, if we did not have this extraordinary cavity-dye setup, because the rest mass term in the Schrödinger equation is then just zero. However, in the setting we are analyzing, it is possible to consistently map cavity photons onto an ensemble of massive trapped bosons. In the previous section we introduced the Fock space for the photons (2.155). This is now the same space to efficiently describe the massive trapped bosons.

3.1 Ultra cold versus room temperature Bose gas

The determination of the phase boundary between the gas and the BEC phase is of fundamental interest. In the case of ultra cold Bose gases, one considers the critical temperature $T_{\mathrm{crit}}(N)$ as a function of the particle number N. However, in the present experimental setting the temperature T is given-namely the room temperature $T = 300\ K$-and the unknown critical particle number $N_{\mathrm{crit}}(T)$ for the onset of Bose-Einstein condensation has to be calculated. The comfort of this situation is that we do not have to extract the temperature by inverting the equation of state for the particle number. Another interesting fact to note is that the ratio of the trap energy versus the thermal energy $\beta\hbar\omega \approx 1/150$ is roughly the same as for the atomic BEC experiments. The harmonic oscillator energy $\hbar\omega$ for the cavity photons and the thermal energy $k_{\mathrm{B}}T$ at room temperature ~ 300 K are both about

a factor 10^9 larger than for the usual atomic BEC, with typical trap frequencies in the ~ 100 Hz regime and ultra cold temperatures of 10^{-7} K. In three dimensions, the semiclassical treatment of the Bose gas in a trap yields a sufficient description. However, in lower dimensions the interacting Bose gas in a semiclassical treatment is problematic, because it involves some polylogarithmic functions which have to be careful approximated. The present work circumvents this difficulties by calculating every quantity quantum mechanically, meaning, we evaluate the occurring discrete sums without any semiclassical approximation.

3.2 Density matrix

Expectation values of general states in quantum many-body theory can be calculated with the help of the density matrix $\widehat{\rho}$

$$\left\langle \widehat{O} \right\rangle = \mathrm{tr}\left\{ \widehat{\rho}\,\widehat{O} \right\}, \tag{3.1}$$

where $\widehat{O}$ is any observable of the system. The density matrix $\widehat{\rho}$ is a positive definite hermitian trace class operator with $\mathrm{tr}(\widehat{\rho}) = 1$. Depending on the quantum state one considers different forms of the underlying density matrix. We examine a thermal ensemble of bosons, because the key ingredient is the thermalization of photons in the transverse modes. This corresponds to

$$\widehat{\rho} = \frac{1}{Z} \mathrm{e}^{-\beta \widehat{H}} \tag{3.2}$$

with the inverse temperature $\beta = 1/k_{\mathrm{B}}T$ and the grand-canonical partition function Z defined as

$$Z = \mathrm{tr}\left\{ \mathrm{e}^{-\beta \widehat{H}} \right\}. \tag{3.3}$$

All relevant thermodynamic properties can be deduced from the effective action

$$\Gamma = -\frac{1}{\beta} \ln Z. \tag{3.4}$$

The introduced effective action Γ of course depends on the order parameters ψ, ψ^* of the system. The extremalization of the effective action with respect to the corresponding order parameter

$$\left. \frac{\delta \Gamma[\psi^*(\mathbf{x}), \psi(\mathbf{x})]}{\delta \psi^*(\mathbf{x})} \right|_{(\psi^*_{\mathrm{ext}}(\mathbf{x}), \psi_{\mathrm{ext}}(\mathbf{x}))} \stackrel{!}{=} 0 \tag{3.5}$$

yields the extremal order parameters $\psi^*_{\mathrm{ext}}(\mathbf{x}), \psi_{\mathrm{ext}}(\mathbf{x})$, which are physically realized. The effective action with extremal physical fields is then identical to the free energy [24] of the system,

$$F = \Gamma[\psi^*_{\mathrm{ext}}(\mathbf{x}), \psi_{\mathrm{ext}}(\mathbf{x})]. \tag{3.6}$$

In order to perform further investigations, it is required to have a closer look at how to calculate the partition function or the effective action, respectively.

3.3 Effective action

Calculating the grand-canonical partition function or the effective action respectively requires the system Hamiltonian in second quantization. Before we specify the full field Hamiltonian, we discuss a possible interaction. In the case of electromagnetic fields additional interaction terms can be implemented by modeling the dye solution as a non-linear material, e.g. with the Kerr-effect

$$D_i = \epsilon_0 E_i + P_i = \epsilon_0 E_i + \epsilon_0 \sum_j \chi_i^j E_j + \epsilon_0 \sum_{jkl} \chi_i^{jkl} E_j E_k E_l. \tag{3.7}$$

Here, χ_i^j denotes the components of the linear susceptibility and χ_i^{jkl} are the elements of the non-linear susceptibility. The Kerr-effect is an effect of third order in the electromagnetic fields which is especially strong in certain liquids and crystals. This interaction leads to effects like self-focussing and self-phase modulation.
Assuming that the dye solution is an isotropic medium and the resulting polarization is parallel to the electric field, the linear susceptibility $\chi_i^j = \chi$ has identical components for all three directions. Due to the isotropy and for further simplification, the non-linear susceptibility has identical entries $\chi_i^{jkl} = \chi^{(2)}$. With these assumptions, Equation (3.7) can be simplified to

$$\mathbf{D} \approx \epsilon_0 (1 + \chi + \chi^{(2)} |\mathbf{E}|^2) \mathbf{E}, \tag{3.8}$$

where the non-linear polarisation is further reduced to the field intensity times the electric field. The definition of the polarization (3.8) does not fix the order of the electromagnetic fields and their conjugate. We only know that the conjugate non-linear polarization has to involve two conjugate fields and a non-conjugate one. Furthermore there is no explicit scalar product for the fields in the brackets since it depends on how to simplify the non-linear susceptibility tensor. Thus the alternative introduction for the non-linear polarization is

$$\mathbf{D} = \epsilon_0 (1 + \chi) \mathbf{E} + \epsilon_0 \chi^{(2)} \mathbf{E}^* (\mathbf{E} \cdot \mathbf{E}), \tag{3.9}$$

$$\mathbf{D}^* = \epsilon_0 (1 + \chi) \mathbf{E}^* + \epsilon_0 \chi^{(2)} (\mathbf{E}^* \cdot \mathbf{E}^*) \mathbf{E}. \tag{3.10}$$

Defining the fields in this way directly leads to a normal ordered Hamiltonian, which is later advantageous for the field quantization. The expression in the brackets (3.8) is the refraction index squared. Expanding for $\chi^{(2)} \ll 1$, the Kerr non-linearity directly leads to an intensity dependent refraction index

$$n = (1 + \chi + \chi^{(2)} |\mathbf{E}|^2)^{\frac{1}{2}} \approx n_0 + \frac{1}{2} \chi^{(2)} |\mathbf{E}|^2 \approx n_0 + n_2 I \tag{3.11}$$

with the linear refraction index of the medium $n_0 = \sqrt{1 + \chi}$ and the non-linear refraction index $n_2 = \chi^{(2)} / [2(1 + \chi)]$. Taking into account the non-linearity, the Hamiltonian for the electromagnetic field H_{em} becomes

$$\begin{aligned} H_{\text{em}} =& \frac{\epsilon_0}{2} N^2 \int_{\text{vol}_c} dA \, \left\{ \mathbf{E}^* \cdot \mathbf{E} + c^2 \mathbf{B}^* \cdot \mathbf{B} \right\} \\ &+ \epsilon_0 n_2 N^4 \int_{\text{vol}_c} dA \, \left\{ \mathbf{E}^* \cdot \mathbf{E}^* \mathbf{E} \cdot \mathbf{E} \right\} + \mathcal{O}(n_2^2). \end{aligned} \tag{3.12}$$

According to Equation (2.147), the first line already contains the linear polarization and the second line involves the non-linear part. Under the condition $n_2 \ll 1$ the occurring higher order interaction terms are omitted. The fields are arranged in normal order and we consider (3.12) as the starting Hamiltonian for the quantization. For the ongoing calculation we reexpress the Hamiltonian in terms of the vector potential (2.7), (2.8). Then we use the normalization constant N from (2.152) and the definition of $\mathbf{A}$ (2.108) to find

$$\begin{aligned} H_{\text{em}} = &\int_{\text{vol}_c} dA \sum_{jk} \sum_{lm} \hbar \sqrt{\omega_{jk}\omega_{lm}} \mathbf{A}_{jk}^* \cdot \mathbf{A}_{lm} \\ &+ \frac{\tilde{g}}{2} n_2 \int_{\text{vol}_c} dA \left\{ \sum_{jk} \sum_{lm} \mathbf{A}_{jk}^* \cdot \mathbf{A}_{lm}^* \right\} \left\{ \sum_{op} \sum_{rs} \mathbf{A}_{op} \cdot \mathbf{A}_{rs} \right\}. \end{aligned} \tag{3.13}$$

Taking into account relation $\mathbf{E} = ic|\mathbf{k}|\mathbf{A}$ from (2.7) and the leading order of $|\mathbf{k}| = k_\parallel$ from (2.119), yields an interaction parameter $\tilde{g} = \hbar^2 c^2 k_\parallel^2 / \epsilon_0$. According to (2.159) we introduce the vector-valued field operators $\widehat{\mathbf{A}}$ and $\widehat{\mathbf{A}}^\dagger$ and realize that the Hamiltonian (3.13) has the quantized form

$$\widehat{H}_{\text{em}} = \int_{\text{vol}_c} dA\, \widehat{\mathbf{A}}^\dagger(\mathbf{x}) h_0 \widehat{\mathbf{A}}(\mathbf{x}) + \frac{\tilde{g}}{2} n_2 \int_{\text{vol}_c} dA\, \widehat{\mathbf{A}}^\dagger(\mathbf{x}) \widehat{\mathbf{A}}^\dagger(\mathbf{x}) \widehat{\mathbf{A}}(\mathbf{x}) \widehat{\mathbf{A}}(\mathbf{x}) \tag{3.14}$$

where we used the orthogonality of the Fock base and replaced the eigenvalue $\hbar\omega_{lm}$ with the corresponding two dimensional single-particle Hamiltonian h_0

$$h_0(\mathbf{x}) u_{lm} = \hbar \omega_{lm} u_{lm}. \tag{3.15}$$

Here u_{lm} is the scalar seed function (2.87) for vector field $\mathbf{A}_{lm}$. The derivation of the paraxial Helmholtz equation showed that it suffices to describe the cavity photon gas as a two-dimensional harmonic oscillator plus the kinetic energy term the z-direction

$$h_0(\mathbf{x}) = \frac{\mathbf{p}^2}{2m_{\text{ph}}} + V(\mathbf{x}) = -\frac{\hbar^2 \Delta}{2m_{\text{ph}}} + \frac{m_{\text{ph}}}{2} \omega^2 \rho^2. \tag{3.16}$$

Plugging (3.16) into (3.14) we find

$$\begin{aligned} \widehat{H}_{\text{em}} = &\int_{\text{vol}_c} dA\, \widehat{\mathbf{A}}^\dagger(\mathbf{x}) \left[-\frac{\hbar^2 \Delta}{2m_{\text{ph}}} + V(\mathbf{x}) - \mu' \right] \widehat{\mathbf{A}}(\mathbf{x}) \\ &+ \frac{\tilde{g}}{2} n_2 \int_{\text{vol}_c} dA\, \widehat{\mathbf{A}}^\dagger(\mathbf{x}) \widehat{\mathbf{A}}^\dagger(\mathbf{x}) \widehat{\mathbf{A}}(\mathbf{x}) \widehat{\mathbf{A}}(\mathbf{x}) \end{aligned} \tag{3.17}$$

where μ' is the chemical potential. In the last steps we have linked the electromagnetic Hamiltonian with interaction term to a second quantized massive trapped bosonic Hamiltonian. The expression arising from the Kerr non-linearity provides the interaction, while the harmonic oscillator expression corresponds to the non-interacting field Hamiltonian. Introducing the bosonic field operators $\widehat{\psi}^\dagger, \widehat{\psi}$, the

quantization of the electromagnetic field (2.156) already yields the mode expansion for our effective massive boson field

$$\widehat{\psi}(\mathbf{x}) = \widehat{\mathbf{A}}(\mathbf{x}) = \sum_{lm} \mathbf{A}_{lm\epsilon_1}(\mathbf{x})\widehat{a}_{lm\epsilon_1} + \mathbf{A}_{lm\epsilon_2}(\mathbf{x})\widehat{a}_{lm\epsilon_2} \tag{3.18}$$

$$\widehat{\psi}^\dagger(\mathbf{x}) = \widehat{\mathbf{A}}^\dagger(\mathbf{x}) = \sum_{lm} \mathbf{A}^*_{lm\epsilon_1}(\mathbf{x})\widehat{a}^\dagger_{lm\epsilon_1} + \mathbf{A}^*_{lm\epsilon_2}(\mathbf{x})\widehat{a}^\dagger_{lm\epsilon_2}. \tag{3.19}$$

The respective canonical commutation relations are

$$\left[\widehat{\psi}^\dagger_i(\mathbf{x}), \widehat{\psi}_j(\mathbf{x}')\right] = \delta^{(2)}_\perp(\mathbf{x} - \mathbf{x}')\delta_{ij}, \tag{3.20}$$

$$\left[\widehat{\psi}_i(\mathbf{x}), \widehat{\psi}_j(\mathbf{x}')\right] = \left[\widehat{\psi}^\dagger_i(\mathbf{x}), \widehat{\psi}^\dagger_j(\mathbf{x}')\right] = 0. \tag{3.21}$$

Thus, the derivation of the effective two-dimensional massive Hamiltonian is just an reinterpretation of the field operators. These field operators inherit the vector character from the mode functions $\mathbf{A}_{lm\epsilon_i}$. Redefining the chemical potential, we compensate the constant energy offset arising from fixed longitudinal wave vector $k_\parallel$

$$\mu = \mu' + \frac{\hbar^2 k_\parallel^2}{2m}, \tag{3.22}$$

and get the second quantized Hamiltonian for an effective massive two-dimensional harmonic oscillator

$$\begin{aligned}\widehat{H} = &\int_{\mathrm{vol_c}} dA\, \widehat{\psi}^\dagger(\mathbf{x}) \left[-\frac{\hbar^2\Delta}{2m_{\mathrm{ph}}} + V(\mathbf{x}) - \mu\right] \widehat{\psi}(\mathbf{x}) \\ &+ \frac{\tilde{g}}{2} n_2 \int_{\mathrm{vol_c}} dA\, \widehat{\psi}^\dagger(\mathbf{x})\widehat{\psi}^\dagger(\mathbf{x})\widehat{\psi}(\mathbf{x})\widehat{\psi}(\mathbf{x}).\end{aligned} \tag{3.23}$$

The two-dimensional Hamiltonian (3.23) is consequently an effective two-dimensional harmonic oscillator with a modulation in ζ-direction, which is mainly the z-axis, see Figure 3.1. The spatial intensity modulation is the relict from the translation of

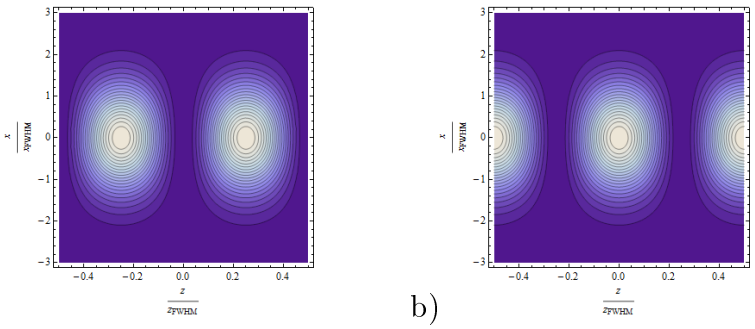

a) b)

Figure 3.1: Intensity profile in xz-plane for the ground-state of Dirichlet modes a) and von Neumann modes b). The z-axis is horizontal and the x-axis vertical.

three-dimensional Helmholtz equation into a two-dimensional Hamiltonian.

3.3.1 Condensate and fluctuations

Before we determine the phase transition, it is useful to investigate the order parameter for Bose-Einstein condensation, and the dependency of the partition function on the order parameter. This section provides tools and methods for the evaluation of the partition function.
If the ground state has a macroscopic occupation, we can separate the field operators into a condensate term $lm = 00$ and the non-condensate excited components $lm \neq 00$

$$\widehat{\psi}(\mathbf{x}) = \psi_{00}(\mathbf{x}) + \delta\widehat{\psi}(\mathbf{x}) \tag{3.24}$$

$$\widehat{\psi}^\dagger(\mathbf{x}) = \psi^*_{00}(\mathbf{x}) + \delta\widehat{\psi}^\dagger(\mathbf{x}) \tag{3.25}$$

with the condensate wave function ψ_{00} and the fluctuation $\delta\widehat{\psi}$ defined as

$$\psi_{00}(\mathbf{x}) = \sum_\epsilon \mathbf{A}_{00\epsilon}(\mathbf{x}) a_{00\epsilon} \qquad \delta\widehat{\psi}(\mathbf{x}) = \sum_{lm\neq 00,\epsilon} \mathbf{A}_{lm\epsilon}(\mathbf{x})\widehat{a}_{lm\epsilon} \tag{3.26}$$

$$\psi^*_{00}(\mathbf{x}) = \sum_\epsilon \mathbf{A}^*_{00\epsilon}(\mathbf{x}) a^*_{00\epsilon} \qquad \delta\widehat{\psi}^\dagger(\mathbf{x}) = \sum_{lm\neq 00,\epsilon} \mathbf{A}^*_{lm\epsilon}(\mathbf{x})\widehat{a}^\dagger_{lm\epsilon}. \tag{3.27}$$

The condensate function has two different contributions arising from the polarizations. The expression of the field operators (3.24), (3.25) implicitly introduced the Bogoliubov approximation, in which the operators $\widehat{a}_{00\epsilon}$ and $\widehat{a}^\dagger_{00\epsilon}$ are replaced by the complex numbers $a_{00\epsilon} = \sqrt{N_{00\epsilon}}$ and $a^*_{00\epsilon} = \sqrt{N^*_{00\epsilon}}$ such that $\langle \widehat{a}^\dagger_{00\epsilon}\widehat{a}_{00\epsilon}\rangle = N_{00\epsilon}$ yields the average occupation number of the ground state with the respective polarization ϵ. Thus the total photon number for the degenerate ground state is $N_{00} = N_{00\epsilon_1} + N_{00\epsilon_2}$. Along the lines of Yamamoto [25], we will describe the phase transition due to spontaneous symmetry breaking as follows. The definition of the field operators (3.24), (3.25) already implies that the expectation value of $\langle\widehat{\psi}(\mathbf{x})\rangle$ is non-zero. This would not be possible if the condensate state is in a Fock state $|N_0\rangle$. The classical wave function ψ_{00}, which is in the present case the sum of vector potentials $A_{00\epsilon_1} + A_{00\epsilon_2}$, plays the role of the order parameter in the cavity system and determines the condensate density $n_{00}(\mathbf{x}) = |\psi_{00}|^2$. While the ground state particle number N_{00} fixes the amplitude of the wave function or the vector potential respectively, the phase of the order parameter e.g. $e^{i\alpha}$ is left completely arbitrary. For a BEC phase transition, the condensate system spontaneously chooses a particular phase α. From a quantum field theoretical point of view this spontaneous breaking of gauge symmetry is taken into account by saying that the condensate state is in or close to a coherent state [26],

$$\widehat{a}_{00\epsilon}\,|\alpha_\epsilon\rangle = \alpha_\epsilon\,|\alpha_\epsilon\rangle \tag{3.28}$$

with $|\alpha_\epsilon|^2 = N_{00\epsilon}$. Expressed in the Fock base the coherent state is

$$|\alpha\rangle = \mathrm{e}^{-\frac{|\alpha|^2}{2}} \sum_{n=0}^{\infty} \frac{\alpha^n}{\sqrt{n!}}|n\rangle. \tag{3.29}$$

The Bogoliubov decomposition allows an explicit treatment of the order parameter $\psi_{00}(\mathbf{x})$.

3.3.2 Two-dimensional phase transitions

As mentioned the order parameter has $U(1)$ symmetry. The phase transition to the BEC phase is described by spontaneous symmetry breaking. However we will discuss here an another kind phase transition, namely the Berezinskii–Kosterlitz–Thouless transition (BKT transition) [27, 28]. This is a phase transition of infinite order, while the classical BEC theory is described by a phase transition of second order. In the BKT case one especially considers the phase factor of the order parameter, whose gradient yields a velocity field. The occurrence of vortices and the periodic structure of the phase lead to a correlation in two dimensions whose long-range order decays algebraically. Usually, an exponential behavior is expected. The explicit check whether or not the BKT applies here, might be an additional subject for this particular system but not for the present thesis.
Plugging the Bogoliubov decomposition (3.24) and (3.25) into the second quantized Hamiltonian $\widehat{H}$ (3.23) with the rescaled μ (3.22), we find

$$\begin{aligned}\widehat{H}_0 = \int dA \psi_{00}^*(\mathbf{x}) \left[h_0(\mathbf{x}) - \mu\right] \psi_{00}(\mathbf{x}) + \delta\widehat{\psi}^\dagger(\mathbf{x}) \left[h_0(\mathbf{x}) - \mu\right] \psi_{00}(\mathbf{x}) \\ + \psi_{00}^*(\mathbf{x}) \left[h_0(\mathbf{x}) - \mu\right] \delta\widehat{\psi}(\mathbf{x}) + \delta\widehat{\psi}^\dagger(\mathbf{x}) \left[h_0(\mathbf{x}) - \mu\right] \delta\widehat{\psi}(\mathbf{x}).\end{aligned} \tag{3.30}$$

which, due to the normal mode expansion (3.18), (3.19) reduces to

$$\widehat{H}_0 = \int \psi_{00}^*(\mathbf{x}) \left[h_0(\mathbf{x}) - \mu\right] \psi_{00}(\mathbf{x}) + \int \delta\widehat{\psi}^\dagger(\mathbf{x}) \left[h_0(\mathbf{x}) - \mu\right] \delta\widehat{\psi}(\mathbf{x}). \tag{3.31}$$

The orthogonality of the vector modes $\mathbf{A}_{lm\epsilon}$ cannot be used in the interacting case, because the product of four mode functions has to be evaluated. Thus the decomposed interacting part in normal order is

$$\begin{aligned}\widehat{H}_{\text{int}} = \frac{g}{2} \int \left|\psi_{00}(\mathbf{x})\right|^4 + 2\left|\psi_{00}(\mathbf{x})\right|^2 \psi_{00}^*(\mathbf{x}) \delta\widehat{\psi}(\mathbf{x}) + (\psi_{00}^*(\mathbf{x}))^2 \delta\widehat{\psi}(\mathbf{x}) \delta\widehat{\psi}(\mathbf{x}) \\ + 2\left|\psi_{00}(\mathbf{x})\right|^2 \psi_{00}(\mathbf{x}) \delta\widehat{\psi}^\dagger(\mathbf{x}) + 4\left|\psi_{00}(\mathbf{x})\right|^2 \delta\widehat{\psi}^\dagger(\mathbf{x}) \delta\widehat{\psi}(\mathbf{x}) \\ + 2\psi_{00}^*(\mathbf{x}) \delta\widehat{\psi}^\dagger(\mathbf{x}) \delta\widehat{\psi}(\mathbf{x}) \delta\widehat{\psi}(\mathbf{x}) + (\psi_{00}(\mathbf{x}))^2 \delta\widehat{\psi}^\dagger(\mathbf{x}) \delta\widehat{\psi}^\dagger(\mathbf{x}) \\ + 2\psi_{00}(\mathbf{x}) \delta\widehat{\psi}^\dagger(\mathbf{x}) \delta\widehat{\psi}^\dagger(\mathbf{x}) \delta\widehat{\psi}(\mathbf{x}) + \delta\widehat{\psi}^\dagger(\mathbf{x}) \delta\widehat{\psi}^\dagger(\mathbf{x}) \delta\widehat{\psi}(\mathbf{x}) \delta\widehat{\psi}(\mathbf{x}).\end{aligned} \tag{3.32}$$

Here the interaction parameter g is defined as

$$g = \tilde{g} n_2. \tag{3.33}$$

The precise value of g depends on the material, namely on the non-linear refraction index n_2 which is assumed to be small. In a later section we will give the its explicit number. All terms of zeroth order in the fluctuation operators $\delta\widehat{\psi}, \delta\widehat{\psi}^\dagger$ represent the usual Gross-Pitaevskii theory. The terms proportional to $\delta\widehat{\psi}^\dagger \delta\widehat{\psi}$ are the Hartree and the Fock contributions. Expressions containing $\delta\widehat{\psi}^\dagger \delta\widehat{\psi}^\dagger$ and $\delta\widehat{\psi}\delta\widehat{\psi}$ correspond to the Bogoliubov channel. The higher order fluctuation terms can be considered as corrections to the mentioned theories.

For the calculation of the effective action (3.4) we need to evaluate the exponential of (3.30), (3.32)

$$\Gamma = -\frac{1}{\beta} \ln \left\{ \mathrm{tr} \left(\exp[-\beta(\widehat{H}_0 + \widehat{H}_{\mathrm{int}})] \right) \right\} \tag{3.34}$$

The fundamental problem of this operator exponential are the terms which are not quadratic or quartic in the fluctuation operators $\delta\widehat{\psi}$, $\delta\widehat{\psi}^\dagger$ so we cannot close the algebra. This exponential produces an infinite series of nested commutators without hitting the unit element or the normal form $\delta\widehat{\psi}^\dagger\delta\widehat{\psi}$; for further reading check Zassenhausen formula [29] for exponentials of operators. The Hamiltonian $\widehat{H}_0$ contains only zeroth order and quadratic terms in $\delta\widehat{\psi}$, whereas the interacting Hamiltonian $\widehat{H}_{\mathrm{int}}$ also involves terms of the order $\delta\widehat{\psi}, \delta\widehat{\psi}^3$. The problem is not exactly solvable, but we can try to find a solution with a perturbative approach in the interaction Hamiltonian $\widehat{H}_{\mathrm{int}}$.

3.3.3 Perturbation theory in the interacting Hamiltonian

The parameter g will be small in comparison to the non-interacting term as long as the intensity of the electromagnetic field is not extraordinary high. A first perturbative approach to the effective action (3.34) with respect to the interacting part leads to

$$\Gamma = -\frac{1}{\beta} \ln \left\{ \mathrm{tr} \left(\mathrm{e}^{-\beta\widehat{H}_0}[1 - \beta\widehat{H}_{\mathrm{int}}] \right) \right\}. \tag{3.35}$$

Using the series expansion of the logarithm

$$\ln(1-x) = -\sum_{p=1}^{\infty} \frac{x^p}{p}, \tag{3.36}$$

the definition of the partition function (3.3) and the unperturbed expectation value

$$\langle \bullet \rangle_{(0)} = \frac{1}{Z_0} \mathrm{tr} \left(e^{-\beta\widehat{H}_0} \bullet \right), \tag{3.37}$$

we finally get the effective action with a linearized interaction part

$$\Gamma = -\frac{1}{\beta} \ln Z_0 + \left\langle \widehat{H}_{\mathrm{int}} \right\rangle_{(0)}. \tag{3.38}$$

The trace is performed over the Fock base $|\mathbf{n}\rangle = |\{n_{lm\epsilon}\}\rangle_{l\in\mathbb{N}, m\in\mathbb{Z}\setminus l=0, m=0}$, where the ground state is excluded according to the definition of $\delta\widehat{\psi}, \delta\widehat{\psi}^\dagger$ in (3.26), (3.27). The unperturbed Hamiltonian $\widehat{H}_0$ in (3.31) is diagonalized in the Fock base. Performing the trace always means summing over the diagonal elements of the full Hamiltonian. Thus, we can simplify the expectation value of the perturbed Hamiltonian in the

effective action

$$\Gamma = -\frac{1}{\beta}\ln Z_0 + \left\langle \widehat{H}_{\text{int}} \right\rangle_{(0)} \tag{3.39}$$

$$\begin{aligned} &= -\frac{1}{\beta}\ln Z_0 \\ &\quad + \frac{g}{2}\int \left\langle |\psi_{00}(\mathbf{x})|^4 + 4\,|\psi_{00}(\mathbf{x})|^2\,\delta\widehat{\psi}^\dagger(\mathbf{x})\delta\widehat{\psi}(\mathbf{x}) + \delta\widehat{\psi}^\dagger(\mathbf{x})\delta\widehat{\psi}^\dagger(\mathbf{x})\delta\widehat{\psi}(\mathbf{x})\delta\widehat{\psi}(\mathbf{x})\right\rangle_{(0)} \\ &\quad + \left\langle \mathcal{O}(\delta\hat{\psi}^\dagger, \delta\hat{\psi}, \delta\hat{\psi}\delta\hat{\psi}, \delta\hat{\psi}^\dagger\delta\hat{\psi}^\dagger, \delta\hat{\psi}^\dagger\delta\hat{\psi}\delta\hat{\psi}, \delta\hat{\psi}^\dagger\delta\hat{\psi}^\dagger\delta\hat{\psi})\right\rangle_{(0)} \end{aligned} \tag{3.40}$$

$$\begin{aligned} &= -\frac{1}{\beta}\ln Z_0 + \frac{g}{2}\int |\psi_{00}(\mathbf{x})|^4 \\ &\quad + \frac{g}{2}\int 4\,|\psi_{00}(\mathbf{x})|^2 \left\langle \delta\widehat{\psi}^\dagger(\mathbf{x})\delta\widehat{\psi}(\mathbf{x})\right\rangle_{(0)} + \frac{g}{2}\int \left\langle \delta\widehat{\psi}^\dagger(\mathbf{x})\delta\widehat{\psi}^\dagger(\mathbf{x})\delta\widehat{\psi}(\mathbf{x})\delta\widehat{\psi}(\mathbf{x})\right\rangle_{(0)}. \end{aligned} \tag{3.41}$$

Applying the Wick-rule in order to simplify the expectation value of the four field operators, we get

$$\left\langle \delta\widehat{\psi}^\dagger(\mathbf{x})\delta\widehat{\psi}^\dagger(\mathbf{x})\delta\widehat{\psi}(\mathbf{x})\delta\widehat{\psi}(\mathbf{x})\right\rangle_{(0)} = 2\left\langle \delta\widehat{\psi}^\dagger(\mathbf{x})\delta\widehat{\psi}(\mathbf{x})\right\rangle^2_{(0)}. \tag{3.42}$$

Then the effective action can be written in the compact form

$$\begin{aligned} \Gamma = &-\frac{1}{\beta}\ln Z_0 + \frac{g}{2}\int |\psi_{00}(\mathbf{x})|^4 + 2g\int |\psi_{00}(\mathbf{x})|^2 \left\langle \delta\widehat{\psi}^\dagger(\mathbf{x})\delta\widehat{\psi}(\mathbf{x})\right\rangle_{(0)} \\ &+ g\int \left\langle \delta\widehat{\psi}^\dagger(\mathbf{x})\delta\widehat{\psi}(\mathbf{x})\right\rangle_{(0)} \left\langle \delta\widehat{\psi}^\dagger(\mathbf{x})\delta\widehat{\psi}(\mathbf{x})\right\rangle_{(0)}. \end{aligned} \tag{3.43}$$

3.4 Effective action for ideal cavity photon gas

Calculating the effective action for the ideal cavity photon gas, i.e. $g = 0$, we have to evaluate

$$\Gamma_0 = -\frac{1}{\beta}\ln Z_0 = -\frac{1}{\beta}\ln\left\{\sum_{\mathbf{n}} \langle \mathbf{n}|\, \mathrm{e}^{-\beta\widehat{H}_0}\,|\mathbf{n}\rangle\right\}. \tag{3.44}$$

The mode functions $A_{lm\epsilon}(\mathbf{x})$ in the bosonic field operators are eigenstates of the single-particle non-interacting Hamiltonian h_0 (3.16). By taking advantage of the constructed orthogonal modes, the second quantized non-interacting Hamiltonian $\widehat{H}_0$ (3.31) reads

$$\begin{aligned} \widehat{H}_0 = &\sum_\epsilon (\hbar\omega - \mu)\int dA\,|\mathbf{A}_{00\epsilon}(\mathbf{x})|^2 \\ &+ \sum_\epsilon \sum_{lm\neq 00} (\hbar\omega_{lm} - \mu)\int dA\,\left\{\mathbf{A}^*_{lm\epsilon}(\mathbf{x})\cdot\mathbf{A}_{lm\epsilon}(\mathbf{x})\widehat{a}^\dagger_{lm\epsilon}\widehat{a}_{lm\epsilon}\right\}, \end{aligned} \tag{3.45}$$

where $|\psi_{00}(\mathbf{x})|^2 = \sum_\epsilon |\mathbf{A}_{00\epsilon}(\mathbf{x})|^2$ is the condensate density and the expression in curly brackets is the density operator $\widehat{n}_{lm\epsilon}(\mathbf{x})$ of the respective excited states. Additionally, the mode functions are normalized, which yields

$$\widehat{H}_0 = \sum_\epsilon (\hbar\omega - \mu) N_{00\epsilon} + \sum_\epsilon \sum_{lm\neq 00} (\hbar\omega_{lm} - \mu) \widehat{a}^\dagger_{lm\epsilon} \widehat{a}_{lm\epsilon}. \tag{3.46}$$

Taking into account that the photon number operator $\widehat{a}^\dagger_{lm\epsilon}\widehat{a}_{lm\epsilon} = \widehat{n}_{lm\epsilon}$ acts only on its distinct energy slot of the total state $|\mathbf{n}\rangle$, the effective action becomes

$$\Gamma = -\frac{1}{\beta} \ln \left\{ \mathrm{e}^{-\beta \sum_\epsilon (\hbar\omega - \mu) N_{00\epsilon}} \prod_{\epsilon, lm\neq 00} \sum_{n_{lm\epsilon}=0}^{\infty} \langle n_{lm\epsilon}| \, \mathrm{e}^{-\beta(\hbar\omega_{lm} - \mu)\widehat{n}_{lm\epsilon}} \, |n_{lm\epsilon}\rangle \right\}. \tag{3.47}$$

Here the sum over the different energy levels $lm\epsilon$ in the exponential is rewritten into a product of the summands. The sum appearing behind the product is just the rewritten trace for each energy slot, since every energy level can be occupied by an arbitrary number $n_{lm\epsilon}$, whereas the occupation number of the condensate is fixed to $N_{00} = N_{00\epsilon_1} + N_{00\epsilon_2}$. Due to the two polarizations the photonic ground state is degenerate, whereas the usual massive BEC with its scalar-valued field operators is non-degenerate.
Demanding that $\mu < E_{lm}$, we apply the geometric series

$$\sum_{p=0}^{\infty} x^p = \frac{1}{1-x} \quad \text{for all } |x| < 1 \tag{3.48}$$

to Equation (3.47). The trace is evaluated in the eigenstates of the Hamiltonian. Thus, replacing the operators $\widehat{n}_{lm\epsilon}$ in Equation (3.47) by the eigenvalues $n_{lm\epsilon}$ and using the geometric series results in

$$\Gamma = (\hbar\omega - \mu)\, N_{00} - \frac{1}{\beta} \ln \prod_{lm\neq 00} \frac{1}{(1 - \exp\{-\beta[E_{lm} - \mu]\})} \frac{1}{(1 - \exp\{-\beta[E_{lm} - \mu]\})}. \tag{3.49}$$

The explicit product of the same expression reminds of the two distinct polarizations. With the help of the logarithmic laws and the Taylor expansion of the logarithm (3.36), we find

$$\Gamma = (\hbar\omega - \mu)\, N_{00} - \frac{2}{\beta} \sum_{p=1}^{\infty} \sum_{ml\neq 00} \frac{\exp\{-\beta(E_{lm} - \mu)p\}}{p}. \tag{3.50}$$

The prefactor two arises naturally from the two possible polarizations. In the case of a broken symmetry between the polarizations, as for example by polarized mirrors or different energy eigenvalues for the each polarization, this simplification would not hold any longer.

Inserting the explicit form of the energy eigenvalues E_{lm} from (2.119), we find

$$\begin{aligned}\Gamma &= (\hbar\omega - \mu)\, N_{00} \\ &\quad - \frac{2}{\beta}\sum_{p=1}^{\infty}\frac{\mathrm{e}^{-\beta(\hbar\omega-\mu)p}}{p}\left\{\sum_{l=0}^{\infty}\sum_{m=-\infty}^{\infty}\mathrm{e}^{-\beta\hbar\omega 2lp}\mathrm{e}^{-\beta\hbar\omega|m|p}-1\right\} \qquad (3.51)\\ &= (\hbar\omega - \mu)\, N_{00} \\ &\quad - \frac{2}{\beta}\sum_{p=1}^{\infty}\frac{\mathrm{e}^{-\beta(\hbar\omega-\mu)p}}{p}\left\{\sum_{l=0}^{\infty}\left(2\sum_{m=0}^{\infty}\mathrm{e}^{-\beta\hbar\omega 2lp}\mathrm{e}^{-\beta\hbar\omega|m|p}-\mathrm{e}^{-\beta\hbar\omega 2lp}\right)-1\right\}. \qquad (3.52)\end{aligned}$$

The geometric series over the radial quantum number l and the angular momentum quantum number m leads to

$$\begin{aligned}\Gamma &= (\hbar\omega - \mu)\, N_{00} - \\ &\quad \frac{2}{\beta}\sum_{p=1}^{\infty}\frac{\mathrm{e}^{-\beta(\hbar\omega-\mu)p}}{p}\left\{\frac{2}{(1-\mathrm{e}^{-\beta\hbar\omega 2p})(1-\mathrm{e}^{-\beta\hbar\omega p})}-\frac{1}{(1-\mathrm{e}^{-\beta\hbar\omega 2p})}-1\right\}. \qquad (3.53)\end{aligned}$$

This concise form of the effective action Γ is the fundament for the determination of the relevant thermodynamic quantities.

3.5 Critical number for non-interacting cavity photon gas

We have found a reduced expression for the non-interacting effective action Γ in (3.53). In thermodynamics, the particle number is defined as

$$\begin{aligned}N &= -\frac{\partial F}{\partial\mu} = -\frac{\partial\Gamma}{\partial\mu} \qquad (3.54)\\ &= N_{00} + 2\sum_{p=1}^{\infty}\mathrm{e}^{-\beta(\hbar\omega-\mu)p}\left\{\frac{2}{(1-\mathrm{e}^{-\beta\hbar\omega 2p})(1-\mathrm{e}^{-\beta\hbar\omega p})}-\frac{1}{(1-\mathrm{e}^{-\beta\hbar\omega 2p})}-1\right\}.\end{aligned}$$

In order to obtain the critical particle number for the onset of the phase transition, we need to determine the critical chemical potential. Applying the Gross-Pitaevskii theory, the extremalization of the effective action Γ_0 (3.44) with respect to the condensate field $\psi^*_{00\epsilon}$ yields

$$\frac{\delta\Gamma}{\delta\psi^*_{00\epsilon}} = (h_0(\mathbf{x}) - \mu)\psi_{00\epsilon}(\mathbf{x}) \stackrel{!}{=} 0. \qquad (3.55)$$

Note here once again that this has to be performed for both polarizations ϵ_1, ϵ_2. Equation (3.55) is the Gross-Pitaevskii equation for the ideal Bose gas. This equation possesses two solutions; either $\psi_{00\epsilon} = 0$ which corresponds to the gas phase or $\hbar\omega = \mu$ and $\psi_{00\epsilon} \neq 0$, where latter describes the condition for a BEC. Thus, the critical chemical potential for the non-interacting case corresponds to ground state energy

$$\mu_{\mathrm{crit}} = E_{00} = \hbar\omega. \qquad (3.56)$$

Since we are looking for the phase boundary between the gas phase and the BEC, we set $N_{00} = 0$ and plug μ_{crit} from (3.56) into Equation (3.54)

$$N_{\mathrm{crit}} = 2\sum_{p=1}^{\infty}\left\{\frac{2}{(1-\mathrm{e}^{-\beta\hbar\omega 2p})(1-\mathrm{e}^{-\beta\hbar\omega p})} - \frac{1}{(1-\mathrm{e}^{-\beta\hbar\omega 2p})} - 1\right\} \tag{3.57}$$

The sum is absolutely convergent, and its value can be determined numerically with a program like mathematica. The critical particle number for an effective two dimensional ideal photon gas in a curved micro cavity can be specified to

$$N_{\mathrm{crit}} \approx 74300. \tag{3.58}$$

Using the semiclassical approximation $\beta\hbar\omega \ll 1$ for harmonically trapped Bose gases in two dimensions yields

$$N_{\mathrm{crit,semi}} = 2\frac{\zeta(2)}{(\beta\hbar\omega)^2} \approx 72800. \tag{3.59}$$

The deviation of about two percent from the quantum mechanical exact value can be explained by finite-size corrections [30] which can be included via

$$N_{\mathrm{crit,semi+fs}} = 2\left\{\frac{\zeta(2)}{(\beta\hbar\omega)^2} + \frac{-\ln(\beta\hbar\omega)+\gamma-1/2}{\beta\hbar\omega}\right\} \approx 74300, \tag{3.60}$$

with the Euler-Mascheroni constant γ. The good agreement of both results is found in the small ratio of $\beta\hbar\omega = 0.0067 \ll 1$ which allows a semiclassical expansion. However, provided the temperature is given, one should apply the quantum summation which already includes finite-size effects and can even be used for anisotropic traps. Comparing with the experimental result $N_{\mathrm{crit}} = (6.3 \pm 2.4)\cdot 10^4$, the theoretical prediction lies within the error bar. Experimentally, the particle number is controlled via the pump laser. When reaching a critical input power, which corresponds to a certain photon number, the condensation sets in. Thus the total photon number N is the control parameter for the cavity system, see Figure 3.2. The condensate fraction in terms of the total number is

$$\frac{N_{00}}{N} = 1 - \frac{N_{\mathrm{crit}}}{N}, \tag{3.61}$$

where N_{crit} contains the all excited states. Of course, below a critical particle number the ground state is occupied, but this is rather negligible. Hence the condensate fraction first rises significantly for $N > N_{\mathrm{crit}}$ and correspondingly $\mu = \mu_{\mathrm{crit}}$. In order to avoid divergences in the ground state occupation number for $\mu = \mu_{\mathrm{crit}}$, we have treated the ground state explicitly. This is the reason for a rather sharp phase transition shown in Figure 3.2.
In the next section, we will study the impact of interaction on this result.

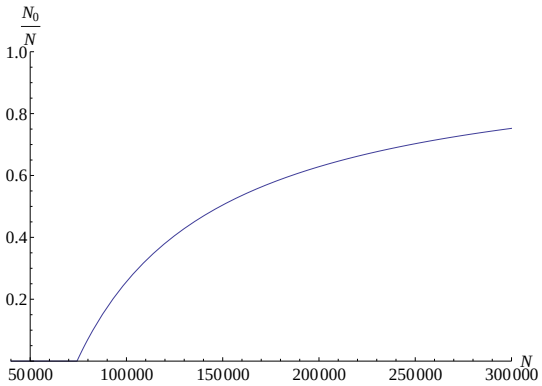

Figure 3.2: Condensate fraction as function of the total photon number N.

3.6 Effective action for interacting cavity photon gas

The interaction considered here arises from the Kerr-effect (3.8). Within a perturbative approach in the interaction parameter g, the effective action can be written in the form (3.43),

$$\begin{aligned}\Gamma = &-\frac{1}{\beta}\ln Z_0 + \frac{g}{2}\int |\psi_{00}(\mathbf{x})|^4 + 2g\int |\psi_{00}(\mathbf{x})|^2 \left\langle \delta\widehat{\psi}^\dagger(\mathbf{x})\delta\widehat{\psi}(\mathbf{x})\right\rangle_{(0)} \\ &+ g\int \left\langle \delta\widehat{\psi}^\dagger(\mathbf{x})\delta\widehat{\psi}(\mathbf{x})\right\rangle_{(0)} \left\langle \delta\widehat{\psi}^\dagger(\mathbf{x})\delta\widehat{\psi}(\mathbf{x})\right\rangle_{(0)} \end{aligned} \tag{3.62}$$

A quantity to determine is the expectation value of $\delta\widehat{\psi}^\dagger(\mathbf{x})\delta\widehat{\psi}(\mathbf{x})$. By definition this term is

$$\begin{aligned}\left\langle \delta\widehat{\psi}^\dagger(\mathbf{x})\delta\widehat{\psi}(\mathbf{x})\right\rangle_{(0)} = &\frac{1}{Z_0}\left\{\sum_{\mathbf{n}}\langle\mathbf{n}| \sum_{lm\epsilon, lm\neq 00}\sum_{l'm'\epsilon', l'm'\neq 00}\right. \\ &\left.\mathbf{A}^*_{lm\epsilon}(\mathbf{x})\cdot\mathbf{A}_{l'm'\epsilon'}(\mathbf{x})\widehat{a}^\dagger_{lm\epsilon}a_{l'm'\epsilon'}\mathrm{e}^{-\beta\widehat{H}_0}|\mathbf{n}\rangle\right\}. \end{aligned} \tag{3.63}$$

Applying the orthogonality of the Fock base immediately leads to

$$\left\langle \delta\widehat{\psi}^\dagger(\mathbf{x})\delta\widehat{\psi}(\mathbf{x})\right\rangle_{(0)} = \frac{1}{Z_0}\sum_{\mathbf{n}}\langle\mathbf{n}|\sum_{lm\epsilon, lm\neq 00}\mathbf{A}^*_{lm\epsilon}(\mathbf{x})\cdot\mathbf{A}_{lm\epsilon}(\mathbf{x})\widehat{n}_{lm\epsilon}\mathrm{e}^{-\beta\widehat{H}_0}|\mathbf{n}\rangle \tag{3.64}$$

Since the trace is performed in the eigenstates of the number operators $\widehat{n}_{lm\epsilon}$ we replace them by their eigenvalues (2.155), and with definition of the partition function (3.3), the expectation value reads

$$\begin{aligned}\left\langle \delta\widehat{\psi}^\dagger(\mathbf{x})\delta\widehat{\psi}(\mathbf{x})\right\rangle_{(0)} = &\frac{\mathrm{e}^{-\beta(\hbar\omega-\mu)N_{00}}}{Z_0}\prod_{op\epsilon''\neq lm\epsilon, lm\neq 00}\sum_{n_{op\epsilon''}=0}^{\infty}\mathrm{e}^{-\beta(E_{op}-\mu)n_{op\epsilon''}} \\ &\times\sum_{n_{lm\epsilon}=0}^{\infty}\sum_{lm\epsilon, lm\neq 00}\mathbf{A}^*_{lm\epsilon}(\mathbf{x})\cdot\mathbf{A}_{lm\epsilon}(\mathbf{x})n_{lm\epsilon}\mathrm{e}^{-\beta(E_{lm}-\mu)n_{lm\epsilon}}, \end{aligned} \tag{3.65}$$

where the trace and the exponential are decomposed as in the previous sections. The occurring $n_{lm\epsilon}$ in the sum can be replaced by its respective energy derivative; this is a trick from classical statistics in order to simplify the calculation of the particle number expectation value. The geometric series for the summation over $n_{lm\epsilon}$ and each Fock base slot $n_{op\epsilon''}$ converts the expectation value to

$$\begin{aligned}\left\langle \delta\widehat{\psi}^\dagger(\mathbf{x})\delta\widehat{\psi}(\mathbf{x})\right\rangle_{(0)} =& -\frac{\mathrm{e}^{-\beta(\hbar\omega-\mu)N_{00}}}{\beta Z_0}\prod_{op\epsilon''\neq lm\epsilon, lm\neq 00}\frac{1}{\{1-\mathrm{e}^{-\beta(E_{op}-\mu)}\}^2} \\ &\times\frac{1}{1-\mathrm{e}^{-\beta(E_{lm}-\mu)}}\sum_{lm\epsilon}\mathbf{A}^*_{lm\epsilon}(\mathbf{x})\cdot\mathbf{A}_{lm\epsilon}(\mathbf{x})\frac{\partial}{\partial E_{lm}}\frac{1}{1-\mathrm{e}^{-\beta(E_{lm}-\mu)}},\end{aligned} \tag{3.66}$$

where one geometric series factor with lm arises from $n_{op\epsilon''}=n_{lm\epsilon''}\neq n_{lm\epsilon}$ with another polarization $\epsilon''\neq\epsilon$, which is currently not summed in the second line. Taking the derivative and the definition of the partition function Z_0, we get

$$\left\langle \delta\widehat{\psi}^\dagger(\mathbf{x})\delta\widehat{\psi}(\mathbf{x})\right\rangle_{(0)} = \sum_{lm\epsilon, lm\neq 00}|\mathbf{A}_{lm\epsilon}(\mathbf{x})|^2\frac{1}{\mathrm{e}^{\beta(E_{lm}-\mu)}-1}. \tag{3.67}$$

The result is the mode density times the Bose-Einstein statistics. Inserting the expectation value (3.67) into the effective action for the interacting case (3.43) leads to

$$\begin{aligned}\Gamma =& -\frac{1}{\beta}\ln Z_0+\frac{g}{2}\int|\psi_{00}(\mathbf{x})|^4+g\int 2\,|\psi_{00}(\mathbf{x})|^2\sum_{lm\epsilon,lm\neq 00}|\mathbf{A}_{lm\epsilon}(\mathbf{x})|^2\frac{1}{\mathrm{e}^{\beta(E_{lm}-\mu)}-1} \\ &+g\int\left(\sum_{lm\epsilon,lm\neq 00}|\mathbf{A}_{lm\epsilon}(\mathbf{x})|^2\frac{1}{\mathrm{e}^{\beta(E_{lm}-\mu)}-1}\right)^2.\end{aligned} \tag{3.68}$$

The evaluation of the mode function product involving the double sum over the quantum numbers l and m is explicitly performed in the Appendix C.11, it is closely connected to the Wick rotated propagator and the Green function. The rewritten double sum (3.67) is

$$\sum_{lm\epsilon,lm\neq 00}|\mathbf{A}_{lm\epsilon}(\mathbf{x})|^2\frac{1}{\mathrm{e}^{\beta(E_{lm}-\mu)}-1} = \frac{k}{\pi a}\sum_{p=1}^{\infty}\mathrm{e}^{-\beta(\hbar\omega-\mu)p}\left\{\frac{\mathrm{e}^{-\frac{k}{a}\tanh(\hbar\omega p/2)\rho^2}}{(1-\mathrm{e}^{-\beta 2\hbar\omega p})}-\mathrm{e}^{-\frac{k}{a}\rho^2}\right\}. \tag{3.69}$$

Here the quantity k is the absolute value of the vector, which is in leading order $k=k_\parallel$. The small a is the scaling constant derived from the boundary value problem $a=\sqrt{RL/2}$. In combination the parameter k/a is exactly $k_\perp^2$. What is left from the double sum in (3.69) is a single sum over rescaled Gaussians. This is a tremendous simplification which now allows the determination of the integrals in (3.68). The condensate density $|\psi_{00}(\mathbf{x})|^2$ (3.26) is a scalar product of the lowest vector mode functions $\mathbf{A}_{00}$. All appearing scalar products of mode functions are evaluated approximatively with an expansion in the micro cavity and large curvature limes $k_\parallel z=\text{const}$ and $k_\perp=\text{const}$, while $z\to 0$ and the curvature radius $R\to\infty$.

Thus the first integral in (3.62) is the product of the condensate densities

$$I_{00^2} = \frac{g}{2}\int dA\,|\psi_{00}(\mathbf{x})|^4 \tag{3.70}$$

$$\approx \frac{g}{2}N_{00}^2\frac{k}{a\pi}2\frac{k}{a}\int \mathrm{e}^{-\frac{k}{a}2\rho^2}\rho d\rho \tag{3.71}$$

$$= \frac{g}{2}\frac{k}{2\pi a}N_{00}^2, \tag{3.72}$$

where N_{00} is the defined condensate particle number and the other occurring constants arise from the normalization which can be found in Appendix A.23. The integration over condensate and excited states yields

$$I_{00\mathrm{exc}} = 2g\int dA\,|\psi_{00}(\mathbf{x})|^2 \sum_{lm\epsilon,lm\neq 00} |\mathbf{A}_{lm\epsilon}(\mathbf{x})|^2 \frac{1}{\mathrm{e}^{\beta(E_{lm}-\mu)}-1} \tag{3.73}$$

$$\approx 2gN_{00}\frac{k}{a\pi}\frac{2k}{a}\sum_{p=1}^{\infty}\mathrm{e}^{-\beta(\hbar\omega-\mu)p}\int \mathrm{e}^{-\frac{k}{a}\rho^2}\left\{\frac{\mathrm{e}^{-\frac{k}{a}\tanh(\hbar\omega p/2)\rho^2}}{(1-\mathrm{e}^{-\beta 2\hbar\omega p})} - \mathrm{e}^{-\frac{k}{a}\rho^2}\right\}\rho d\rho \tag{3.74}$$

$$= 2gN_{00}\frac{k}{\pi a}\sum_{p=1}^{\infty}\mathrm{e}^{-\beta(\hbar\omega-\mu)p}\left\{\frac{1}{(1+\tanh(\hbar\omega p/2))(1-\mathrm{e}^{-\beta 2\hbar\omega p})} - \frac{1}{2}\right\}. \tag{3.75}$$

Finally the integral containing the excited state squared is equal to

$$I_{\mathrm{exc}^2} = g\int dA\left(\sum_{lm\epsilon,lm\neq 00}|\mathbf{A}_{lm\epsilon}(\mathbf{x})|^2\frac{1}{\mathrm{e}^{\beta(E_{lm}-\mu)}-1}\right)^2 \tag{3.76}$$

$$\begin{aligned} = g\frac{k}{\pi a}\sum_{q=1}^{\infty}\sum_{p=1}^{\infty}\mathrm{e}^{-\beta(\hbar\omega-\mu)(p+q)}\Bigg\{&\frac{1}{2} - \frac{1}{(1+\tanh(\hbar\omega q/2))(1-\mathrm{e}^{-\beta 2\hbar\omega q})} \\ &- \frac{1}{(1+\tanh(\hbar\omega p/2))(1-\mathrm{e}^{-\beta 2\hbar\omega p})} \\ &+ \frac{1}{(\tanh(\hbar\omega q/2)+\tanh(\hbar\omega p/2))(1-\mathrm{e}^{-\beta 2\hbar\omega p})(1-\mathrm{e}^{-\beta 2\hbar\omega q})}\Bigg\}. \end{aligned} \tag{3.77}$$

The appearing sums over p and q converge, because we have taken out the ground state. The effective action for interacting photon gas is

$$\Gamma = -\frac{1}{\beta}\ln Z_0 + I_{00^2}(\mu) + I_{00\mathrm{exc}}(\mu) + I_{\mathrm{exc}^2}(\mu). \tag{3.78}$$

3.7 Shift of chemical potential due to interaction

Due to the interaction, there will be a shift of the chemical potential and furthermore the ground state is changed. We expand both the ground state wave function which is the order parameter ψ_{00} and the chemical potential μ in orders of g

$$\psi_{00}(\mathbf{x}) = \psi_{00}^{(0)}(\mathbf{x}) + \psi_{00}^{(1)}(\mathbf{x}) + \dots, \qquad \mu = \mu^{(0)} + \mu^{(1)} + \dots \quad . \tag{3.79}$$

Extremizing the effective action (3.43) with respect to the condensate wave function ψ_{00}^* yields

$$\frac{\delta\Gamma}{\delta\psi_{00}^*} = \left\{[h_0 - \mu + g|\psi_{00}(\mathbf{x})|^2] + 2g\left\langle\delta\widehat{\psi}^\dagger(\mathbf{x})\delta\widehat{\psi}(\mathbf{x})\right\rangle_{(0)}\right\}\psi_{00}(\mathbf{x}) \stackrel{!}{=} 0. \tag{3.80}$$

The expression in the squared brackets represents the Gross-Pitaevskii equation for an interacting Bose gas. Plugging in the expansion for ψ_{00} and μ and then sorting the orders of g yields in zeroth order

$$[h_0 - \mu^{(0)}]\psi_{00}^{(0)}(\mathbf{x}) \stackrel{!}{=} 0. \tag{3.81}$$

Thus, the zeroth order of μ is identical to the ground state energy

$$\mu^{(0)} = E_{00} = \hbar\omega \tag{3.82}$$

for condensate phase, where $\psi_{00}^{(0)} \neq 0$. The first order in g is

$$\left[h_0 - \mu^{(0)}\right]\psi_{00}^{(1)}(\mathbf{x}) = -\left\{g\left|\psi_{00}^{(0)}(\mathbf{x})\right|^2 - \mu^{(1)} + 2g\left\langle\delta\widehat{\psi}^\dagger(\mathbf{x})\delta\widehat{\psi}(\mathbf{x})\right\rangle_{(0)}\right\}\psi_{00}^{(0)}(\mathbf{x}). \tag{3.83}$$

This is just one equation for the two unknown $\psi_{00}^{(1)}(\mathbf{x})$ and $\mu^{(1)}$. Multiplying (3.83) with $\psi_{00}^{*(0)}(\mathbf{x})$ from the left and then integrating results in

$$\begin{aligned}\int\psi_{00}^{*(0)}(\mathbf{x})\left[h_0 - \mu^{(0)}\right]\psi_{00}^{(1)}(\mathbf{x}) = \\ -\int\psi_{00}^{*(0)}(\mathbf{x})\left\{g\left|\psi_{00}^{(0)}(\mathbf{x})\right|^2 - \mu^{(1)} + 2g\left\langle\delta\widehat{\psi}^\dagger(\mathbf{x})\delta\widehat{\psi}(\mathbf{x})\right\rangle_{(0)}\right\}\psi_{00}^{(0)}(\mathbf{x}).\end{aligned} \tag{3.84}$$

Due to the hermiticity of h_0 and Equation (3.82), the left-hand side vanishes and the remainder can be solved for $\mu^{(1)}$

$$\mu^{(1)} = \frac{g}{N_{00}}\int\psi_{00}^{*(0)}(\mathbf{x})\left\{\left|\psi_{00}^{(0)}(\mathbf{x})\right|^2 + 2\left\langle\delta\widehat{\psi}^\dagger(\mathbf{x})\delta\widehat{\psi}(\mathbf{x})\right\rangle_{(0)}\right\}\psi_{00}^{(0)}(\mathbf{x}). \tag{3.85}$$

The expression on the right-hand side corresponds to $[2I_{00^2}(\mu^{(0)}) + I_{00\mathrm{exc}}(\mu^{(0)})]/N_{00}$. The critical chemical potential until first order in g is

$$\mu_{\mathrm{crit}} = \hbar\omega + \frac{1}{N_{00}}[2I_{00^2}(\hbar\omega) + I_{00\mathrm{exc}}(\hbar\omega)]. \tag{3.86}$$

3.8 Critical number for the interacting cavity photon gas

The critical particle number for an interacting photon gas follows from

$$N = -\frac{\partial F}{\partial\mu} = -\frac{\partial\Gamma}{\partial\mu}. \tag{3.87}$$

Here we take the effective action with interaction (3.78). In order to get the critical point between the gas phase and the condensate phase, we set $N_{00} = 0$ and $\mu = \mu_{\mathrm{crit}}$ to find

$$\begin{aligned} N_{\mathrm{crit}} =& 2\sum_{p=1}^{\infty} \mathrm{e}^{-\beta(\hbar\omega-\mu_{\mathrm{crit}})p} \left\{ \frac{2}{(1-\mathrm{e}^{-\beta\hbar\omega 2p})(1-\mathrm{e}^{-\beta\hbar\omega p})} - \frac{1}{(1-\mathrm{e}^{-\beta\hbar\omega 2p})} - 1 \right\} \\ & - \frac{\partial I_{\mathrm{exc}^2}(\mu)|_{\mu=\mu_{\mathrm{crit}}}}{\partial\mu}. \end{aligned} \tag{3.88}$$

Inserting (3.77) and (3.86) into Equation (3.88) and expanding up first order in g yields

$$\begin{aligned} N_{\mathrm{crit}} =& 2\sum_{p=1}^{\infty} \left\{ \frac{2}{(1-\mathrm{e}^{-\beta\hbar\omega 2p})(1-\mathrm{e}^{-\beta\hbar\omega p})} - \frac{1}{(1-\mathrm{e}^{-\beta\hbar\omega 2p})} - 1 \right\} \\ & \times \left(1 + pg2\frac{k}{a\pi} \sum_{l=1}^{\infty} \left\{ \frac{1}{(1+\tanh(\hbar\omega l/2))(1-\mathrm{e}^{-\beta 2\hbar\omega l})} - \frac{1}{2} \right\} \right) \\ & - g\beta\frac{k}{a\pi} \sum_{q=1}^{\infty}\sum_{p=1}^{\infty} (q+p) \left\{ \frac{1}{2} - \frac{1}{(1+\tanh(\hbar\omega q/2))(1-\mathrm{e}^{-\beta 2\hbar\omega q})} \right. \\ & - \frac{1}{(1+\tanh(\hbar\omega p/2))(1-\mathrm{e}^{-\beta 2\hbar\omega p})} \\ & \left. + \frac{1}{(\tanh(\hbar\omega p/2)+\tanh(\hbar\omega q/2))(1-\mathrm{e}^{-\beta 2\hbar\omega p})(1-\mathrm{e}^{-\beta 2\hbar\omega q})} \right\}. \end{aligned} \tag{3.89}$$

In order to evaluate these sums, the interaction parameter g is required. This parameter includes the non-linear refraction index n_2, which is a material parameter. Fortunately, there exists an estimate based on numerical simulations of the Gross-Pitaevskii equation, which were fitted to the experimental data [31]. The parameter has the definition

$$g = \frac{\hbar^2}{m_{\mathrm{ph}}}\overline{g}, \tag{3.90}$$

where $\overline{g}$ is the dimensionless parameter obtained from the Gross-Pitaevskii fit. Its value is $\overline{g} = 7 \cdot 10^{-4}$. Defining g in this way, the prefactor of the interacting term resembles the familiar expression for a two-dimensional harmonically trapped Bose gas

$$g\beta\frac{k}{a\pi} = \frac{\overline{g}\beta}{\pi}\frac{\hbar^2}{m_{\mathrm{ph}}}\frac{m_{\mathrm{ph}}\omega}{\hbar} = \frac{\overline{g}}{\pi}\beta\hbar\omega \tag{3.91}$$

with the effective photon mass term $m_{\mathrm{ph}} = \hbar k_{\parallel}/c$.
The result obtained with the program mathematica is

$$N_{\mathrm{crit}} \approx 74300 + 100 - 150 = 74250. \tag{3.92}$$

The interaction has only a small contribution to the critical photon number, which is not surprising, since the interaction parameter for the atomic BECs is $\overline{g} = 10^{-2} -$

10^{-1} [32]. Here we introduced the Kerr-effect as an effective two-body contact interaction in our second quantized Hamiltonian (3.23). We suggest to implement other possible interactions in the geometry which shifts the oscillator level trap frequency or possibly the higher order correction from the mode analysis lead to a non-negligible contribution, when evaluated in the double sums for the free energy.

3.9 Density and correlation

In this section, we take advantage of the vector modes and present the mode profiles for the BEC of photons. Of course, these profiles include the thermal contribution and the condensate part. The bilocal density of the introduced bosonic field operators is

$$n(\mathbf{x},\mathbf{x}') = \left\langle \widehat{\psi}^\dagger(\mathbf{x})\widehat{\psi}(\mathbf{x}')\right\rangle_{(0)} = \mathrm{tr}\left\{\widehat{\rho}\left(\sum_{lm\epsilon}\sum_{l'm'\epsilon'}\mathbf{A}^*_{lm\epsilon}(\mathbf{x})\cdot\mathbf{A}_{l'm'\epsilon'}(\mathbf{x}')\widehat{a}^\dagger_{lm\epsilon}\widehat{a}_{l'm'\epsilon'}\right)\right\}. \tag{3.93}$$

Applying the orthogonality of the Fock base and the Bogoliubov decomposition (3.24), (3.25) immediately leads to

$$\begin{aligned} n(\mathbf{x},\mathbf{x}') =& \frac{1}{Z_0}\sum_{\mathbf{n}}\langle\mathbf{n}|\sum_{\epsilon}\psi^*_{00\epsilon}(\mathbf{x})\psi_{00\epsilon}(\mathbf{x}')\mathrm{e}^{-\beta\widehat{H}_0}|\mathbf{n}\rangle \\ &+\frac{1}{Z_0}\sum_{\mathbf{n}}\langle\mathbf{n}|\sum_{lm\epsilon,lm\neq 00}\mathbf{A}^*_{lm\epsilon}(\mathbf{x})\cdot\mathbf{A}_{lm\epsilon}(\mathbf{x}')\widehat{n}_{lm\epsilon}\mathrm{e}^{-\beta\widehat{H}_0}|\mathbf{n}\rangle\,. \end{aligned} \tag{3.94}$$

The evaluation of the trace is performed as in the section of the free energy for the interacting photon gas, thus the obtained expression is similar to (3.67),

$$n(\mathbf{x},\mathbf{x}') = \sum_{\epsilon}\psi^*_{00\epsilon}(\mathbf{x})\psi_{00\epsilon}(\mathbf{x}') + \sum_{lm\epsilon,lm\neq 00}\mathbf{A}^*_{lm\epsilon}(\mathbf{x})\cdot\mathbf{A}_{lm\epsilon}(\mathbf{x}')\frac{1}{\mathrm{e}^{\beta(E_{lm}-\mu)}-1}. \tag{3.95}$$

Here the bilocal density contains the condensate and the excited states which are required for the full density profile. According to Appendix (C.9), the excited state density can be rewritten into

$$\begin{aligned} n(\mathbf{x},\mathbf{x}') =& \sum_{\epsilon}\psi^*_{00\epsilon}(\mathbf{x})\psi_{00\epsilon}(\mathbf{x}') \\ &+\frac{k}{a\pi}\sum_{p=1}^{\infty}\mathrm{e}^{-\beta(\hbar\omega-\mu)p}\mathrm{e}^{-\frac{k}{2a}(\rho^2+\rho'^2)}\left\{\frac{\mathrm{e}^{-\frac{z}{(1-z)}\frac{k}{a}(\rho^2+\rho'^2)}}{(1-z)}\mathrm{e}^{2\frac{k}{a}\frac{\sqrt{\rho^2\rho'^2 z}}{(1-z)}\cos(\phi-\phi')}-1\right\}, \end{aligned} \tag{3.96}$$

where the parameter z is $z=\mathrm{e}^{-\beta\hbar\omega 2p}$. In the special case $\mathbf{x}=\mathbf{x}'$, we find the spatial autocorrelation of the field which corresponds to the intensity. The autocorrelation has the simple form (C.11)

$$n(\mathbf{x}) = |\psi_{00}(\mathbf{x})|^2 + \frac{k}{a\pi}\sum_{p=1}^{\infty}\mathrm{e}^{-\beta(\hbar\omega-\mu)p}\left\{\frac{\mathrm{e}^{-\frac{k}{a}\rho^2\tanh(\hbar\omega p/2)}}{(1-\mathrm{e}^{-\beta\hbar\omega 2p})}-\mathrm{e}^{-\frac{k}{a}\rho^2}\right\}. \tag{3.97}$$

In the following section the transverse wave number $k_\perp$ is denoted as $k_\perp = k_{trans} = \sqrt{k/a}$ in order to correspond with mathematica plots. Figure 3.3 shows a plot of the autocorrelation below and above criticality. The condensate part is localized in the trap center, whereas the excited states dominate for $\rho k_{\text{trans}} > 2$. The logarithmic plot in Figure 3.3 illustrates the Gaussian decay of the ground state. Evaluating the Gaussian of the ground state, we can specify the spatial extension of the BEC

$$\mathrm{e}^{-\frac{k}{a}\rho^2} \stackrel{!}{=} \mathrm{e}^{-1}, \tag{3.98}$$

which leads to

$$\rho_0 = \sqrt{\frac{a}{k}} = 14.1\ \mu\text{m}. \tag{3.99}$$

This result coincides with the estimate of the Equipartition theorem for the harmonic oscillator

$$\frac{m_{\text{ph}}\omega^2\rho^2}{2} = \frac{\hbar\omega}{2}. \tag{3.100}$$

Solving for the radius we get

$$\rho_0 = \sqrt{\frac{\hbar}{m_{\text{ph}}\omega}} = \sqrt{\frac{\hbar c a}{\hbar k c}} = \sqrt{\frac{a}{k}}, \tag{3.101}$$

where we used the definition of the effective photon mass (2.125) and the result for the trap frequency (2.126).
Due to the knowledge of the complete mode structure it is possible to determine the spatial correlation for the photon gas (3.97). Figure 3.4 shows a radial correlation at a spatial point, where the trapped BEC gives only a small contribution due to the spatial inhomogeneity. Above criticality, the correlation decays slower in central direction, due to the presence of the condensate, whereas abroad the center ,for $\rho k_{\text{trans}} > 2$, the decay is almost alike. It is remarkable to see that in the central region the condensate yields the major contribution. For large ρ, i.e. $\rho k_{\text{trans}} > 2$, the thermal excited states begin to dominate.

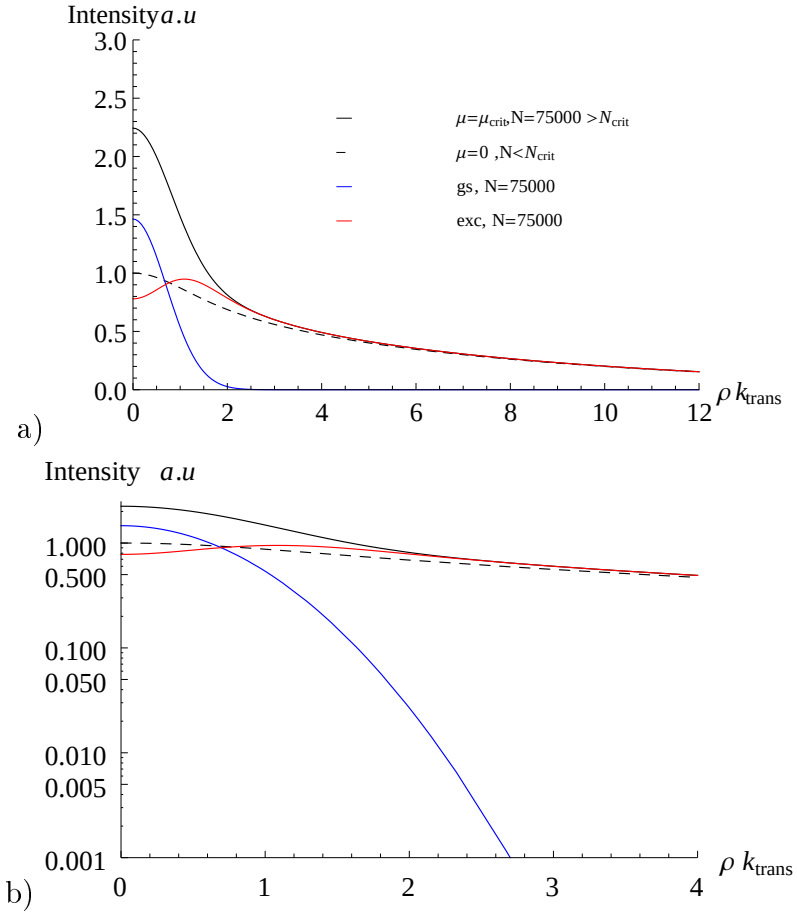

Figure 3.3: a) Radial autocorrelation below and above criticality, normalized to density of the photons gas below criticality at $\rho = 0$ and $k_{\text{trans}} = \sqrt{k/a}$. The intensity is decomposed in ground state (gs) and excited states (exc). b) Logarithmic plot of a).

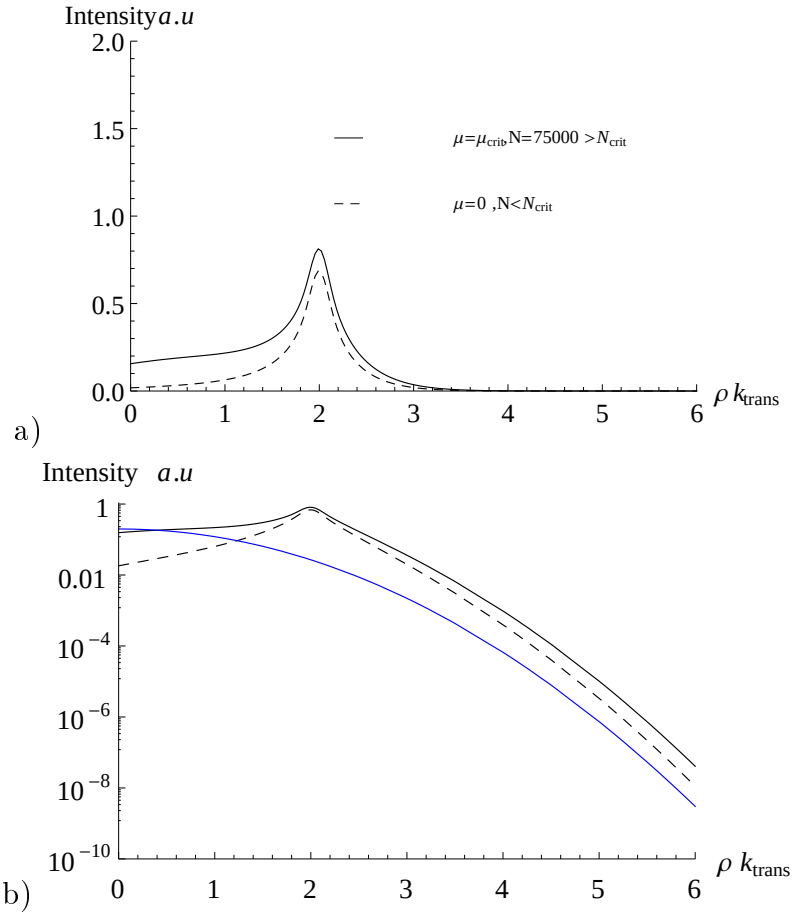

Figure 3.4: a)Radial correlation below and above criticality at $\rho k_{\text{trans}} = 2$ with $k_{\text{trans}} = \sqrt{k/a}$, normalized to the density of the photons gas below criticality at $\rho = 0$. b) Logarithmic plot of a) with additionally ground state (blue curve) plotted.

Chapter 4

Conclusion and outlook

This thesis systematically derived the Bose-Einstein condensation of photons from classical electrodynamics. We studied the mode functions in a resonator, revealing a classical frequency offset. The resonator geometry mimics an effective potential, which is a prerequisite for a BEC. Fixing the longitudinal quantum number as prescribed in the experiment, the underlying mode structure corresponds to that of a massive two-dimensional harmonically trapped Bose gas. Here we have explicitly shown the analogy between the quantized electromagnetic field with a fixed quantum number and the bosonic field operators, which inherit the structure from the solutions of the classical Maxwell equations. Finally, correlations and densities were studied to confirm the signatures of BEC. The obtained boundary value problem for this resonator yields in leading order the trap frequency described in the Weitz experiment [9], as well as the effective mass term. Furthermore, the whole wave vector structure and the dispersion relation could be recovered. The main result is the complete construction of the electromagnetic field, which grants access to relevant quantities such as correlations, intensities and photon numbers.
In particular, the BEC of photons inherits a vector character, arising from the two different polarizations and the wave vector $\mathbf{k}$. A consequence is the degeneracy of the ground state, but also of all other states. To reveal the vectorial structure of the photon BEC, we suggest to put a polarization filter in front of the detector. Depending on the decrease of the corresponding intensity, one can check whether one of the two polarizations is preferred, i.e whether the BEC is right- or left-handed. Furthermore, one should discuss the feasibility of polarized BEC with some special media in the resonator or polarized pump light. Investigating the modes, the creation of a doughnut-shaped ground state is interesting. This requires a mechanism which forbids the Gaussian ground state, as for example a dye excitation and reemission, which macroscopically populates the $|m| = 1$ state and blocks the $|m| = 0$ state due to selection rules. We do not know whether or not dyes with a suitable dipole transition exist. There are still open questions concerning the phase transition of this two-dimensional system. In the present work, the phase transition was calculated as if it was arising from spontaneous breaking of the $U(1)$ symmetry. However, it should be possible to check whether or not the BKT-theory [33] applies to the BEC of photons.

Appendix A

Normalizing the vector modes

In this chapter we present the calculation of the normalized modes in (2.145). Mostly we will use the Einstein sum convention, meaning upper and lower indices are summed. The integral (2.144) is the L^2 scalar product of the vectorial mode function $\mathbf{A_{lm}}$

$$
\begin{aligned}
1 \overset{!}{=} & \int_{\mathrm{vol_c}} dA\, \mathbf{A_{lm}} \cdot \mathbf{A^*_{lm}} && \text{(A.1)}\\
= & \Gamma^2_{lm} \int_{\mathrm{vol_c}} dA\, (\nabla \times \mathbf{e}_+ u_{\mathrm{vN}lm}) \cdot (\nabla \times \mathbf{e}^*_+ u^*_{\mathrm{D}lm}) \\
& + \frac{\Gamma^2_{lm}}{k^2_{lm}} (\nabla \times \nabla \times \mathbf{e}_+ u_{\mathrm{D}lm}) \cdot (\nabla \times \nabla \times \mathbf{e}^*_+ u^*_{\mathrm{vN}lm}), && \text{(A.2)}
\end{aligned}
$$

where in the second step we already left out the scalar product of the mixed terms, since we know that the $\nabla\times$-mode and the $\nabla\times\nabla\times$-mode are orthogonal by construction. The subscript D and vN indicates the Dirichlet and von Neumann boundary condition for the scalar function P, respectively.
The following vector analytic identity simplifies the occurring curl expressions

$$
\begin{aligned}
\nabla \times \mathbf{T} \cdot \nabla \times \mathbf{T}^* = & \epsilon_{ijk}\epsilon_{lmn} \mathbf{e}^i \cdot \mathbf{e}^l \partial^j T^k \partial^m T^{*n} && \text{(A.3)}\\
= & \partial_j T_k \partial^j T^{*k} - \partial_j T_k \partial^k T^{*j} && \text{(A.4)}\\
= & \partial^j \left[(\partial_j T_k) T^{*k} \right] - (\Delta T_k) T^{*k} + (\partial_j \partial_k T^k) T^{*j} - \partial^k \left[(\partial_j T_k) T^{*j} \right]. && \text{(A.5)}
\end{aligned}
$$

We wrote this expression explicitly without integral. Due to the two-dimensional integral in (A.2), we have take care of the occurring z-derivatives, because partial integration with respect to z does not apply. Plugging (A.5) into the second line in (A.2) with $\mathbf{T} = \nabla \times \mathbf{e}_+ u_{\mathrm{D}lm}$, the divergence term $\partial_k T^k$ vanishes automatically. The x, y divergence expressions of $\partial^j \left[(\partial_j T_k) T^{*k} \right]$ and $\partial^k \left[(\partial_j T_k) T^{*j} \right]$ vanish by integration over the xy-plane due to the rapid decay of scalar solution, only the divergence with

respect to z remains. So we are left the integral

$$1 \stackrel{!}{=} \Gamma_{lm}^2 \int\limits_{\mathrm{vol_c}} dA (\nabla \times \mathbf{e}_+ u_{\mathrm{vN}lm}) \cdot (\nabla \times \mathbf{e}_+^* u_{\mathrm{vN}lm}^*) + (\nabla \times \mathbf{e}_+ u_{\mathrm{D}lm}) \cdot (\nabla \times \mathbf{e}_+^* u_{\mathrm{D}lm}^*) \tag{A.6}$$

$$+ \frac{\Gamma_{lm}^2}{k_{lm}^2} \partial^z \int\limits_{\mathrm{vol_c}} dA \left[(\partial_z T_k) T^{*k} - (\partial_j T_z) T^{*j} \right] \tag{A.7}$$

The second line can be neglected, because the largest contribution arises from the derivative with respect to z. In order to compensate the term $1/k_{lm}^2$, it requires two z-derivatives. We set $j = z$ for first term in the second line and $j = k = z$ for second term to find the leading order

$$\partial_z \left[(\partial_z T_k) T^{*k} - (\partial_z T_z) T_z^* \right] = \partial_z \left[(\partial_z T_x) T^{*x} + (\partial_z T_y) T^{*y} \right] \tag{A.8}$$

$$= \partial_z \left[(\partial_z \partial_z u_{\mathrm{D}lm}) u_{\mathrm{D}lm}^* - (\partial_z \partial_z u_{\mathrm{D}lm}) u_{\mathrm{D}lm}^* \right] \tag{A.9}$$

$$= 0. \tag{A.10}$$

Above we showed how to shift the operator $\nabla\times$ and then replace it by $-\Delta\mathbf{T} = k_{lm}^2 \mathbf{T}$. Applying (A.5) again to (A.6) with $\mathbf{T} = \mathbf{e}_+ u_{\mathrm{D}lm}$ and $\mathbf{P} = \mathbf{e}_+ u_{\mathrm{vN}lm}$, we get

$$1 \stackrel{!}{=} -\Gamma_{lm}^2 \int\limits_{\mathrm{vol_c}} dA \Delta (u_{\mathrm{D}lm} u_{\mathrm{D}lm}^* + u_{\mathrm{vN}lm} u_{\mathrm{vN}lm}^*) \tag{A.11}$$

$$+ \Gamma_{lm}^2 \int\limits_{\mathrm{vol_c}} dA \, \partial^j (\partial_j T_k T^{*k} + \partial_j P_k P^{*k}) \tag{A.12}$$

$$+ \Gamma_{lm}^2 \int\limits_{\mathrm{vol_c}} dA \, \partial_j T^k \partial_k T^{*j} + \partial_j P^k \partial_k P^{*j}. \tag{A.13}$$

Integrating the divergence expressions in the second line over x and y, only the integral over the divergence with respect to z remains

$$\partial_z T_k T^{*k} + \partial_z P_k P^{*k} = k_\parallel |R_{lm}(x,y)|^2 (-\sin(k_\parallel z)\cos(k_\parallel z) + \sin(k_\parallel z)\cos(k_\parallel z)) \tag{A.14}$$

$$= 0, \tag{A.15}$$

where $R_{lm}(x,y)$ is transversal solution (2.65), which is independent from z. The third line (A.13) does not involve any z-derivatives, because the vectors do not have a z-component. The arguments x and y always appear in a quadratic form in the mode function $u_{\mathrm{D}lm}$ and $u_{\mathrm{vN}lm}$ (2.87). Thus, the derivative of each mode function is of the order $k_\parallel \rho / a \ll k_\parallel$, deriving the obtained prefactor another time would result in $k_\perp^2 = k_\parallel$. However, due to the single appearing derivatives we neglect the third line (A.13). The result is then

$$1 \stackrel{!}{=} -\Gamma_{lm}^2 \int\limits_{\mathrm{vol_c}} dA \, \Delta (u_{\mathrm{D}lm} u_{\mathrm{D}lm}^* + u_{\mathrm{vN}lm} u_{\mathrm{vN}lm}^*) \tag{A.16}$$

$$= \Gamma_{lm}^2 k_{lm}^2 \int\limits_{\mathrm{vol_c}} dA \, (u_{\mathrm{D}lm} u_{\mathrm{D}lm}^* + u_{\mathrm{vN}lm} u_{\mathrm{vN}lm}^*). \tag{A.17}$$

In the next steps we calculate the normalization factor Γ_{lm}. In paraxial approximation the quantization volume is the area perpendicular to the optical axis. Since this area is rotational invariant under the azimuthal angle ϕ, we perform the integration of (A.17) in polar coordinates

$$1 \stackrel{!}{=} \Gamma_{lm}^2 k_{lm}^2 \int_0^{2\pi} \int_0^{\infty} |R_{lm}(\rho)|^2 \left[P_{\mathrm{D}}^2(z) + P_{\mathrm{vN}}^2(z)\right] \rho d\rho d\phi \tag{A.18}$$

$$= \Gamma_{lm}^2 k_{lm}^2 2\pi \int_0^{\infty} |R_{lm}(\rho)|^2 \rho d\rho, \tag{A.19}$$

where we used that the absolute value of the mode function (2.87) is independent from ϕ and the functions $P_{\mathrm{D}}^2(z) = \sin^2(k_\parallel z)$ and $P_{\mathrm{vN}}^2(z) = \cos^2(k_\parallel z)$ add up to 1. Discussing the transverse extension of these modes, we have already recognized a strong confinement close the optical axis, i.e. the z-axis, which means contributions from abroad are only tiny perturbative corrections. Furthermore, in the limit for small curvature meaning $a \to \infty$, it is justified to set the upper integration limit $\rho_0 = \infty$, while the angle $\theta \approx \rho/a$ in oblate spheroidal coordinates remains small or at least constant, check also the discussion on open and closed cavities (2.67) and Figure 2.3. In order to integrate (A.19), we substitute $x = \rho^2 k_{lm}/a$ to arrive at

$$1 \stackrel{!}{=} \Gamma_{lm}^2 \left(\frac{a}{k_{lm}}\right)^m a k_{lm} 2\pi \int_0^{\infty} \mathrm{e}^{-x} x^m \left\{L_l^m(x)\right\}^2 dx, \tag{A.20}$$

where we used the transverse solution $R(\rho)$ from (2.65). The integral expression is the exact definition for the L^2-measure of the Laguerre polynomials. This is what we expected from the orthogonal mode system. The Laguerre integral has the value

$$\int_0^{\infty} \mathrm{e}^{-x} x^m \left\{L_l^m(x)\right\}^2 dx = \frac{(l+m)!}{l!}. \tag{A.21}$$

Thus the evaluated total mode function integral is explicit

$$1 \stackrel{!}{=} \Gamma_{lm}^2 \left(\frac{a}{k_{lm}}\right)^m a k_{lm} \pi \frac{(l+m)!}{l!}. \tag{A.22}$$

Hence the normalization constant is

$$\Gamma_{lm} = \sqrt{\left(\frac{k_{lm}}{a}\right)^{m-1} \frac{1}{\pi a^2} \frac{l!}{(l+m)!}}. \tag{A.23}$$

Appendix B

Transverse delta function

We present an outline of the derivation for the canonical commutation relation of the constructed transverse vector potential operators $\widehat{\mathbf{A}}$ and $\widehat{\mathbf{A}}^\dagger$ in (2.159). The canonical commutator for the vector potential $\widehat{\mathbf{A}}$ and its canonical conjugate field $\widehat{\mathbf{\Pi}} = \dot{\widehat{\mathbf{A}}}$ is

$$N^2\left[\widehat{A}_i^\dagger(\mathbf{x}), \widehat{\Pi}_j(\mathbf{x}')\right] = iN^2\left[\widehat{A}_i^\dagger(\mathbf{x}), \omega\widehat{A}_j(\mathbf{x}')\right] \tag{B.1}$$

$$= iN^2 \sum_{(n)lm\epsilon}\sum_{op\epsilon'} \mathbf{e}_i \cdot \mathbf{e}_j \omega_{op} A^{i*}_{(n)lm\epsilon}(\mathbf{x}) A^j_{op\epsilon'}(\mathbf{x}') \times \left[\widehat{a}^\dagger_{lm\epsilon}, \widehat{a}_{op\epsilon'}\right] \tag{B.2}$$

$$= i\sum_{lm\epsilon} N_{lm}^2 \delta_{ij}\omega_{lm} A^{i*}_{lm\epsilon}(\mathbf{x}) A^j_{lm\epsilon}(\mathbf{x}') \tag{B.3}$$

$$= C_{ij\epsilon 1}(x,x') + C_{ij\epsilon 2}(x,x'), \tag{B.4}$$

where we used the commutator for the annihilation and creation operators (2.153) which yields $\delta_{lo}\delta_{mp}\delta_{\epsilon\epsilon'}$. The appearing N_{lm} (2.152) gives the components of A_i of the vector modes $\mathbf{A}$ the proper dimension. In the next steps we will treat each polarization ϵ separate. With the definition of the vector fields (2.94) and the scalar mode function $u_{\mathrm{vN}lm}$ (2.87) we get for one polarization

$$C_{ij\epsilon 1}(x,x') = i\sum_{lm} N_{lm}^2 \Gamma_{lm}^2 \omega_{(n)lm} \epsilon_{ikt}\epsilon_{iop} \partial^k \left[\mathbf{e}_+ u_{\mathrm{vN}lm}(\mathbf{x})\right]^t \partial'^o \left[\mathbf{e}_+^* u^*_{\mathrm{vN}lm}(\mathbf{x}')\right]^p \tag{B.5}$$

$$= i\sum_{lm} N_{lm}^2 \Gamma_{lm}^2 \omega_{lm} (\delta_{ko}\delta_{tp} - \delta_{kp}\delta_{to}) \partial^k \left[\mathbf{e}_+ u_{\mathrm{vN}lm}(\mathbf{x})\right]^t \partial'^o \left[\mathbf{e}_+^* u^*_{\mathrm{vN}lm}(\mathbf{x}')\right]^p . \tag{B.6}$$

The index t on $\left[\mathbf{e}_+ u_{\mathrm{vN}lm}(\mathbf{x})\right]^t$ denotes the component t from the vector $\mathbf{e}_+ u_{\mathrm{vN}lm}$. Summing over the components t and p of $\mathbf{e}_+$ and $\mathbf{e}_+^*$, only the components of the same index do not cancel out. Taking into account that a derivative with a prime ∂'_o acts only on primed variables, we take out the partial derivatives

$$= i\left(\partial_k \partial'^k - \partial_k \partial'^o\right) \sum_{lm\epsilon} N_{lm}^2 \Gamma_{lm}^2 \omega_{lm} u_{\mathrm{vN}lm}(\mathbf{x}) u^*_{\mathrm{vN}lm}(\mathbf{x}'). \tag{B.7}$$

$$\tag{B.8}$$

Performing analogous steps for the other polarization yields

$$C_{ij\epsilon 2}(x,x') = i\sum_{lm}\delta_{ij}N_{lm}^2\frac{\Gamma_{lm}^2}{k_{lm}^2}\omega_{lm}\left[\nabla\times\nabla\times\mathbf{e}_+u_{\mathrm{D}lm}(\mathbf{x})\right]^i\left[\nabla'\times\nabla'\times\mathbf{e}_+^*u_{\mathrm{D}lm}^*(\mathbf{x}')\right]^j. \tag{B.9}$$

Again the primed variables do not act on the unprimed variables. Thus, we can take out $(\nabla\times\nabla\times)(\nabla'\times\nabla'\times)$. Using the indentity $(\nabla\times\nabla\times) = \nabla\nabla\cdot - \Delta$ and the argument for summation over all the vector components of $\mathbf{e}_+$ and $\mathbf{e}_+^*$ we find

$$= i\left(\partial_k\partial^k - \partial_k\partial^o\right)\left(\partial_k'\partial'^k - \partial_k'\partial'^o\right)\sum_{lm}N_{lm}^2\frac{\Gamma_{lm}^2}{k_{lm}^2}\omega_{lm}u_{\mathrm{D}lm}(\mathbf{x})u_{\mathrm{D}lm}^*(\mathbf{x}'). \tag{B.10}$$

Finally the full commutator has the form

$$\begin{aligned} N^2\left[\widehat{A}_i^\dagger(\mathbf{x}),\widehat{\Pi}_j(\mathbf{x}')\right] = & \\ & i\left(\partial_k\partial'^k - \partial_k\partial'^o\right)\sum_{lm}N_{lm}^2\Gamma_{lm}^2\omega_{lm}u_{\mathrm{vN}lm}(\mathbf{x})u_{\mathrm{vN}lm}^*(\mathbf{x}') \\ & + i\left(\partial_k\partial^k - \partial_k\partial^o\right)\left(\partial_k'\partial'^k - \partial_k'\partial'^o\right)\sum_{lm}N_{lm}^2\frac{\Gamma_{lm}^2}{k_{lm}^2}\omega_{lm}u_{\mathrm{D}lm}(\mathbf{x})u_{\mathrm{D}lm}^*(\mathbf{x}'). \end{aligned} \tag{B.11}$$

In the next step we explicitly write down the scalar function u (2.87) and use the constants Γ_{lm} (A.23) and N_{lm} (2.152)

$$\begin{aligned} D(x,x') = & \sum_{lm}\frac{l!}{(l+m)!}\frac{\hbar}{\epsilon_0 ka\pi}\left(\frac{k}{a}\rho\rho'\right)^{|m|}L_l^{|m|}\left(\frac{k}{a}\rho^2\right)L_l^{|m|}\left(\frac{k}{a}\rho'^2\right) \\ & \times \mathrm{e}^{-\frac{k}{2a}(\rho'^2+\rho^2)}\mathrm{e}^{im(\phi-\phi')}P(k_\parallel z)P(k_\parallel z'). \end{aligned} \tag{B.12}$$

Here $P(z)$ is the transverse solution (2.65), with no fixed boundary condition, such that the next steps hold four both polarizations.
We need to show the completeness relation for the Laguerre polynomials. Therefore we introduce the symmetric kernel polynomial

$$K_n^m(x,y) := \sum_{i=0}^{l}\frac{i!L_i^m(x)L_i^m(y)}{(i+m)!} \tag{B.13}$$

$$= \frac{(l+1)!}{(l+m)!}\frac{L_l^{(\alpha)}(x)L_{l+1}^m(y) - L_{l+1}^m(x)L_l^m(y)}{x-y}. \tag{B.14}$$

Such a kernel exists for all orhtogonal polynomials (Christoffel-Darboux theorem). Combining the kernel with the respective L^2 measure of the Laguerre polynomials leads to a delta function in L^2, which is then understood distribution in a convolution integral

$$y^m e^{-y}K_n^m(\cdot,y) \to \delta(y-\cdot). \tag{B.15}$$

Setting $x = \frac{k}{a}\rho^2$ and $y = \frac{k}{a}\rho'^2$ we apply (B.15) to (B.12), then the l sum can be replaced

$$D(x,x') = \sum_m \frac{\hbar}{\epsilon_0 k a \pi} \left(\frac{\rho'}{\rho}\right)^{|m|} \mathrm{e}^{-\frac{k}{a}(\rho'^2-\rho^2)} \delta\left[\frac{k}{a}\rho^2 - \frac{k}{a}\rho'^2\right] \mathrm{e}^{im(\phi-\phi')} P(k_\parallel z) P(k_\parallel z'). \tag{B.16}$$

A property of the delta distribution is

$$\delta[f(x)] = \sum_{x_0} \frac{\delta(x-x_0)}{|f'(x_0)|}, \tag{B.17}$$

where the x_0 fulfill $f(x_0) = 0$. Using this property the sum gets the form

$$D(x,x') = \sum_m \frac{\hbar}{\epsilon_0 k a \pi} \frac{a}{k 2\rho} \delta\left[\rho - \rho'\right] \mathrm{e}^{im(\phi-\phi')} P(k_\parallel z) P(k_\parallel z'). \tag{B.18}$$

Another representation of the delta function is

$$\delta(x) = \frac{1}{2\pi} \sum_{n=-\infty}^{\infty} \mathrm{e}^{inx}, \tag{B.19}$$

which reduces the sum to

$$D(x,x') = \frac{\hbar}{k^2 \epsilon_0 \rho} \delta(\rho-\rho')\delta(\phi-\phi') P(k_{\parallel n} z) P(k_{\parallel n} z'). \tag{B.20}$$

We can further replace in the second line of (B.10) the operator $\partial'_k \partial'^k \to -k_{lm}^2$ and omit the expression $\partial'_k \partial'^o$, because the scaling with $1/k_{lm}^2$ makes this term negligible. Then the commutator (B.1) is

$$\begin{aligned} N^2 \left[\widehat{A}_i^\dagger(\mathbf{x}), \widehat{\Pi}_j(\mathbf{x}')\right] = \\ \frac{i\hbar}{\epsilon_0} \delta_{ij} \left(\partial_k \partial^k - \partial_k \partial^o\right) \frac{1}{k^2 \rho} \delta(\rho-\rho')\delta(\phi-\phi') \left\{\cos(k_\parallel(z+z))\right\}. \end{aligned} \tag{B.21}$$

The term in curly brackets is $\cos(k_{\parallel n}(z+z)) = \cos(k_n z)\cos(k_n z') - \sin(k_n z)\sin(k_n z')$ with longitudinal cut-off wave number $k_\parallel$.
Since the considered mode functions $u_{\mathrm{D}(n)lm}$ and $u_{\mathrm{vN}(n)lm}$ are well behaved, it is always possible to Fourier transform, which means we can interchange derivatives with wave vectors. Thus we further simply the obtained expression,

$$N^2 \left[\widehat{A}_i^\dagger(\mathbf{x}), \widehat{\Pi}_j(\mathbf{x}')\right] = \frac{i\hbar}{\epsilon_0} \left(\delta_{ij} - \partial_i \frac{1}{k^2} \partial_j\right) \delta^{(2)}(\mathbf{x}-\mathbf{x}') \cos(k_\parallel(z+z)), \tag{B.22}$$

which then resembles the definition of the transverse delta function [34]

$$\delta_\perp^{ij}(\mathbf{x}-\mathbf{x}') = \left\{\delta_{ij} - \partial_i \frac{1}{\Delta} \partial_j\right\} \delta^{(3)}(\mathbf{x}-\mathbf{x}'). \tag{B.23}$$

The fixed longitudinal quantum number makes (B.22) to an effective two-dimensional transverse delta function with spatial modulation in z-direction.

Appendix C

Correlation function

This appendix deals with the explicit calculation of the double sum over the quantum numbers l and m appearing in the expectation value of the excited states in (3.67) and as bilocal expression in (3.95). The expectation value is

$$\left\langle \delta\widehat{\psi}^{\dagger}(\mathbf{x})\delta\widehat{\psi}(\mathbf{x}')\right\rangle_{(0)} = n_{\mathrm{exc}}(\mathbf{x},\mathbf{x}') = \sum_{lm\epsilon,lm\neq 00} \mathbf{A}^{*}_{lm\epsilon}(\mathbf{x})\cdot\mathbf{A}_{lm\epsilon}(\mathbf{x}')\frac{1}{\mathrm{e}^{\beta(E_{lm}-\mu)}-1} \tag{C.1}$$

This expression is also understood as the bilocal density for the excited states $n_{\mathrm{exc}}(\mathbf{x},\mathbf{x}')$. The evaluation of the product of the vectorial mode functions is performed approximatively by taking the micro cavity limes $k_{\parallel}z = \text{const}$ and $k_{\perp} = \text{const}$ while $z \to 0$, see also Appendix (A), where the scalar product is performed always regarding the leading order terms. Applying the definition of the vector modes (2.145) with the scalar solution (2.87), the expansion yields

$$\begin{aligned} n_{\mathrm{exc}}(\mathbf{x},\mathbf{x}') =& \frac{1}{a\pi}\sum_{lm\neq 00} k_{lm}\frac{l!}{(l+|m|)!}\frac{1}{\mathrm{e}^{\beta(E_{lm}-\mu)}-1}\mathrm{e}^{-im(\phi-\phi')} \\ &\times\left(\frac{k_{lm}\rho\rho'}{a}\right)^{|m|}\mathrm{e}^{-\frac{k_{lm}}{2a}(\rho^2+\rho'^2)}L_l^{|m|}\left(\frac{k_{lm}\rho^2}{a}\right)L_l^{|m|}\left(\frac{k_{lm}\rho'^2}{a}\right). \end{aligned} \tag{C.2}$$

The k_{lm} depends on the summation indices l, m. In paraxial approximation the leading order of the absolute value k_{lm} (2.118) is $k_{lm} = k_{\parallel}$. Thus every combination with ρ^2 and k_{lm} is replaced by $k_{\parallel}\rho^2$ and only the expression directly behind the sum symbols is expanded to the next order. The expansion in k_{lm} (2.118) contains expressions of the form $(2l+|m|)/a$, which have to be summed. An analysis of the summands yields expressions proportional to

$$\frac{l!}{(l+|m|)!}\left(k_{\parallel}+\frac{(2l+|m|)}{a}\right)\frac{1}{\mathrm{e}^{\beta\hbar\omega(2l+|m|)}-1}\mathrm{e}^{-\frac{k_{\parallel}}{a}(\rho^2\rho'^2)}L_l^m\left(\frac{k_{\parallel}}{a}\rho^2\right)L_l^m\left(\frac{k_{\parallel}}{a}\rho'^2\right). \tag{C.3}$$

Since $k_{\parallel}$ is about 1000 times larger than $1/a$, only summands larger than $l = 500$ are comparable with $k_{\parallel}$. Then the exponential $1/(\mathrm{e}^{\beta\hbar\omega 2l}-1)$ from the Bose-Einstein statistics effectively surpresses the contribution, because the factor $\beta\hbar\omega 2l$ becomes much larger than 1. Figure C.1 illustrates the behavior of the summand as function

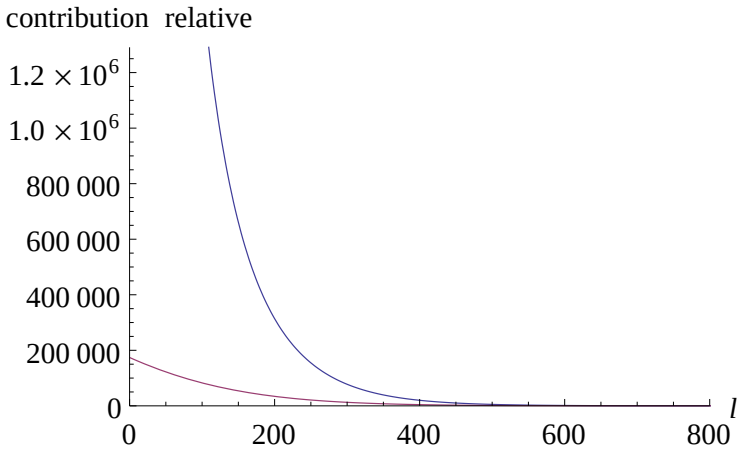

Figure C.1: Relative contributions of the summands in (C.3) as function of l for $m = 0$ and $\rho = \rho' = 0$. The contribution of next order in k_{lm} (red curve) is negligible in comparison to the leading order $k_\parallel$ (blue curve). For large l the Bose-Einstein statistics surpresses all contributions.

of l. An Analogous argument holds for the sum over m. Physically this effective suppression originates from the enhanced cut-off energy or more precise it arises from the large energy spacing between the longitudinal and the transversal modes. If $k_\parallel$ was much smaller, the additional contribution from l and m would be non-negligible.
Rewriting the Bose-Einstein factor into a geometric series and using the explicit form of the scalar solution (2.87) leads to

$$\begin{aligned} n_{\mathrm{exc}}(\mathbf{x},\mathbf{x}') =& \frac{k_\parallel}{a\pi}\sum_{p=1}^{\infty} \mathrm{e}^{-\beta[\hbar\omega-\mu]p}\mathrm{e}^{-\frac{k_\parallel}{2a}(\rho^2+\rho'^2)} \\ &\times\left\{\sum_{m=-\infty}^{\infty}\sum_{l=0}^{\infty} k_\parallel \mathrm{e}^{-\beta[\hbar\omega(2l+|m|)p}\frac{l!}{(l+|m|)!}\left(\frac{k_\parallel\rho\rho'}{a}\right)^{|m|}\right. \\ &\left.\times L_l^{|m|}\left(\frac{k_\parallel\rho^2}{a}\right)L_l^{|m|}\left(\frac{k_\parallel\rho'^2}{a}\right)\mathrm{e}^{-im(\phi-\phi')}-1\right\} \end{aligned} \tag{C.4}$$

The following identity is adapted from Gradshteyn and Ryzhik [20, 8.976]

$$\sum_{l=0}^{\infty}\frac{l!}{\Gamma(l+m+1)}L_l^m(x)L_l^m(y)z^l = \frac{(xyz)^{-\frac{1}{2}m}}{1-z}\exp\left(-z\frac{x+y}{1-z}\right)I_m\left(2\frac{\sqrt{xyz}}{1-z}\right), \tag{C.5}$$

for all $|z| < 1$. Here I_m is the modified Bessel function and Γ is the gamma function. First we identify $x = k_z/a\rho^2$, $y = k_z/a\rho'^2$ and $z = \mathrm{e}^{-\beta\hbar\omega 2p}$. Then formula (C.5) leads

to

$$n_{\mathrm{exc}}(\mathbf{x},\mathbf{x}') = \frac{k_\parallel}{a\pi}\sum_{p=1}^{\infty} \mathrm{e}^{-\beta(\hbar\omega-\mu)p}\mathrm{e}^{-\frac{1}{2}(x+y)} \times \left\{ \frac{\mathrm{e}^{-\frac{z}{(1-z)}(x+y)}}{(1-z)} \sum_{m=-\infty}^{\infty} \mathrm{e}^{-im(\phi-\phi')} I_m\left(2\frac{\sqrt{xyz}}{1-z}\right) - 1 \right\}. \tag{C.6}$$

Making explicit use of the Jacobi-Anger identity

$$\mathrm{e}^{q\cos(t)} = I_0(q) + 2\sum_{m=1}^{\infty} I_m(q)\cos(mt), \tag{C.7}$$

and the recursion formula for the the modified Bessel function [20, 8.486.7]

$$I_(q) - m = I_m(q) \qquad \text{for all } m \in \mathbb{Z}, \tag{C.8}$$

the sum over the angular momentum quantum number m can also be resolved. Applying (C.7) to (C.6) and substituting back all variables finally yields

$$n_{\mathrm{exc}}(\mathbf{x},\mathbf{x}') = \frac{k_\parallel}{a\pi}\sum_{p=1}^{\infty} \mathrm{e}^{-\beta(\hbar\omega-\mu)p}\mathrm{e}^{-\frac{k_\parallel}{2a}(\rho^2+\rho'^2)} \times \left\{ \frac{\mathrm{e}^{-\frac{z}{(1-z)}\frac{k_\parallel}{a}(\rho^2+\rho'^2)}}{(1-z)} \mathrm{e}^{2\frac{k_\parallel}{a}\frac{\sqrt{\rho^2\rho'^2 z}}{(1-z)}\cos(\phi-\phi')} - 1 \right\}, \tag{C.9}$$

with $z = \mathrm{e}^{-\beta\hbar\omega 2p}$. In the special case of $\mathbf{x} = \mathbf{x}'$ it can be further simplified to

$$n_{exc}(\mathbf{x}) = \frac{k_\parallel}{a\pi}\sum_{p=1}^{\infty} \mathrm{e}^{-\beta(\hbar\omega-\mu)p} \left\{ \frac{\mathrm{e}^{-\frac{k}{a}\rho^2\frac{1-2\sqrt{z}+z}{(1-z)}}}{(1-z)} - \mathrm{e}^{-\frac{k}{a}\rho^2} \right\} \tag{C.10}$$

$$= \frac{k_\parallel}{a\pi}\sum_{p=1}^{\infty} \mathrm{e}^{-\beta(\hbar\omega-\mu)p} \left\{ \frac{\mathrm{e}^{-\frac{k}{a}\rho^2(\beta\hbar\omega p/2)}}{(1-\mathrm{e}^{-\beta\hbar\omega 2p})} - \mathrm{e}^{-\frac{k}{a}\rho^2} \right\}. \tag{C.11}$$

Bibliography

[1] M.H. Anderson, J.R. Ensher, M.R. Matthews, C.E. Wieman, and E.A. Cornell. Observation of Bose-Einstein condensation in a dilute atomic vapor. *science*, 269(5221):198–201, 1995.

[2] K.B. Davis, M.O. Mewes, M.R. Andrews, N.J. Van Druten, D.S. Durfee, D.M. Kurn, and W. Ketterle. Bose-Einstein condensation in a gas of sodium atoms. *Physical Review Letters*, 75(22):3969–3973, 1995.

[3] C.C. Bradley, C.A. Sackett, and R.G. Hulet. Bose-Einstein condensation of lithium: Observation of limited condensate number. *Physical Review Letters*, 78(6):985, 1997.

[4] H. Deng, G. Weihs, C. Santori, J. Bloch, and Y. Yamamoto. Condensation of semiconductor microcavity exciton polaritons. *Science*, 298(5591):199–202, 2002.

[5] J. Kasprzak, M. Richard, S. Kundermann, A. Baas, P. Jeambrun, J.M.J. Keeling, M.H. F.M Marchetti, et al. Bose–Einstein condensation of exciton polaritons. *Nature*, 443(7110):409–414, 2006.

[6] R. Balili, V. Hartwell, D. Snoke, L. Pfeiffer, and K. West. Bose-Einstein condensation of microcavity polaritons in a trap. *Science*, 316(5827):1007–1010, 2007.

[7] S.O. Demokritov, V.E. Demidov, O. Dzyapko, G.A. Melkov, A.A. Serga, B. Hillebrands, and A.N. Slavin. Bose–Einstein condensation of quasi-equilibrium magnons at room temperature under pumping. *Nature*, 443(7110):430–433, 2006.

[8] J. Klaers, F. Vewinger, and M. Weitz. Thermalization of a two-dimensional photonic gas in a white wall photon box. *Nature Physics*, 6(7):512–515, 2010.

[9] J. Klaers, J. Schmitt, F. Vewinger, and M. Weitz. Bose-Einstein condensation of photons in an optical microcavity. *Nature*, 468(7323):545–548, 2010.

[10] J. Klaers, J. Schmitt, T. Damm, F. Vewinger, and M. Weitz. Bose–Einstein condensation of paraxial light. *Applied Physics B: Lasers and Optics*, pages 1–17, 2011.

[11] J. Klaers, J. Schmitt, T. Damm, F. Vewinger, and M. Weitz. Statistical Physics of Bose-Einstein-Condensed Light in a Dye Microcavity. *Physical Review Letters*, 108(16):160403, 2012.

[12] J. Schmitt, T. Damm, F. Vewinger, M. Weitz, and J. Klaers. Thermalization of a two-dimensional photon gas in a polymeric host matrix. *Arxiv preprint arXiv:1201.4658*, 2012.

[13] J. Kerr. *Phil. Mag.*, 50:337,446, 1875.

[14] J.D Jackson. Klassische Elektrodynamik. *De Gruyter*, 3rd edition:20–22, 2002.

[15] P.M Morse and H. Feshbach. Methods of Theorectical Physics, Part I+II. *McGraw-Hill Book Company*, 1953.

[16] T. Pollock. Separabilität von Helmholtz- und Maxwellgleichungen über heterogenen unbeschränkten Gebieten. *Diploma thesis Freie Universität Berlin*, 2007.

[17] M.J. Lahart. Use of electromagnetic scalar potentials in boundary value problems. *American Journal of Physics*, 72:83, 2004.

[18] W. R. Smythe. Static and dynamic electricity. *McGraw-Hill Book Company*, 1968.

[19] I.N. Bronstein, K.A. Semendjajew, G. Msuiol, H. Mühlig. Taschenbuch der Mathematik. *Verlag Harri Deutsch* , 5:677,4., 2000.

[20] I. S. Gradshteyn and I. M Ryzhik. Table of integrals, series and products. *Academic Press*, 4th Edition, 1981.

[21] A. Aiello, C. Marquardt, and G. Leuchs. Geometric spin hall effect of light. *Arxiv preprint arXiv:0902.4639*, 2009.

[22] G. Grynberg C. Cohen-Tannoudji, J. Dupont-Roc. Photons et atomes. *Savoirs actuels, Edition du CNRS, Paris*, page 57, 1987.

[23] A. Messiah. Mécanique quantique tome 2. *DUNOD, Paris*, page 892, 1995.

[24] R. Jackiw. Functional evaluation of the effective potential. *Physical Review D*, 9(6):1686, 1974.

[25] Y. Yamamoto. APPPHYS 389, Bose-Einstein Condensation and Lasers. *Script, Chapter II*, 2010.

[26] R.J. Glauber. Coherent and incoherent states of the radiation field. *Physical Review*, 131(6):2766–2788, 1963.

[27] V.L. Berezinskii. Destruction of long-range order in one-dimensional and two-dimensional systems possessing a continuous symmetry group. ii. quantum systems. *Soviet Journal of Experimental and Theoretical Physics*, 34:610, 1972.

[28] J.M. Kosterlitz and D.J. Thouless. Ordering, metastability and phase transitions in two-dimensional systems. *Journal of Physics C: Solid State Physics*, 6:1181, 1973.

[29] D. Scholz and M. Weyrauch. A note on the Zassenhaus product formula. *Journal of mathematical physics*, 47:033505, 2006.

[30] B. Klünder and A. Pelster. Systematic semiclassical expansion for harmonically trapped ideal Bose gases. *The European Physical Journal B-Condensed Matter and Complex Systems*, 68(3):457–465, 2009.

[31] J Klaers. Bose-Einstein-Kondensation von paraxialem Licht. *Dissertation Universität Bonn*, 2011.

[32] Z. Hadzibabic and J. Dalibard. Two-dimensional bose fluids: An atomic physics perspective. *Arxiv preprint arXiv:0912.1490*, 2009.

[33] Z. Hadzibabic, P. Krüger, M. Cheneau, B. Battelier, and J. Dalibard. Berezinskii–Kosterlitz–Thouless crossover in a trapped atomic gas. *Nature*, 441(7097):1118–1121, 2006.

[34] W. Greiner and J. Reinhardt. Field Quantization. *Springer*, page 202, 1996.

Danksagung

So long, and thanks for all the fish.
Vielen Dank an alle, die mich unterstützt haben. Axel Pelster danke ich für dieses spannende Thema, seine Organisation, Akrebie und Begeisterung für die Physik und die Details. Besonderer Dank gilt Carsten Henkel, der mich mit seinem Wissen bereicherte und mir in zahlreichen Sitzungen eine Inspiration und Motivation war. Auch Gregor und Harald müssen hier unbedingt erwähnt werden. Dann möchte ich mich noch bei meiner Familie und Bonnilein für ihre rückhaltlose Unterstützung bedanken. Pan Arne und Matzetias verdankt diese Arbeit noch so manche Kommata.

Danke.